FZR
FORSCHUNGSZENTRUM ROSSENDORF

Institute for Safety Research

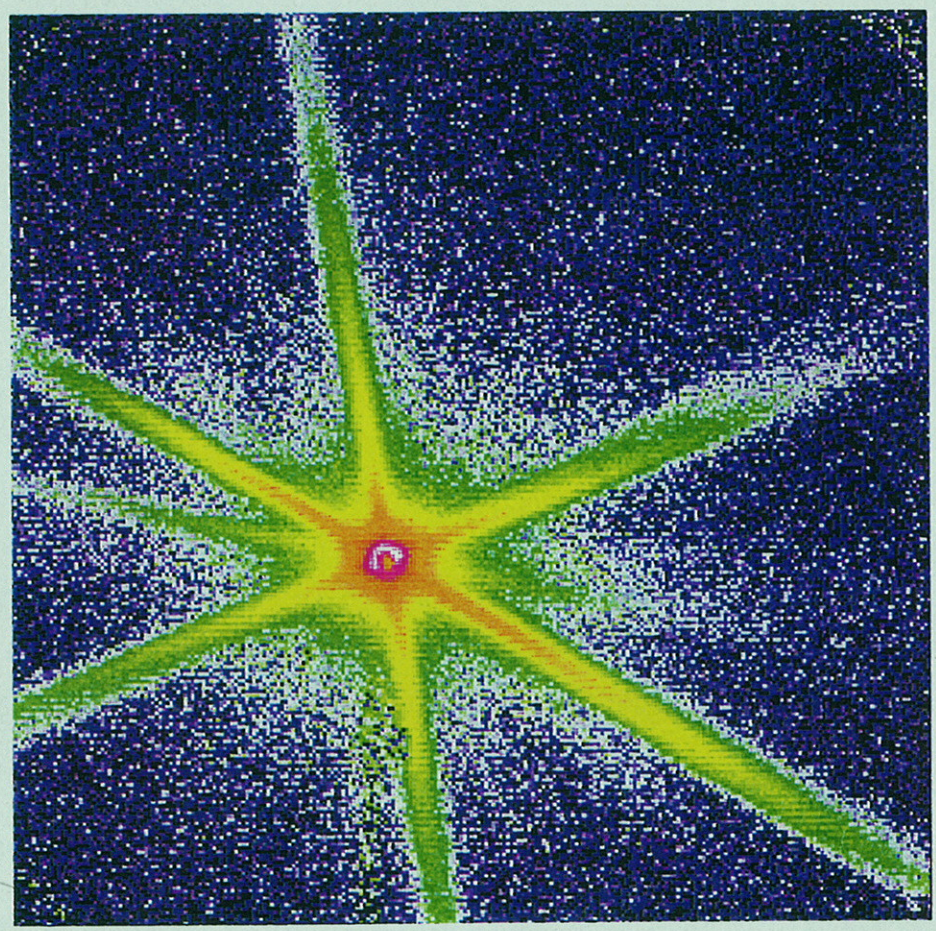

Annual Report 1994

Postfach 51 01 19
D-01314 Dresden, Germany
Tel.: +49-351-3480
Fax: +49-351-3440

Forschungszentrum Rossendorf e. V.

Institut für Sicherheitsforschung

Annual Report 1994

Editors:
F.-P. Weiß, U. Rindelhardt

FZR-126
Juni 1995

For further information on the research projects described in the present annual report, please address the director or one of the authors at the institute.

Cover photograph:
Pattern of the small angle X-ray scattering intensity. The pattern is measured at a bended Al specimen near the crack tip using a beam of 15 μm cross section of the MICROFOCUS beamline at the synchrotron facility ESRF Grenoble.

Postal address:

Postfach 51 01 19
D-01314 Dresden
Germany

Telecommunication:

Tel.: +49 351 260 3480
Fax: +49 351 260 3440
E-mail weissfp@fz-rossendorf.de

CONTENTS

Preface

Generals:

The Institute for Safety Research (IFS) is one of the five scientific institutes of the Research Center Rossendorf, that was founded in the beginning of 1992 as a so called "Blaue Liste" institute which is funded by the Free State of Saxony and by the German federal government with 50% each.

The investigations of IFS cover safety related areas as accident analysis, materials and components safety, risk assessment and risk management.
The developed models, codes and monitoring procedures are applied to nuclear installations, process industries, and to infrastructures of waste management.

Striving for the assessment and enhancement of design based safety, for improving operational safety, and for risk management IFS is engaged in the following methodical fields:

- experimental and theoretical thermo-fluiddynamics,
- 3-dimensional neutron kinetics,
- characterization of the mechanical behaviour of aged materials and microstructural analysis,
- transport calculations of particle and radiation fields,
- early failure diagnostics of processes and plants,
- hazard ranking of non-nuclear waste deposits and support of the selection of appropriate remediation procedures by means of decision analysis.

In 1994, special efforts were directed to the extension of experimental facilities needed for radioactive materials testing and for two phase flow investigations. Moreover, first research projects on the safety of VVER reactors could successfully be finished.

Most important results:

First experiments on the depressurization of runaway chemical batch reactions were carried out at small scaled facilities. The experimentel results and calculations for vessel depressurization over steam release contributed to the conception of a bigger experiment. The construction has just begun. Her it will even be possible to study the influence of foam on the efficiency of pressure decrease. These experiments will also serve as basis for theoretical model development on foam dilution and flow.

A new tool is now available for the improved safety analysis of the Russian type VVER-reactors. The 3-dimensional neutron kinetics code DYN3D, which was developed at IFS, has been coupled with the thermo-hydraulic code ATHLET, that was put at disposal by Gesellschaft für Reaktorsicherheit (GRS). That new coupled code system offers enhanced capabilities for the analysis of reactivity induced accidents, transients, and small break loss of coolant accidents without scram, where the space dependency of thermo-hydraulics and neutron kinetics are important. In that context DYN3D was completed with a burn-up module.

The IFS is going to establish a complex of preparative and testing laboratories for neutron irradiated materials. In October 1994 the first radioactive preparation A-laboratory was lincensed by the Saxon regulatory body. At present, above all reactor pressure vessel (RPV) steels are characterized. During the years coming more and more RPV internals specimens are expected.

The mechanical testing results are complemented by microstructural analysis. For the first time a combination of Small Angle Neutron Scattering (SANS) and Abnormal Small Angle X-Ray Scattering (ASAXS) has been applied to irradiated RPV steels. Thereby it could be proved that neutron irradiation produces hierarchical damage structures of different types. The widely expected Cu-rich precipitates could not be found.

The group for theoretical transport calculations of particle and radiation fields contributed to the Novosibirsk/Russia concept of an intensive 14 MeV-plasma-neutron-source by developing two Monte Carlo codes, which simulate the transport of fast ions and of neutral particles in the Deuterium/Trition plasma under the influence of an external magnetic field. Coupling of these two modules is envisaged to enable a consistent plasma description. Reasonable calculation times shall be achieved by implementing on parallel computers.

A finite element theoretical vibration model for VVER-440 reactors could widely be finished. A special fluid-structure element takes into account additional inertial forces, damping, and stiffness due to the fluid flow in the downcomer. This interaction particularly influences those eigenfrequencies of the primary circuit which are connected with relative desplacements between core barrel and RPV. The whole model is thought to be an efficient supporting instrument for early failure detection and diagnostics.

Considerable progress was also achieved in neural network based acoustic leakage detection and localization. Three layer perceptron networks were shown to be best suited to localize leaks even when the related locations could not be trained. The networks were designed in such a way that the activities of the two output neurons correspond to the leak coordinates in the cross section of the monitored plant.

A collaboration of IFS and Nuclear Engineering and Analytics, Inc. also located at the Rossendorf research site, aimed at the development of a decision analytical tool which is to support the responsible institutions in the selection of appropriate remediation procedures for non-nuclear waste deposits.

Main components of that decision support tool are a system of decision relevant criteria, an interactive module for the generation of probability density functions which describe the uncertainty of geological, chemical, and commercial data that characterize a waste deposit. Moreover, decision preferences of the participating responsible persons can be considered. After extended testing of that tool, it shall be coupled with an expert system for hazard ranking of waste sites which is used in the Free State of Saxony.

Selected Reports

CONTRIBUTIONS OF FZ ROSSENDORF TO THE IAEA STANDARD PROBLEM EXERCISE NO. 4

E. Krepper, H.-M. Prasser, F. Schäfer

1. Introduction

The integral test facility PMK-2 in Budapest is operated by the KFKI Atomic Energy Research Institute. This facility aims to the modelling of the thermalhydraulic behaviour of the Russian pressurized water reactor VVER-440 (NPP Paks). The six loops of the nuclear power plant are modelled by one loop. The volume scaling of the facility is 1:2070. All elevations are kept 1:1. The maximum power of the fuel rod simulator is 1 MW.

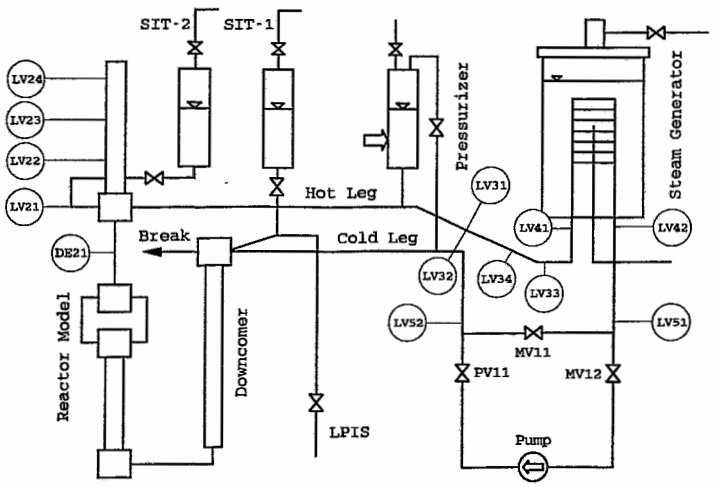

Fig. 1: Scheme of the PMK facility and location of the void fraction probes during the SPE-4 experiment

For many years, the test rig PMK was the only integral model of the primary circuit addressed to VVER type reactors. Soon the idea was born to use the facility as a source of experimental data for so-called Standard Problem Exercises (SPE), which were launched by the IAEA for the training of the theoretic groups dealing with accident simulation in the East. The approach of the SPE is similar to the International Standard Problems (ISP) organized by the OECD for Western reactor types. At first, the participants have to carry out pre-test calculations of the given accident scenario. Then the experiment is carried out and the results are distributed. Assessing these data, the participants can try to eliminate weak points and errors of the pre-test calculations in the stage of post-test calculations. All results are compared and summarized in a final report.

Today, verification of Western thermal hydraulic system codes applied to the specifics of VVER is a topical task for research work. Codes as RELAP, ATHLET and CATHARE are widely used both by licensing organisations and utilities in Eastern countries. The approach of Standard Problem Exercises is similar to what has to be done to verify a computer code. Therefore, the SPEs can contribute to the code verification if the experiment covers VVER specific phenomena.

The experiment of the IAEA standard problem exercise No. 4 was carried out in April 1993. It was a 3.2 mm break at the downcomer head. The high pressure injection cooling was assumed to be not available. As an accident management measure bleed and feed at the secondary side of the steam generator was applied.

There are many VVER specific phenomena covered by this test, such as natural circulation in the two-phase flow regime, ECC mixing and condensation, loop-seal behaviour in the hot leg, heat transfer in partly uncovered core, heat transfer in horizontal steam generators. The experiment is therefore suitable for code verification. For this reason, the Research Center Rossendorf, which is concerned with the verification of ATHLET, the German thermal hydraulic system code developed by the Gesellschaft für Anlagen- und Reaktorsicherheit (GRS), took part in the 4. IAEA Standard Problem Exercise.

2. Contributions to the experiment

Research Center Rossendorf contributed to the SPE-4 experiment by supplying needle shaped conductivity probes for the measurement of local void fractions in the primary circuit of the PMK-II test facility. The probes were developed for the application under primary circuit conditions, where they have to withstand high mechanical and corrosive loads. As a part of the cooperation between the KFKI Atomic Energy Research Institute and the Research Center Rossendorf the probes from Rossendorf have already been applied to various experiments at PMK in the past. During SPE-4 the probes were placed practically all around the circuit (with exception of the core simulator and the downcomer, Fig. 1) and for the first time they have provided data which characterise the phase distribution within the whole primary circuit.

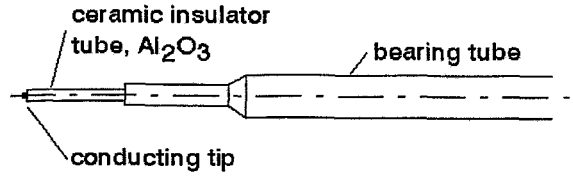

Fig. 2: Principle of the needle shaped conductivity probe

The needle shaped conductivity probes (Fig. 2) are local void fraction sensors. Their function is based on the interruption of the electrical current between the tip of the probe and the conducting fluid by the gas fraction. The void fraction is determined by integrating the time of the gas contact divided by the measuring time. As a second information the average frequency of the phase changes at the probe tip can be measured.

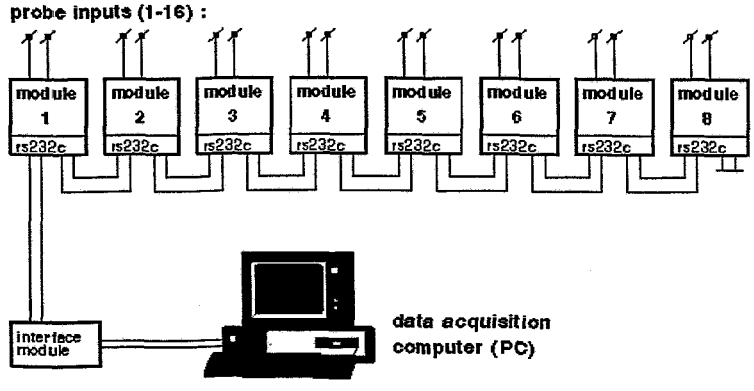

Fig. 3: Data acquisition system

The measuring system consists of a network of preamplifier modules equipped with microcomputers and a central data acquisition PC (Fig. 3). The modules perform a data preprocessing and control a digital interface which is necessary to manage the high electrical disturbance levels typical for integral test facilities. As the result the time behaviour of the void fraction and the frequency of the phase changes (bubble frequency) are recorded with a sampling time of 1 sec.

An overview of the signals of all probes is given in Fig. 4 for the first 500 seconds of the process time. Important events, such as first coolant flashing, depletion of the upper plenum and hot leg loop-seal clearing are marked at the plot. With the help of the needle shaped conductivity probes a couple of general conclusions for intermediate cold leg breaks can be drawn or at least substantiated. So it was observed that the hot leg loop-seal clearing occurs twice. For the first time in this experiment it leads to an entrainment of steam into the steam generator. The pressure drop caused by the onset of condensation leads to an intensification of the ECC water injection by the accumulators and a refilling of the loop seal. The final hot leg loop-seal clearing occurs only after the emptying of the hydroaccumulators. The cold leg loop-seal (pump seal) clearing occurs before the final hot leg loop-seal clearing has taken place. This effect is explained by the evaporation of water in the cold leg and in the steam generator tubes, while the water in the hot leg is subcooled due to the ECC injection. At the end of the process, the operation of the low pressure injection system leads to the reappearance of two-phase flow at the reactor outlet. It has to be remarked that the experiment was stopped before the cold leg loop-seal was refilled and a natural circulation of water was not yet reestablished.

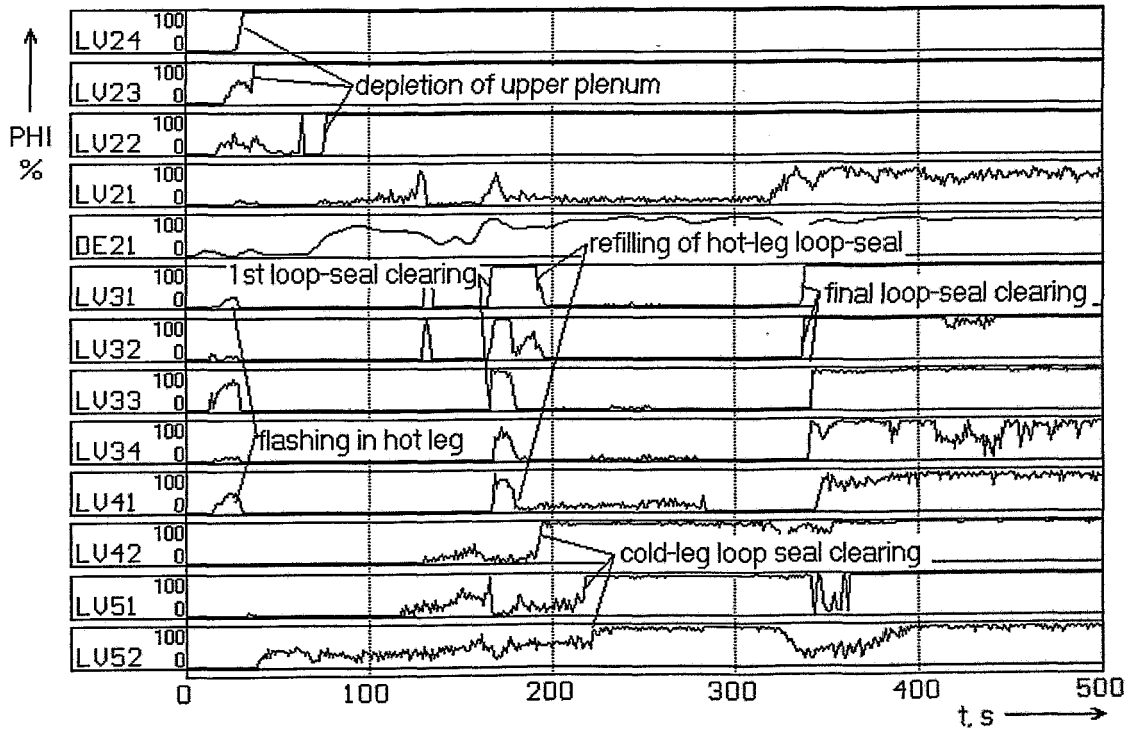

Fig. 4: Signals of void fraction probes

3. Results of ATHLET calculations

Phase 1: 0 - 30 sec

During the first thirty seconds of the experiment, the primary pressure PR21 decreases quite fast (see Fig. 5). In this period at 11.4 MPa the core power starts to decrease according the decay heat curve. At 9.5 MPa the pump coast down starts, which is modelled in the PMK facility by gradually closing the valve PV11. At a primary pressure (PR21) of 5.9 MPa the hydroaccumulators start to inject cold fluid into the primary circuit.

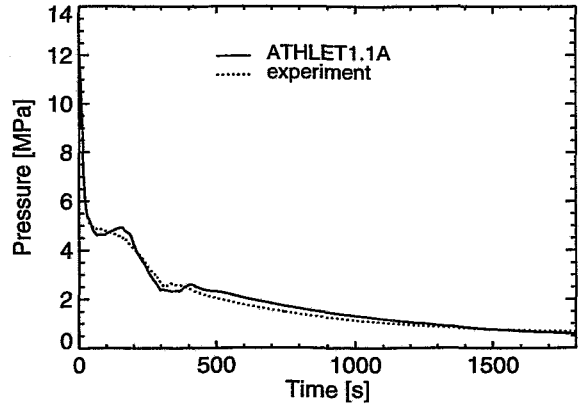

Fig. 5: Primary pressure (PR21)

Phase 2: 30 - 160 sec

Achieving saturation conditions, further primary pressure decreasing stagnates. During the next time period the course of the transient is determined by several overlapping occurrences:

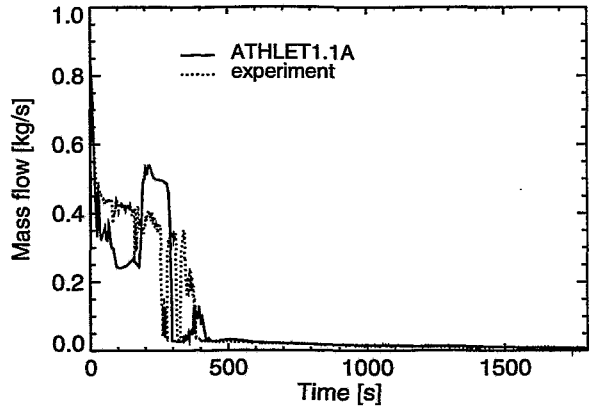

Fig. 6: Break mass flow (FL01)

Due to the pump coast down, the mass flow decreases. This induces enhanced flashing in the primary circuit. The pressure is increased and the core level LE11 is remarkably decreased (see Fig. 7). The exact modelling of the gradually closing pump valve has a large influence on the accuracy of the calculation. Difficulties arise, because during coast down steam and water flow through the pump. For the calculation of the pump behaviour under two phase conditions, no data were available.

The cold fluid, which is injected by the hydroaccumulators, induces condensation of the steam in the primary circuit and the pressure is decreased. There is a strong feedback, because the amount of the injected water is governed by the decreasing primary pressure.

Due to the continuing break mass flow the primary pressure decreases. During this time period the calculated break mass flow is something too low (see Fig. 6). The calculated mass flow depends not only on the applied discharge model, but also on the thermal-hydraulic conditions, particularly the void fraction and the liquid temperature, in the discharge volume. Difficulties in the calculation may arise, since the discharge volume on

the top of the downcomer is also influenced by the cold fluid from the hydroaccumulator and three-dimensional effects might play a growing role.

Phase 3: 160 - 400 sec

150 seconds after start of the pump coast down at about t = 160 s the bleed valve at the secondary steam generator is opened. Simultaneously the pump valve PV11 is completely closed and the bypass valve MV11 is opened. This causes a loop seal clearing in the hot leg (see the void fraction probe signals LV33 and LV41) and a sudden increase of the core collapsed level (LE11). From this time the primary pressure drops faster again and the accumulator injection is accelerated. During the next period the following processes are essential:

The continued steam production in the core blows the cold hydroaccumulator fluid towards the hot leg (counter current flow regime). This is shown by comparison of the void fraction signals LV21 and DE21 (see Fig. 4). In the hot leg the steam is condensed and the loop seal is refilled. After refilling of the hot leg loop seal the subcooled fluid is blown into the steam generator.

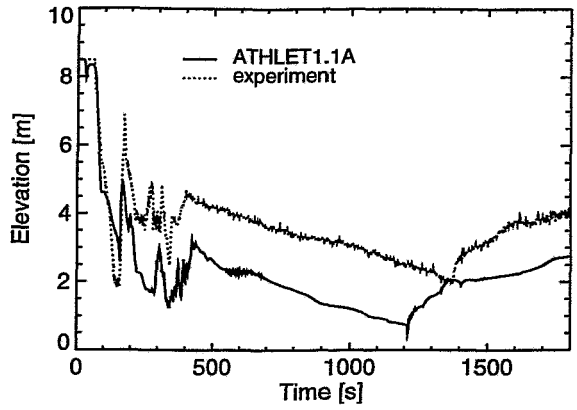

Fig. 7: Core collapsed level (LE11)

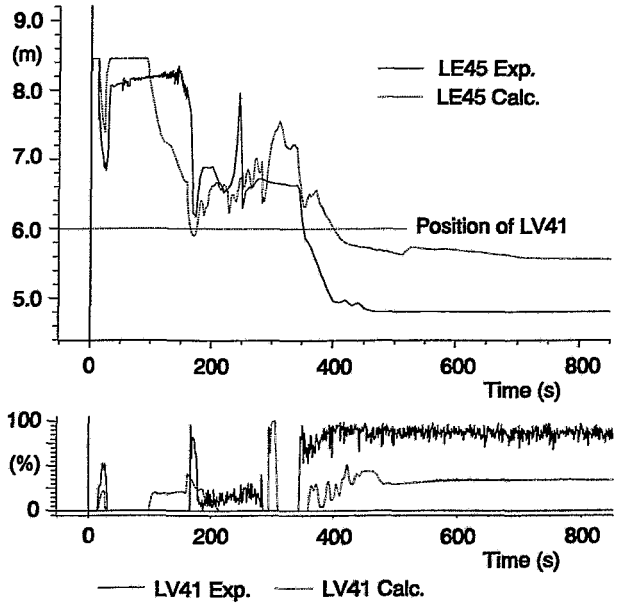

Fig. 8: Collapsed level (LE45) and void fraction in the hot leg

The cold fluid causes an inverted heat flux from the secondary to the primary circuit. For an appropriate calculation of these effects, a detailed model of the steam generator was used. The 82 primary U-tubes are modelled by four clusters. On the secondary side, fluid circulation is considered by appropriate modelling of a secondary riser and downcomer.

At t = 308 s the hydroaccumulators are depleted. Then the power transferred from the secondary side is too low for evaporation and the cold fluid is blown through the steam generator and refills the cold leg loop seal. In the next period the loop seals of the hot leg (t = 340 s) and of the cold leg (t = 385 s) are finally cleared (see void fraction probe signals LV41, LV51 and LV52 in Fig. 4, Fig. 8 and Fig. 9). At t = 400 s the natural circulation in the primary circuit is interrupted.

Phase 4: 400 - 1800 sec

From this time the core decay heat is removed only through the break flow. The collapsed levels in the core (LE11) and in the downcomer (LE61) decrease continuously. At t = 1125 s the cladding temperatures (TE15) of the rod simulator and the fluid temperature in the upper plenum (TE22) start to increase (see Fig. 10). At 1380 s the decreasing primary pressure initiates the low pressure injection. This stops the temperature excursion and refills the levels LE11 and LE61. At 1800 s the test was stopped.

4. Summary

The calculated results are in good agreement with the experiment. Deviations may be explained by strong feedback, which is difficult to predict (for example the pressure governed hydoaccumulator injection) and by limitations of the one-dimensional model (discharge volume). Using the void fraction probe signals it could be shown, that some collapsed levels in later time periods are measured something too high (e.g. for the core collapsed level LE11). The void fraction probe signals yield valuable information for deeper understanding of the thermalhydraulic occurrences and for code validation.

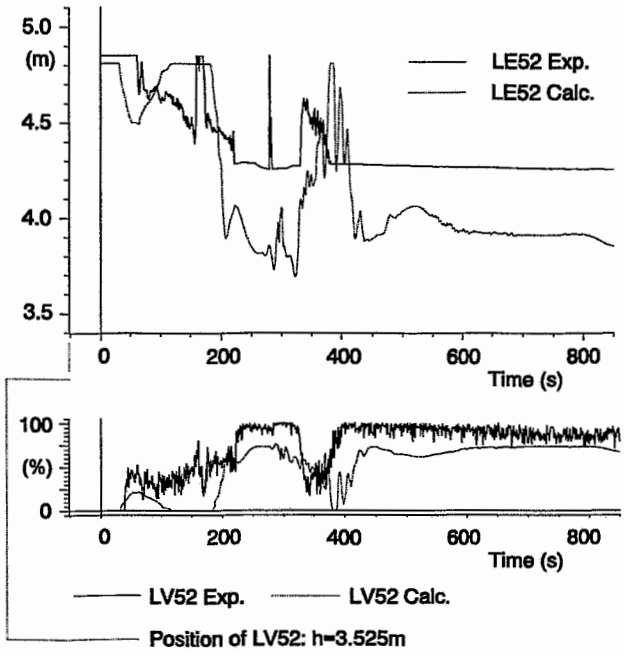

Fig. 9: Collapsed level (LE52) and void fraction (LV52) in the cold leg

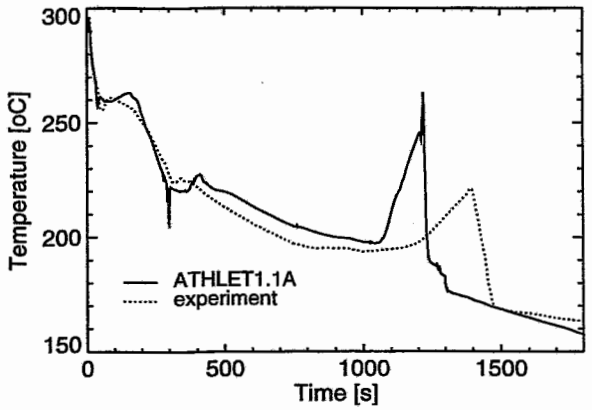

Fig. 10: Temperature in the upper plenum (TE22)

ULTRASONIC TWO-PHASE FLOW MEASUREMENTS BASED ON PATTERN RECOGNITION TECHNIQUES

H.-M. Prasser, F. Hensel, N. Kossok, P. Schütz

1. Basic idea

The idea of using ultrasound for measurement purposes in the field of two-phase flow is promising because of its nonintrusive capability. The state-of-art is characterised by a number of different approaches, which are commonly based on the identification and characterisation of individual voids (bubbles, plugs etc.) applying the techniques of ultrasonic testing and Doppler measurements. The recorded individual events are summarized in order to extract integral flow parameters such as void fraction or flow rates. Unfortunately, an evaluation of individual gas particles is restricted to very low void fractions or to a simple flow structure. Higher void fractions lead to the superposition of the signals produced by the individual voids, which makes it more and more difficult to identify individual particles. Another difficulty arises from the need to apply high frequencies of ultrasound, if small bubbles have to be detected. At these frequencies the sound beam behaves quasi-optically. That means, due to multiple reflection the two-phase mixture soon becomes nontransparent when the void fraction increases.

The main idea of the present work was to overcome these limitations by means of pattern recognition. An ultrasonic beam is modulated by the changing structure of the voids, when they are crossing the beam. Even if there is no model to describe the nature of the resulting signal fluctuations, pattern recognition methods applied on the through-transmission signal ought to be able to identify cases of similar flow structure within certain limitations. The limitations depend on the quality of the pattern recognition method and above all on the significance of the feature vector.

One has to keep in mind that a similar structure of the two-phase flow and therefore a similarity between two through-transmission signals can only be considered if the volume flow densities and the physical properties of both phases, as well as the geometrical and thermal boundary conditions, are kept equal or at least similar. If we restrict to pipe flow, the determining geometrical factors are the inner

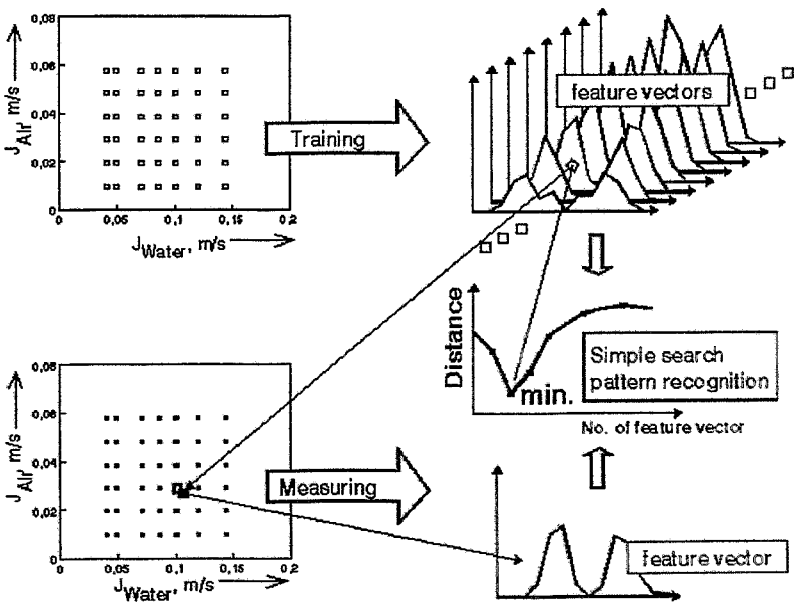

Fig. 1 Determination of the volume flow rates of gas and liquid by pattern recognition methods

diameter, the inclination of the pipe and the distance from the pipe inlet (inlet length).

The determination of the volume flow rates of gas and liquid seems to be feasible if all the other determining factors are equal. The idea was to train a pattern recognition algorithm with the signals recorded at a pipe section and obtained for a matrix of well known volume flow densities. The values of the volume flow densities have to be assigned to the feature vectors stored during the training phase. The classification of a signal recorded at unknown volume flow densities (but otherwise equal conditions) by the trained pattern recognition algorithm ought to restore the volume flow rate couple belonging to the present flow situation (Fig. 1).

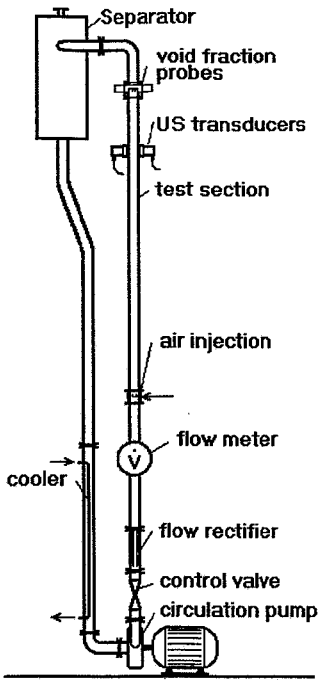

Fig. 2 Experimental air-water loop

Due to the stochastic nature of the through-transmission signal and the presence of disturbances the identification of similarities cannot be achieved by comparing the signals themselves. The comparison has to be carried out on the level of feature vectors calculated from the signal pattern. The components of the feature vector can be created in many different ways. Often statistical methods are applied as for example the calculation of moments of the probability density distribution or different Fourier transform techniques. There is no uniform theory about the optimal choice of pattern extraction methods so that the best method has often to be found experimentally.

As an example for the investigated methods, the results presented below were obtained by so called polar feature extraction methods. The components of the pattern vector are calculated from the probability density distribution $H(\Delta t_E)$ of the time intervals Δt_E between two successive extrema of the signal. An important advantage of this method consists in the independence on the amplitude of the signal. In this way the influence of the attenuation in the wall of the pipe and changes of the transfer coefficient of the instrument chain is suppressed. For more information, see [1].

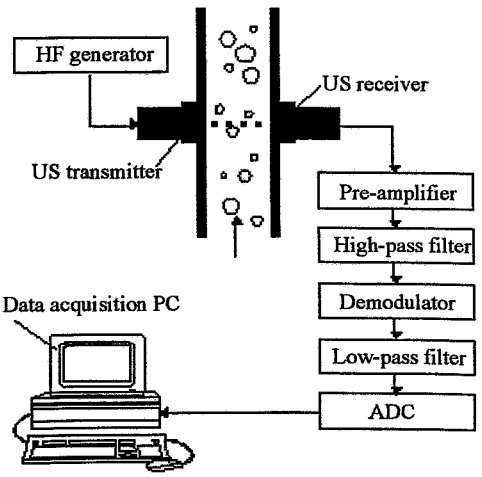

Fig. 3 Measurement chain for ultrasonic through-transmission

2. Experimental tests

The proposed method was tested in experiments that were carried out at a vertical tube section of a nonpressurized air-water driven test loop with an inner diameter of 51.2 mm (Fig. 2). The vertical test channel was made of stainless steel in order to study the influence of the ultrasonic coupling conditions.

The trough-transmission was carried out in a continuous mode at a comparatively low fre quency range from about 300 to 500 kHz in order to maintain the transparency of the two-phase flow at higher gas fractions. It can be realized with a comparatively simple measurement chain (Fig. 3), which is also an advantage of the method. Two ultrasonic transducers (transmitter and receiver) were clamped on at opposite sides of the pipe.

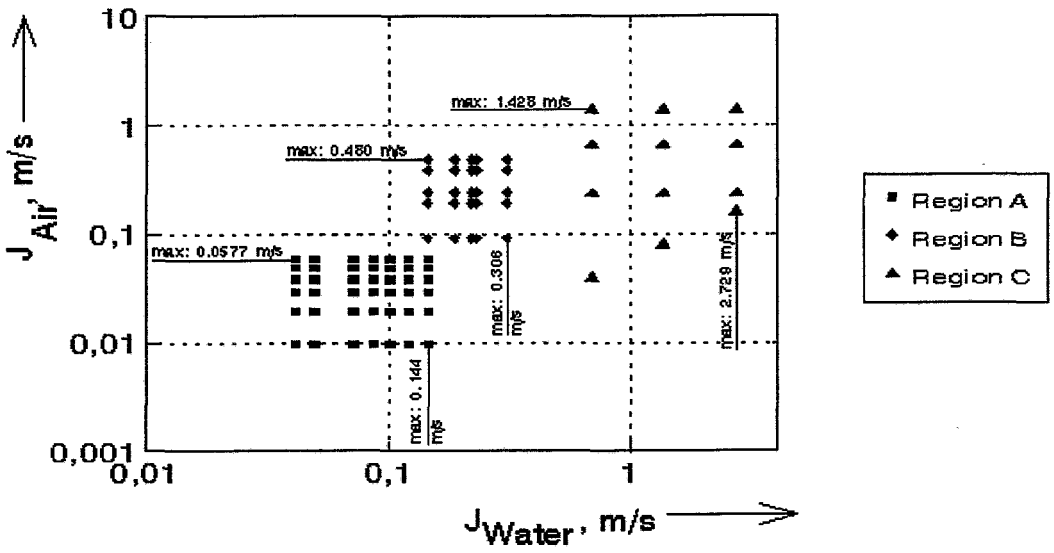

Fig. 4 Matrix of volume flow rate couples of test points

Fig. 4 shows the matrix of test points realized at the loop. The signal for each volume rate couple was recorded several times under constant conditions. One of these samples was used to train the pattern recognition algorithm, while in the classification phase all the obtained signals were treated to be connected with "unknown" flow parameters. They were used to check the reliability of the pattern recognition. The signal was sampled with a frequency of 2 kHz over a 10s interval. In order to proof the sensitivity of the method to the variation of both, water and air volume flow density, the points were placed in a two-dimensional grid.

The points were grouped in three regions. Bubble flow with beginning transition to plug flow dominated in region A. Region B is characterised as fully developed plug flow. In region C again a transition from bubble to plug flow takes place, but at significantly higher water velocities. The regions A and B were partially realized in natural circulation mode.

In Fig. 5 the result of classification of the test points in region A is presented in general.

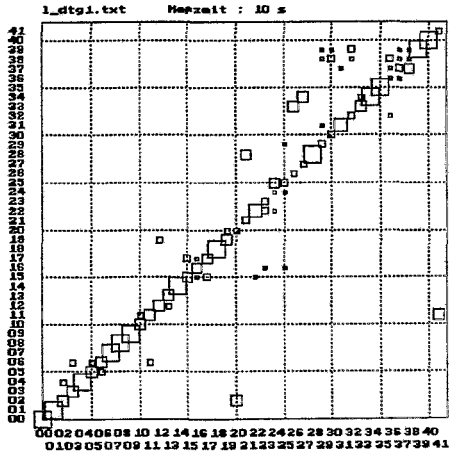

Fig. 5 Result of the classification of region A, $t_{meas} = 10$ s

x-axis: no. of given test point
y-axis: no. of identified test point
magnitude of boxes: number of identified test points

Obviously, the reliability of the pattern recognition is good. The majority of the test points is classified correctly and is therefore placed on the diagonal of the diagram or at least in the neighbourhood of the diagonal.

The influence of the measuring time was studied by dividing the recorded signals into parts. The fragments were subjected to the pattern recognition algorithm. It was found that the reliability of the classification is still quite good. This is illustrated in Fig. 6 by the number of correctly identified test points calculated over all three regions (A-C). The result of over 60% of well-classified points at a measuring time of 10s is satisfying. The fact that the majority of the wrong classifications identified points in the immediate vicinity of the correct points makes the result even more promising. A detailed analysis of the attainable measurement accuracy was published in [1].

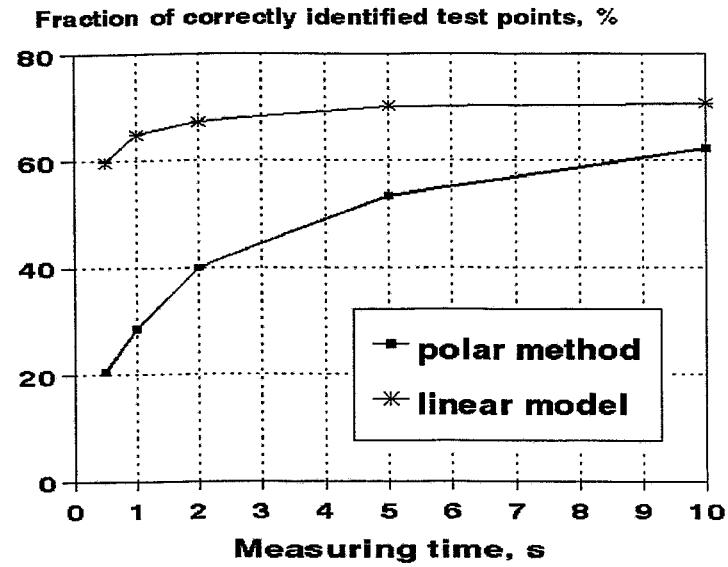

Fig. 6 Number of correctly classified test points over all regions (A-C) of the test matrix

Presently, the work is directed at the identification of optimal feature extraction methods. One of the approaches investigated is the application of a linear prediction model, where the prediction coefficients are used as the components of the feature vector. Preliminary results have shown that the reliability of the classification at a measuring period of 10s is at least as high as in the case of the polar methods, but remains high, when the measuring period is reduced to 1s.

3. Conclusions

The developed method provides an acceptable accuracy for practical applications. Even identifications in transient flow situations seem to be possible. Promissing impulses come from the application of linear prediction models. The universality of the pattern recognition method seems to guarantee the applicability to other two-component or two-phase systems. Nevertheless, in the present state of the investigations transferabillity of pattern vectors to other two-component systems is an open question. The work will be continued.

References

[1] H.-M. Prasser, F. Hensel, P. Schütz
"Ultrasonic two-phase flow measurements based on pattern recognition techniques"
XIII IMEKO world congress, Torino, 5-9 Sept. 1994, proc. vol. 2, pp. 1112-1117.

The project this report is based on is funded by the BMBF (Bundesministerium für Bildung, Wissenschaft, Forschung und Technologie) and is registered with No. 1500967. The authors are responsible for the scientific content of the report.

EMERGENCY VENTING OF PRESSURE VESSELS

H. Steinkamp

1. Introduction

The runaway of exothermal chemical batch reactions may under unfavorable conditions result in uncontrolled releases of toxic, funable and explosive substances. By a runaway exothermal reaction or unintentional external heating the temperature in the pressure vessel increases. In order to prevent an overpressure in the vessel and so damaging of the equipment most chemical reactors, storage tanks and other process vessels are equipped with a rupture disc or an emergency relief valve. The pressure reliefs or safety valves have to be designed for a flow rate, which guarantees that no inadmissible pressure increase occurs in the vessel. So the vessel can be vented through the safety device at a sufficiently high rate to compensate the rate of pressurization. The vented toxic or explosive substances have to be collected in a retention system.

2. Phenomena during depressurization

During emergency venting of a pressure vessel complicated thermodynamic and fluid-dynamic processes take place [1]. Normally the vessel is partially filled with a saturated liquid or completely with a vapour-liquid mixture. The gaseous and the liquid phase are in thermodynamic equilibrium. When the vessel is depressurized, first vapour enters the relief device. This causes a rapid decrease of the pressure in the vessel as to be seen in Fig. 1 [2]. Thermodynamic non-equilibrium occurs between liquid and vapour. By flashing evaporation and phase separation in the superheated liquid, bubbles of vapour are generated. They rise in the liquid and disengage at the surface. Whilst the bubbles remain in the liquid during fast depressurizatio n, they cause an increase of the liquid level. As the mixture level can rise up to the vent, two-phase flow may enter the relief device. The flow behaviour of the two-phase mixture through the relief device differs from that

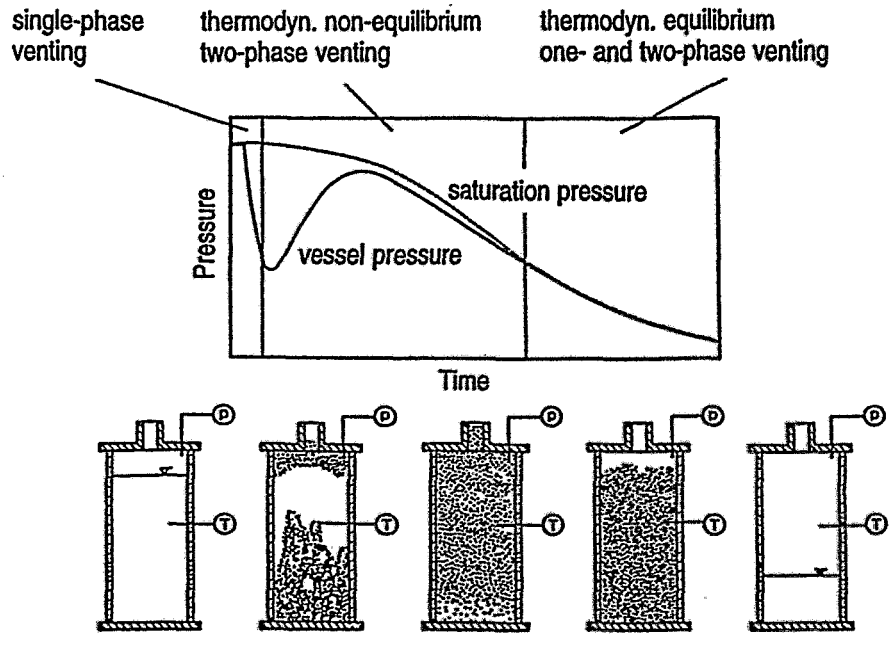

Fig. 1 Hydrodynamic processes during energency venting

of the single-phase. It is strongly de- pendent on the amount of liquid carried in the gas or vapour flow. The composition of the two-phase mixture influences the pressure drop and the maximum flow rate through the valve, the so-called critical flow. The volumetric flow rate of the released two-phase mixture can be smaller than the volumetric flow rate of vapour produced in the vessel. For this reason the pressure may even recover for a short period. By vaporization thermodynamic equilibrium between vapour and liquid is reached again. The venting causes the decrease of mass in the vessel and so the decrease of the mixture level. The depressurization process ends with single-phase vapour venting.

3. Codes for modelling emergency venting

In order to describe the thermo- and fluiddynamic processes during depressurization experimental and theoretical investigations are carried out. The investigations are aiming to model the venting process and to determine the necessary size of the relief vent. Therefore, several numerical models can be used, which are suitable for the analysis of venting transients. In order to compare different models Skouloudis [3] made a benchmark exercise focused on the hydrodynamic aspects of the venting of non-reacting fluids. The experimental data, which were analysed in this benchmark, were carried out at different plants. From the codes applied to analyse the benchmark data the discussion below only refers to the results obtained with RELAP and VESSEL. In order to compare these codes with the code ATHLET calculations are carried out for certain experiments. The codes use different types of two-phase flow models. They dispose of closure relationships, which depend on the flow pattern of the two-phase mixture, but relate the two-phase flow parameters to each other through the mass, momentum and energy conservation equations in different ways.

RELAP and ATHLET are developed to assess the safety of nuclear installations. Based on a one-dimensional approach they describe transient single- and two-phase flow regimes in complex vessel and pipe systems. The non-homogeneous non-equilibrium model for the two-phase system is mapped as system of ordinary differential equations. RELAP5 is developed by the Idaho National Engineering Laboratory (INEL) for the U.S. Nuclear Regulatory Commision (NRC). RELAP5/Mod1 uses separate mass and momentum equations for the individual phase to treat two-phase flow conditions. Due to the assumption that the dominating phase always saturates the minor one, only one energy equation is needed for the two-phase mixture. The selected approach can describe conditions of non-homogeneous flow with different velocities of both phases and thermal non-equilibrium effects during evaporation and condensation. The code includes the description of one-dimensional heat conduction in the vessel wall and the heat transfer between the solid vessel wall and the fluid.

The system code ATHLET is developed by the German Gesellschaft für Anlagen- und Reaktorsicherheit (GRS) for best-estimate analysis in reactor safety [4]. The realistic simulation of two-phase flow and heat transfer phenomena requires detailed models and comprehensive description of the reactor cooling system. The version of the code applied here is built on the five equations thermodynamic non-equilibrium model. There is one mass and one energy equation for each phase, but only one momentum equation for the two-phase mixture. The velocity difference between the two phases is determined by a full-range drift-flux model. Within the non-homogeneous control volume a mixture level is modelled. Above the mixture level a droplet layer is assumed, below the mixture level vapour is modelled as single bubbles surrounded by the liquid.

The code VESSEL is under development at the Joint Research Centre (JRC) Ispra. As used for the benchmark, the pressure vessel can be discretized into several control volumes with a single control volume for the vent line. VESSEL is capable of handling chemical reactions of arbitrary order and can describe the vent line hydrodynamics. External heat transfer through the vessel and the vent line can also be included. Thermal equilibrium has been assumed between the phases. The pressure drop in the vessel due to friction and acceleration forces is neglected. A drift-flux constitutive law relates the momentum of the second phase. The kinetic energy and axial conduction terms in the energy equation are also assumed to be negligible. The mass flow in the vent line is modelled in a simplified manner, taking into account blowdown experiments which were performed at the JRC. The mass flow in both the supercritical and subcritical regions is approximated similar to the gas dynamic theory.

4. Experimental Set-up

The aim of the experimental tests chosen for the benchmark is to describe the phenomena and to demonstrate the importance of some of the parameters related to the venting. The data were generated in depressurization experiments of different liquids without any chemical reaction taken place in the vessel. The experiment this paper refers to was performed in a 280l pressure vessel shown in Fig. 2 [3]. The height of the vessel used in this experiments is 4.27m, the diameter is 0.30m. The diameter of the blow-down orifice is 13mm. Before starting the experiments the vessel was filled with demineralized water up to nearly two-thirds of its height and boiled at atmospheric pressure for 30 minutes to free the supply water from any dissolved gas. The vent on top of the vessel was then closed and the water was heated up to the starting conditions at 385°C and 7MPa. Blow-down was initiated by opening the valve.

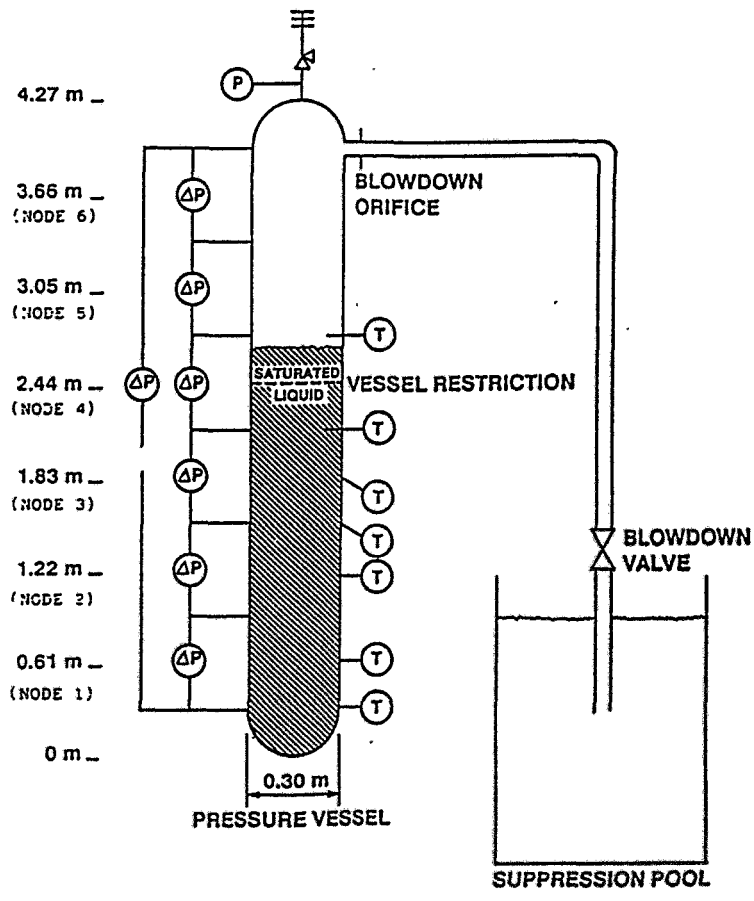

Fig. 2 Experimental set-up

5. Results

In Fig. 3 the measured and calculated pressure in the vessel is shown. The pressure drop in the vessel is measured by the pressure transducer placed on top of the vessel. As mentioned before the pressure in the vessel decreases rapidly after opening the valve. The comparison of experimental and calculated data show that the pressure decrease is almost perfectly described by the code VESSEL. RELAP and ATHLET provide to low values. The high accuracy of the data calculated by VESSEL is due to the consideration of initial void fraction in the vessel.

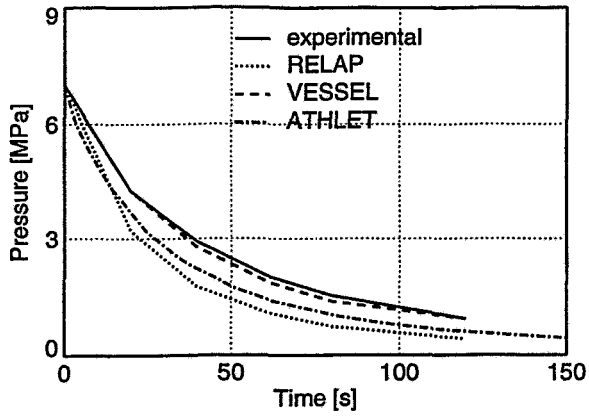

Fig. 3 Time dependent pressure in the vessel

As shown in Fig. 4 the mixture level in the vessel does not reach the relief valve placed on top of the vessel at 4.27m. During depressurization only vapour is vented out of the vessel. The evaporation starts with opening the relief. After about 5s the mixture level has reached its maximum and then decreases continously.

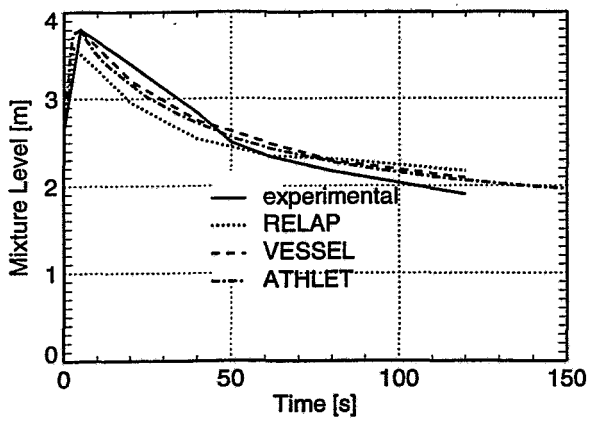

Fig. 4 Time dependent mixture level in the vessel

In Fig. 5 the measured void fraction in different levels of the vessel are compared with ATHLET results. For the calculation with ATHLET the vessel is discretized into six equal sized nodes beginning at the bottom of the vessel (see Fig. 2). In node 2 the initial void fraction is zero and rises up to 30% for both the experiment and the calculation. Node 4 is the volume directly below the initial water level. Due to the rising mixture level the void fraction in this node increases up to 40%. As a consequent of

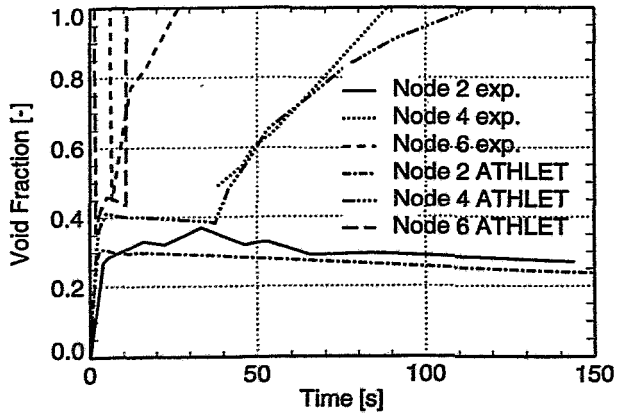

Fig. 5 Time dependent void fraction in different heights of the vessel

the water losses during venting the final level is decreased below of node 4 and there is pure vapour in that node at the end of the experiment. Node 6 already contains vapour at the beginnig. Due to the rising mixture level the void fraction decreases to 45% for a short period.

6. Conclusions

Depressurization through safety and pressure relief valves has gained increasing interest in safety stategies for chemical plants. To prevent runaway reactions the apparatus have to be equipped with safety reliefs. The layout of the venting equipment requires reliable and precise data of the fluid- and thermodynamic processes during depressurization. With the numerical codes developed for safety analysis the venting of steam vessel can be simulated. ATHLET especially is able to predict the void fraction depending on the vessel height. Although these codes contain a one-dimensional model they allow the description of complex geometries due to the detailed nodalization of the considered apparatus. In chemical reactors, however, the venting process is not only influenced by the flashing behaviour but additionally by the running chemical reaction in the vessel. Therefore the codes used for modelling have to consider the kinetics of the chemical reaction. Further multi-component systems and dissolving processes have to be regarded. In order to predict the fluid- and thermodynamic process it could be helpful to use 3-dimensional codes in combination with the one-dimensional codes as used in nuclear industry to get a more detailed describtion of the running processes.

[1] F. Mayinger
"Two-Phase Flow Phenomena with Depressurization - Consequences for the Design and Layout of Safety and Pressure Relief Valves"
Chem. Eng. Process 23(1988)1/11

[2] F. Hardekopf
"Zweiphasenströmung infolge der Druckentlastung eines chemischen Reaktors"
Dissertation, Hannover 1988

[3] A.N. Skouloudis
"Fifteen Benchmark Exercises on Vessel Depressurization "
EUR 12607 EN, 1990

[4] M.J. Burwell, G. Lerchl, J. Teschendorff, K. Wolfert
"The Thermohydraulic Code ATHLET for Analysis of PWR and BWR Systems"
Nureth 4, Karlsruhe, 1989, 2659/2669

BURNUP VERSION OF THE REACTOR CODE DYN3D

S. Mittag

1. Introduction

The three-dimensional nodal reactor core model DYN3D [1] developed in the Research Centre Rossendorf (RCR) is being used in several East European countries and the RCR itself for the simulation of reactivity initiated accidents (RIA). Progress and consequences of such an accident will be influenced by the actual burnup state of the reactor core. In order to enable DYN3D users to independently calculate three-dimensional burnup distributions for all possible states occuring during a reactor cycle, a burnup version of the code has been developed.

2. Burnup Calculation

As thermal power in a reactor is produced by nuclear fission, the reactor operation leads to a continuous loss, i. e. burning out of fissile material (fuel). Adding up the energy produced within a volume element (node) up to the actual moment, and dividing this energy quantity by the mass of the uranium that was originally present within the node yields the so-called nodal burnup value. Thus, the measure of burnup is MWd/kgU (megawatt days per kilogramme uranium). During reactor operation, more and more U-235 nuclei are burnt and replaced by their fission products. Furthermore, other nuclei are converted by reaction with neutrons; especially neutron capture by U-238 produces plutonium, which on its part is burnt by fission. The continuous production and destruction of different nuclei causes a strong dependence of the macroscopic neutron group data (cross sections and diffusion coefficients) on burnup.

In the stationary part of the DYN3D code, the power density is calculated by solving the neutron diffusion equation for a given material distribution within the core. Essentially, the extension of DYN3D to a burnup version is done by putting a burnup loop around the stationary kernel of the code, in which the nodal fluxes and temperatures are calculated. Starting point of the loop is a given material and burnup distribution reflecting the reactor core operational history which may include previous fuel cycles. For the given state, the code generates the actual burnup-specific nodal group data using the special macroscopic neutron group data library MAGRU [2]. Next, the nodal distributions of neutron flux, power density, fuel temperature, coolant density and concentrations of the reactor poisons xenon and samarium (fission products) are calculated by an iteration which includes temperature feedback. The calculation of the critical boron acid concentration is also part of the iteration process which finally leads to a stationary core state. The nodal power densities are assumed to be constant for a certain time interval, in which the nodal burnup values increase only little, compared to their increase during a whole reactor cycle. For this burnup time-step interval, DYN3D calculates a burnup growth within each node using the stationary power densities. Now, a new group data distribution belonging to the updated nodal burnup values is derived for the next time step. In this way, the burnup calculation proceeds step by step until the end of cycle, or an otherwise interesting burnup state is reached, which then can be studied by dynamic DYN3D calculations.

During the whole operation period of a reactor, the material distribution within the core is often modified, for example by changing the positions of partially burnt-out fuel elements, by putting in new ones, and also by control rod movements. All these manipulations as well as changes in total power are modelled by special routines and can easily be controlled by additional input data. Modelling the nodal material and burnup distributions is somewhat complicated in the case of VVER-440 because of the special construction of its control rods. In fact, there are no rods, as usually used in Western type reactors, but absorbing assemblies which have the same hexagonal shape and length as fuel elements. They are followed by real fuel elements which are attached to the absorbers bottom by a coupling part. "Changing control rod positions" in case of VVER-440 means moving such assemblies along the vertical axis. The axial burnup distribution of a fuel follower is moved up or down during "control rod movements". All these special features are taken into account in the DYN3D burnup version.

3. Application of the Burnup Code to VVER-440

The burnup version was tested by participating in the benchmark problem on control rod worth of a VVER-440 in Paks (Hungary) [3]. The problem has been defined in the frame of the Atomic Energy Research (AER) association on VVER physics. As rod worth is a measure of how control rods influence reactivity, i. e. the neutron balance of the reactor core, it depends on the burnup distribution. In the AER problem, the starting burnup distribution was given for the end of the 3rd cycle of Paks unit 2. Starting from this point, the burnup progress had to be calculated through the cycles 4 to 7 using the corresponding shuffle schemes (reloading of fuel elements) and operational histories provided by the utility. Finally the different rod efficiencies had to be calculated for the beginning and the end of the 7th cycle.

The burnup distributions obtained by DYN3D for cycle 7 were compared with reference results provided by Paks. The maximum relative deviations in burnup are less then 5 %, absolute differences are not greater then some 0.5 MWd/kgU. Fig. 1 shows the comparison of fuel element burnup values at the end of the cycle for a 60-degree symmetry sector of the core. The greatest relative deviations are observed at the core boundaries, which may be caused by different boundary treatment in DYN3D and the burnup code used in Paks. In Fig. 1 the fuel elements marked by thick lines are fuel followers of control assemblies. The elements number 1, the central one, and number 7 belong to the 6th control rod group which is

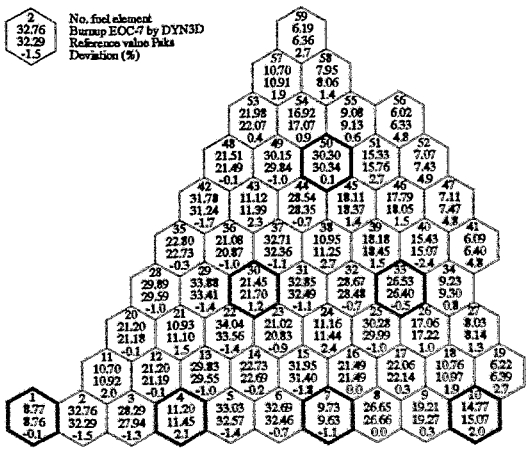

Fig. 1: Burnup distribution in MWd/kgU of Paks-2, end of cycle 7

mainly used for reactor control.

The group differential rod efficiency, calculated by the benchmark participants for the beginning of cycle 7 (BOC-7) and zero power [4], is compared to measured values in Fig. 2. Differential efficiency means the change of reactivity caused by rod movement divided by the (differential) control rod shift. It sensitively depends on the group position. The position of 0 cm means that the absorbing part is fully dived in; in the case of 250 cm the fuel follower is inserted in its total length. Generally DYN3D provides a rather satisfying description of the measured data; in middle-range positions, all applied codes underestimate the experiment.

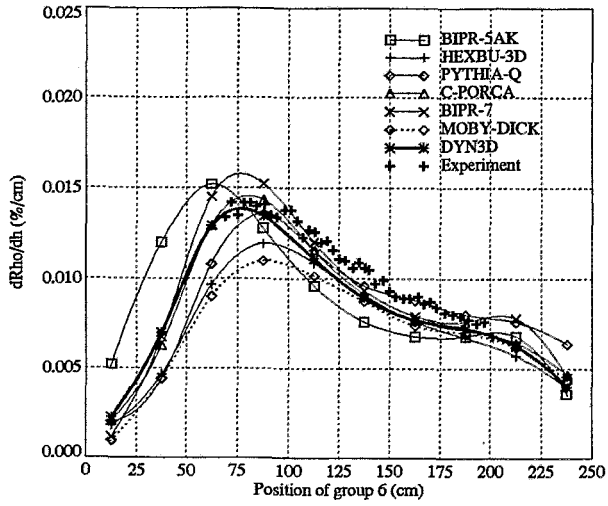

Fig. 2: Differential rod efficiency of group 6, BOC

Fig. 3 shows corresponding results for the end of cycle (EOC-7). Comparing Figs. 2 and 3, it is interesting to observe, how the burnup during cycle 7 affects differential rod efficiency. Especially, the increase in the upper region of rod positions (160...220 cm) is caused by the fuel followers. For 280 days about 60 cm of the fuel followers were not dived-in but were below the core bottom. Only during the last 26 days they were run-up step by step, shifting out the absorbing parts. As the followers contained fresh fuel at the beginning of the cycle, their lower parts (60 cm) were not burnt-up even at EOC-7. Thus, moving these parts into the core would lead to considerable reactivity increase.

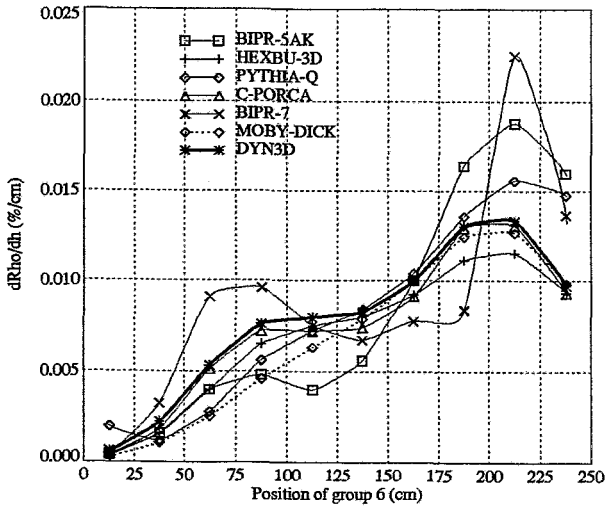

Fig. 3: Differential rod efficiency, group 6, EOC

Furthermore model calculations [4] proved that neglecting the presence of the coupling part (and steel pellets in the follower top) would result in too high peaks in differential efficiencies for upper rod positions (Fig. 4).

4. Conclusions

The AER benchmark test shows the qualification of DYN3D for burnup calcula-tions. Obviously the group data used in the calculations strongly influence the results. The application of different neutron diffusion codes and different group data libraries by the benchmark participants will certainly be the cause of relatively high deviations in rod efficiencies. The results obtained up to now are not sufficient to clarify to what extent both the group data and the reactor codes are responsible for the deviations. Thus it would be useful to repeat the calculations applying the same data library in different codes, or alternatively using different data libraries with the same code. Therefore the link of another macroscopic group data library to DYN3D is under consideration.

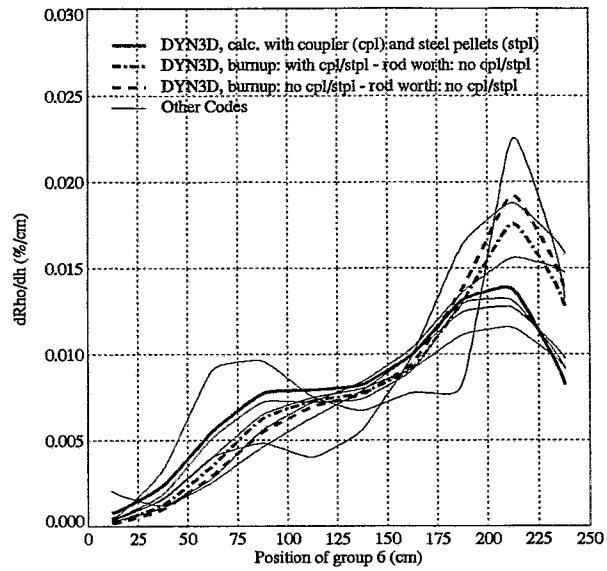

Fig. 4: Differential rod efficiency, group 6, EOC

5. References

[1] U. Grundmann and U. Rohde
"DYN3D/M2 - a Code for Calculation of Reactivity Transients in Cores with Hexagonal Geometry"
IAEA Technical Committee Meeting on Reactivity Initiated Accidents, Vienna, 1989
Report FZR 93-01

[2] G. Agthe und H.-J. Kretzschmar
"Zur automatisierten Bereitstellung neutronenphysikalischer Weniggruppen-parameter für die makroskopische Berechnung von Spaltzonen thermischer Reaktoren"
Kernenergie 33 (1990) 165-170 (Teil 1), 214-218 (Teil 2)

[3] L. Korpás et al.
"AER Benchmark Problem for Calculation of Control Rod Worth of VVER-440 Reactor"
Working Group B Meeting of AER, Pieštany (Slovak Republik), 1992

[4] S. Mittag
"Solution of AER Benchmark Problem on Control Rod Worth of Paks VVER-440 by the Code DYN3D"
4th Symposium of AER, Sozopol (Bulgaria), 1994

The project this report is based on is funded by the BMBF (Bundesministerium für Bildung, Wissenschaft, Forschung und Technologie) and is registered with No. 150 0925. The author is responsible for the scientific content of the report.

ULTRASONIC TIME-OF-FLIGHT DIFFRACTION METHOD FOR MONITORING STABLE CRACK GROWTH

Ute Bergmann, Frank Bergner[1]

1. Introduction

In the elasto-plastic fracture mechanics the resistance of a material against stable crack growth under monotonic loading is described in terms of the crack growth resistance curve (e.g. J-R curve) relating a crack field parameter (e.g. J integral) to the amount of stable crack growth needed in order to obtain J-R curves. The multiple specimen technique requires a set of identical specimens because the crack extension is measured at the fracture surfaces of broken specimens. Therefore each specimen provides a single value of crack extension only. The multiple specimen technique is the basis of existing fracture mechanics standards and the procedure is described there in detail. Single specimen techniques are, in principle, sufficient to obtain a J-R curve. According to the fracture mechanics standards, these methods are allowed as well, if the qualification criterion is fulfilled demanding an agreement of monitored crack extension with physical crack extension within 15 %.

In the past a number of ultrasonic techniques for monitoring stable crack growth in fracture mechanics tests have been investigated. The pulse-reflection or pulse-transmission technique relates the crack length to the amplitude of an ultrasonic pulse reflected at or passed in front of a crack face. Another phenomenon exploited for crack growth monitoring is diffraction at the crack tip. By scanning an ultrasonic transducer along the specimen and tracing the location of maximum amplitude of back diffraction, crack growth can be measured. In our mechanical testing laboratory a crack growth monitoring device based on the ultrasonic time-of-flight diffraction technique has been developed. It is intended to overcome some drawbacks or applicability limits of other methods. In particular, the method should be applicable for bend specimens as small as Charpy type ones or even smaller (plane strain conditions required) as these are preferred dimensions in special fields of fracture mechanics testing (e. g. neutron embrittlement of reactor pressure vessel steels, testing of single crystals).

2. Principle of crack growth monitoring

The measuring principle is based on the phenomenon of the crack-tip-diffraction of an ultrasonic wave. An incidenting longitudinal or transverse plane wave causes a diffracted wave field containing longitudinal and transverse waves in all directions as well as surface waves along the crack faces. A particular realization of this situation is illustrated in Fig.1. A transverse wave is directed onto the crack front by an angle beam transducer and the diffracted transverse wave is picked up by an identical transducer placed symmetrically with respect to the crack plane. If the transducers are assumed to be point-like and to be placed at a distance, x_0 from the crack plane, and if the specimen is not yet loaded in bending, the time of flight in the specimen, T_0-t_0, is a measure of the crack length, a.

[1]Dresden University of Technology, Institute for Material Science

$$a = \sqrt{[C_T \frac{(T_0 - t_0)}{2}]^2 - x_0^2}$$

C_T denotes the transverse wave velocity of the material, T_0 is the measured time of flight, and t_0 is the delay time of the transducers. If the specimen is bent (load point displacement, d), it has to be taken into account that the centre of rotation is shifted a distance, r(W-a), away from the crack tip. W-a is the uncracked ligament, and r is the rotational factor (r = 0.4).

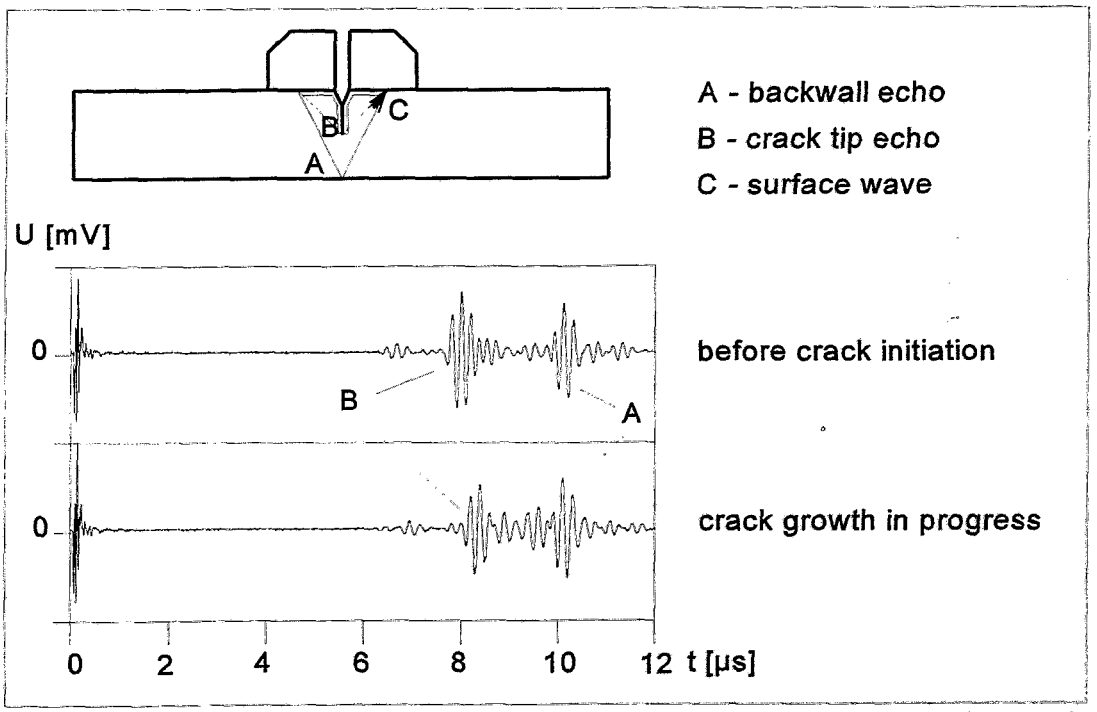

Fig.1 Principle of the time-of-flight diffraction method for stable crack growth monitoring, crack growth is calculated from the time of flight of echo B

The delay time of the transducers, the effective point of sound passage, and the sound velocity of the material have to be known for crack length measurements. They can be determined by calibration experiments using the fracture mechanics specimen without extensive instrumentation.

3. Apparatus and specimens

The computer controlled testing machine is equipped with a three-point bending device. A pulser/receiver together with a pair of 45° angle beam transducers working in the pulse-transmission mode were used in order to transmit and pick up the ultrasonic pulses. The received echo pulses were sampled and stored by means of a digital signal analyzer. This analyzer is connected with a personal computer via GPIB.
Specimens have been taken from two low-carbon low-alloy steels, StE 460 (0.1% C,

1,6%Mn) in the normalized condition and 10CrMo9.10 (0.1% C, 2.25% Cr, 1% Mo) in the quenched and tempered condition. Specimens of dimensions 10 x 10 x 55 mm containing 10% side grooves in order to hold the crack plane fixed were pre-cracked up to an overall depth of about 4 to 5 mm before testing.

4. Results

In Fig.2 the overall crack growth monitored by the ultrasonic method is compared with the crack extension measured by optical examination of the fracture surface. So far the measurements have been confined to crack lenghts in the range from 4 to 6 mm. Fig.2 shows that even for small load point displacements the agreement with physical crack extension is much better if the actual location of the center of rotation is taken into account, i.e. specimen bending cannot be ignored. In all cases the qualification criterion of 15% agreement is fulfilled.

This result has been achieved for rather small specimens without any changes of the specimen design. An important feature of the present technique is the location of the transducers at the crack-bonded surface of the specimen. Consequently, the tip-diffracted transverse wave is the first wave arriving at the receiver and the arrival time can be measured very precisely. Future work should include the extension of the method to other materials and specimen dimensions as well as the utilization of additional information hidden in both time-of-flight and amplitude of consecutive echoes.

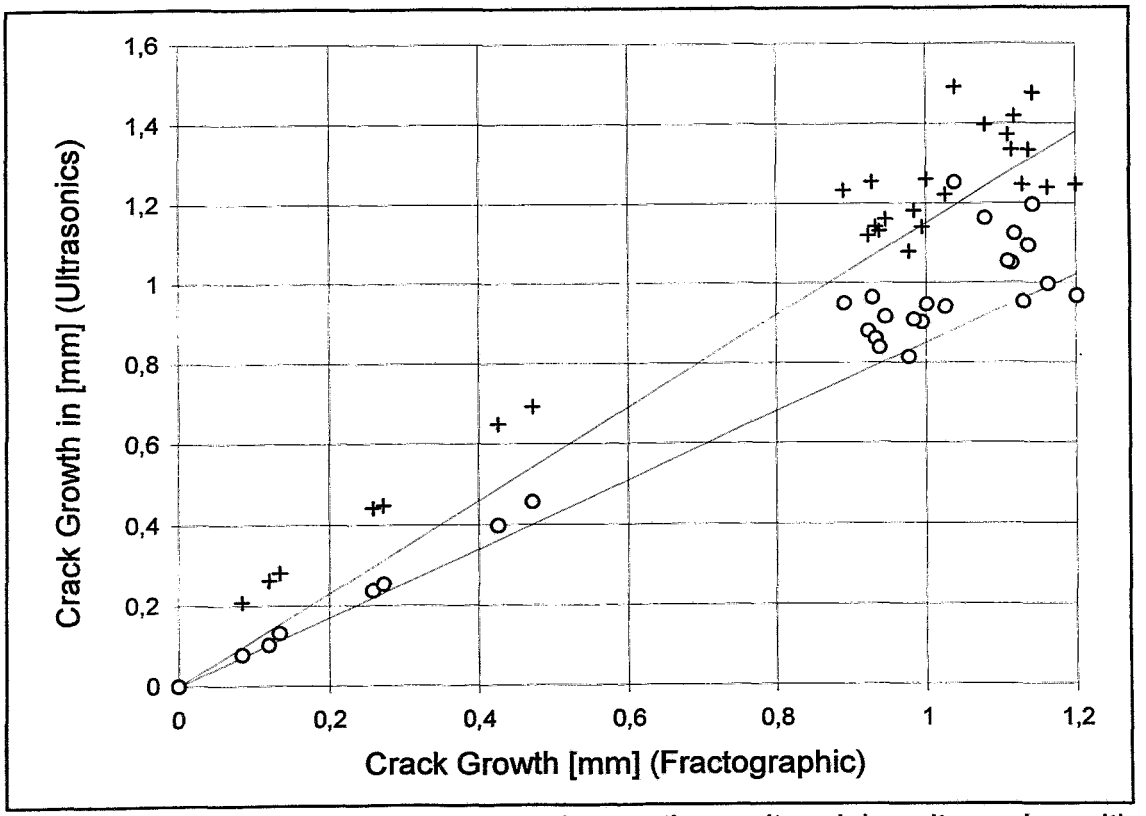

Fig. 2 Comparison of the overall crack growth monitored by ultrasonics with fractographic crack extension and qualification criterion (symbols: + ... specimen bending ignored, o ... location of the center of specimen rotation taken into account)

EVIDENCE AND CONSEQUENCES OF MECHANICAL PROPERTIES GRADIENTS OVER THE WALL OF A VVER-TYPE REACTOR PRESSURE VESSEL

J. Böhmert, M. Große, H.-W. Viehrig

1. Introduction

Reactor pressure vessels (RPV) are thick-walled components with a typical thickness of 150-300 mm. For components of such dimensions gradients of mechanical properties over the wall are inevitable. They can result from differences in the conditions of solidification, in the plastic deformation during the processing, or in the cooling rate by quenching from austenitizing temperature. Safety assessment has to evaluate the slope of these gradients and to consider the worst case of the safety-related parameters. That has especially to be taken into consideration if the deterioration of the mechanical properties during the reactor operation is additionally dependent on the depth position. Neutron embrittlement of the RPV steel and neutron flux attenuation over the RPV wall through self shielding cause such effect.

Within the framework of the US-American HSST programme the through-thickness dependence of the mechanical properties was intensively investigated for rolled plates and forgings of ASTM-type RPV steels. As a typical result it was observed that the strength parameters (yield stress, ultimate tensile stress, hardness) and the toughness parameters (Charpy V-impact energy, fracture toughness, reciprocal brittle-ductile transition temperature) strongly decrease from the surface to the one-quarter-thickness position and are quite constant over the central region of the wall. This course was attributed to the higher cooling rate of the surface region [1]. For VVER-type RPV steels, which have a significantly different design, there has not been yet a comparable investigation.

2. Experimental

The following materials were investigated in this study:

- 140 mm cladded forging segment of 15Kh2MFA steel (test plate with weld) produced in Russia (code: KAB-B, -W)
- 140 mm forging segment of 15Kh2MFAA steel originating from a Russian RPV-ring (code: KU-1)
- 150 mm forging segment of 15Kh2NMFAA steel originating from a Russian testing RPV-ring (code: KU-2)
- ASTM-type steels from the IAEA-CRP-Programme, Phase 3 (227 mm rolled plate A 533 B, cl. 1 - Code: JRQ; 290 mm forging, A508, cl. 3 - code: JFL).

The mechanical properties of specimens cut from different depth positions were determined using several mechanical testing methods (hardness measurements, tensile testing, quasi-static 3-point bending tests and Charpy-V impact testing). The differences of the microstructure were investigated by several structural analysis methods (for instance light microscopy, electron raster and transmission microscopy,

small angle scattering, X-ray diffraction, Auger electron spectroscopy). For the material KAB, irradiated specimens from two depth positions were available.

3. Results

Generally, the VVER-type RPV steels do not show the same through-thickness dependence of strength and toughness properties like the ASTM-type steels. Only the test plate KAB which was produced in the middle of the seventies and has a higher level of impurities (Cu, P, S) exhibits a trend according to the characteristic results in ref. [1]. As an example, the dependence of the yield stress and the transition temperature on the depth position is given in Figs. 1 and 2. The influence of the depth position of VVER-type steels is insignificant and does hardly exceed the scattering range of the results within a depth layer or in adjacent layers.

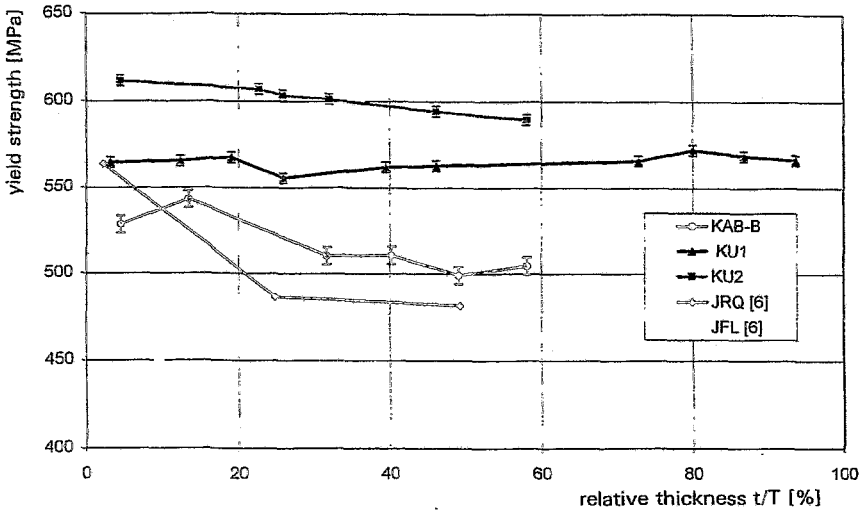

Fig. 1 Dependence of the yield strength on the depth for 15Kh2MFA (KAB, KU-1) 15Kh2NFMFA (KU-2) and ASTM-type steels (JFL, JRQ)

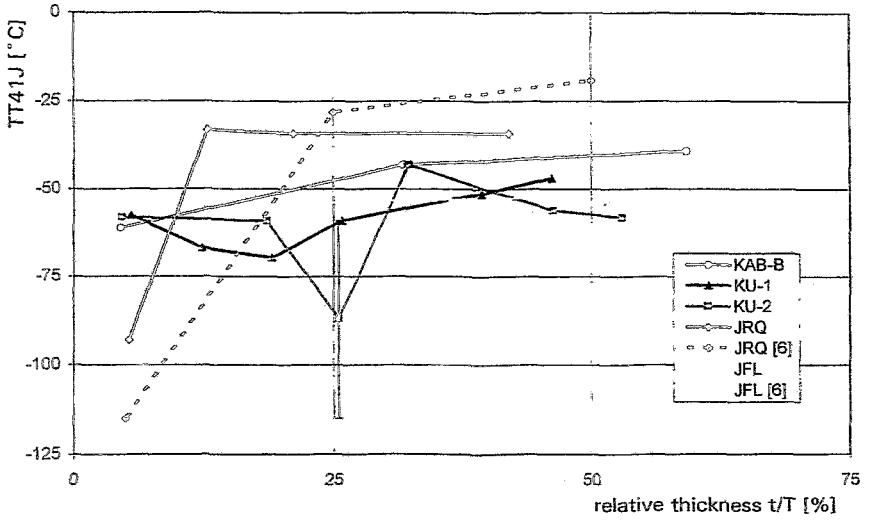

Fig. 2 Dependence of the transition temperature TT_{41J} on the depth for 15Kh2MFA (KAB-, KU-1) 15Kh2NFMFA (KU-2) and ASTM-type steel (JFL, JRQ)

Especially for heats with a lower impurity level (KU-1, KU-2), this is valid even under intensified testing conditions (using side grooved and fatigue cracked Charpy-V notch specimens) and in the brittle fracture temperature range. However, the one-quarter-position is not the position showing the most unfavourable toughness in all cases.

An unambiguous relation between the changes of the mechanical properties and the microstructure cannot be recognized. The microstructure possesses an evident structural hierarchy, as shown in Fig. 3. It is bainitic, consists of different portions of granular or lath-formed tempered bainite, partly also contains different content of pro-eutektoid ferrite. Preferably at the ferrite lath boundaries large carbides (0.2 μm) of the $M_{23}C_6$ type are precipitated. Finally, fine-dispersed vanadium-carbides (10-20nm) are arranged at dislocations within the bainitic ferrite. The type of bainite, the carbide arrangement, or the volume fraction and size of carbides vary in the same range as well for specimens from the same depth layer as for specimens from different layers. As an essential structural parameter that closely correlates to the depth dependence of strength and toughness the content of pro-eutectoid ferrite can be identified. Though the effect could not be analytically revealed, a change of the microdistribution of impurity elements or minor-alloying elements must be supposed. Irradiation and annealing do not particularly modify this through-thickness characteristic. Therefore, it seems that the main factor affecting toughness is the irradiation-induced structural change and, thus, changes between different depth position are not increased but rather decreased.

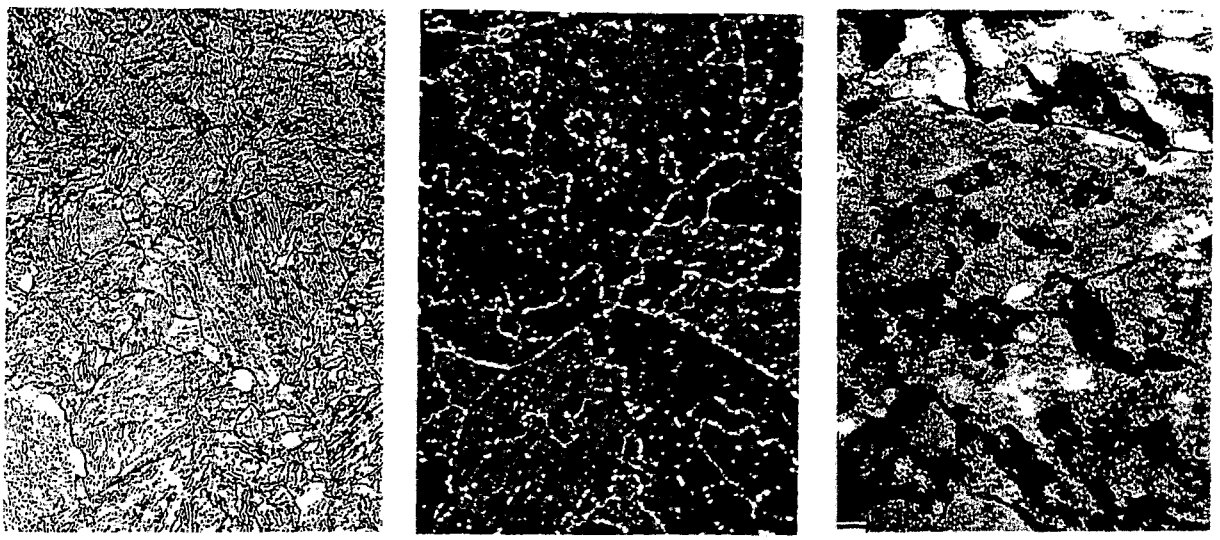

Fig. 3 Typical microstructure of 15Kh2MFA steel (materials: KAB)

4. Safety-related conclusion

The course of the transition temperature over the RPV wall after certain operation times (▲ level of fluence) can be estimated using the depth dependence of the transition temperature of the initial state, the irradiation susceptibility (which is weakly depth dependent), and the self-shielding of the RPV wall. For the Greifswald

typical material KAB the course is given in Fig. 4. In comparison to the behaviour of an ASTM-type steel which is illustrated on the base of results of the HSST programme [2] in Fig. 5, the VVER-type RPV steel does not show a characteristic maximum of the transition temperature near the one-quarter position that increases with the inner wall fluence. Instead the transition temperature weakly descends and, thus, the toughness ascends from inside to outside of the RPV. Therefore it can be concluded that a stable growing inside crack runs into an area of the wall with higher fracture toughness and can be stopped. In this respect, a negative gradient of the transition temperature, as can be seen in Fig. 4, can be assessed as safety-improving, especially under pressurized thermal shock conditions which are particularly critical. Basically, there are no safety-related objections against using one-quarter specimens within the framework of the surveillance programme. In the initial state the depth dependence of the transition temperature or the fracture toughness has to be examined and the most unfavourable position must be found out. Besides, the investigation of variations of the mechanical properties over the wall can be used for quality controling. In connection with a low influence of the specimens orientation a low depth dependence provides the proof of a high quality of the steel marked by a low content of impurities.

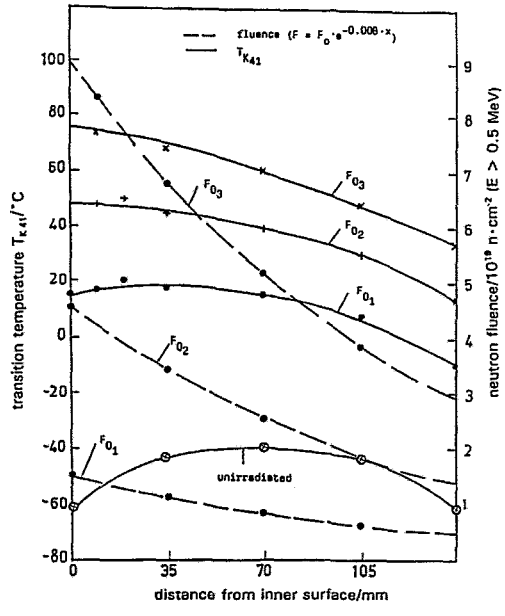

Fig. 4
Transition temperature TT_{41} over the wall of a VVER 440-type RPV, using results obtained from KAB material

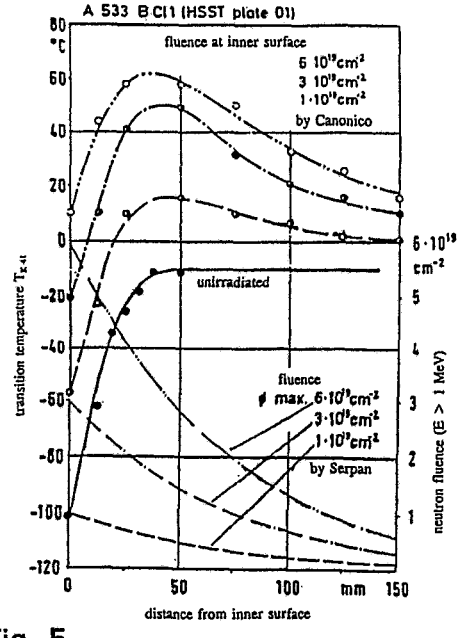

Fig. 5
Transition temperature over the wall of RPV, citation from Kußmaul [2]

References

[1] D.A. Canonico, Nucl. Eng. Des. 17 (1971) 149-160

[2] K. Kußmaul (ed.), Werkstoffe, Fertigung und Prüfung drucktragender Komponenten von Hochleistungsdampfkraftwerken, Vulkan-Verlag, Essen, 1981, p. 84

The project this report is based on is funded by the BMBF (Bundesministerium für Bildung, Wissenschaft, Forschung und Technologie) and is registered with No. 1500918. The authors are responsible for the scientific content of the report.

DETERMINATION OF THE DYNAMIC CRACK-INITIATION TOUGHNESS DURING INSTRUMENTED IMPACT TESTS FOR ELASTIC-PLASTIC MATERIAL BEHAVIOUR

H. Richter and H.-W. Viehrig

1. Introduction

From the fracture mechanical point of view crack-resistance curves (R-curves) are an important tool for the assessment of safety margins of materials with respect to fracture. On the one hand the shape of R-curves depends on the specimen geometry. That is why the test results can only be transfered to components in the framework of the ASTM validation requirements. On the other hand it was found that the crack initiation is a real material value which does not depend on the specimen geometry. According to this fact several methods were developed to determine crack initiation toughness. One of the accepted methods in fracture mechanics to obtain crack initiation toughness is the J-integral based on measurement of the stretch zone width (SZW) in front of the crack tip by using scanning electron microscopy (SEM) [1-6].

A central and still unsolved problem is the detection of crack initiation in the load displacement curves obtained through impact tests. In this case the detection of physical quantities connected with the process of stable crack initiation is necessary. There are only a few methods to detect the crack initiation under dynamic loading, as for instance the optical measurement of crack opening displacement [8] or crack tip stress field recording [1,3].

In this paper first experiments, performed with a special instrumentation for the simultaneous recording of impact force and emitted acoustic waves (AE) [7,12] are presented. Additionally magnetic (ME) and electric emissions (EE) were recorded during impact loading. Further fractographic investigations were accomplished to obtain information about the fracture processes [10-12].

The development of a method like this can be of interest for investigation and fracture mechanical characterisation of reactor pressure vessel (RPV) steels, especially if only a limited quantity of material is available.

2. Experimental

For the determination of loading parameters a pendulum impact tester with a maximum initial energy of 300 J was modified. The block diagramm in Fig.1 gives an overview of the experimental arrangement.

The pendulum is instrumented to measure the impact force according to recently recommended methods [13,14]. A supplementary measuring system was designed and installed to detect events produced by fracture of the specimen. For that a piezoelectric non-commercial AE-broadband sensor was placed within a drilled hole of the impact tup. The distance to the expected main AE source - the fatigue precracked

crack front- is 29 mm. The broadband sensor is connected with a 40dB/60dB preamplifier which includes a passive high pass filter to suppress low frequency noise.

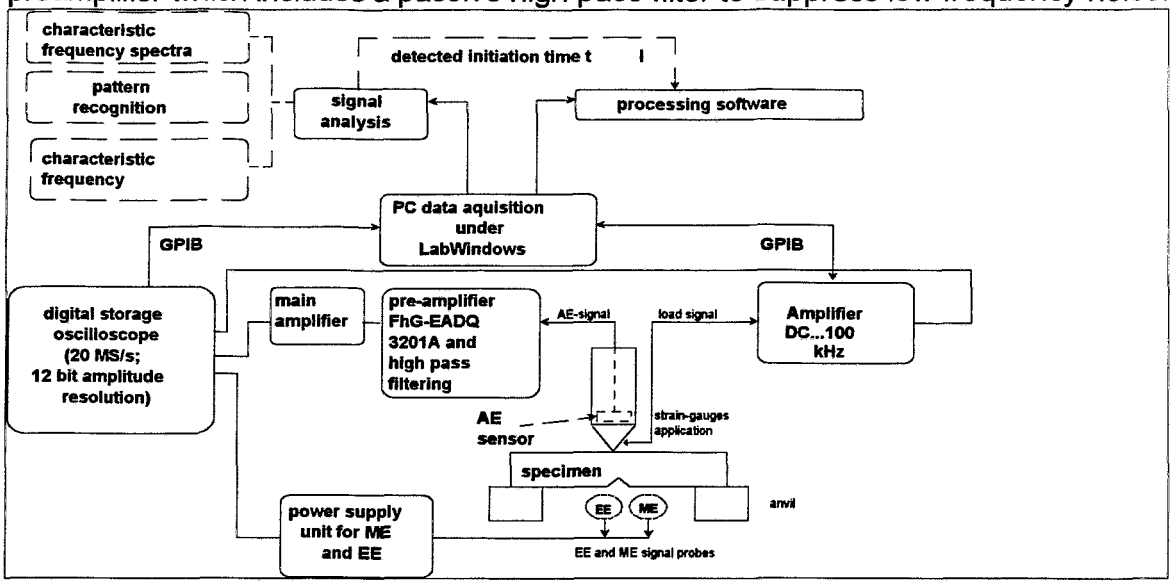

Fig.1: Block diagram of the special instrumentation

After main amplification the signals can be recorded with 20 MHz sampling rate on a digital storage oscilloscope (DSO). The sampling rate and the amplitude resolution should be appropriate to study even low energy fracture initiation events. The system was calibrated with ultrasonic shock waves.

The second sensor, a twin probe, is able to measure electric and magnetic field emissions associated with fast fracture processes. It is placed at a distance of 5 mm from the crack. The EE- and ME-signals are also stored by the DSO. The main parts of the arrangement are controlled through the GPIB interface of a PC. Conventional or fracture mechanical toughness values can immediately be computed by PC software. Moreover, the acquired signal can be subjected to a variety of standard signal analysis procedures. So, typical fracture events can be characterised in time and frequency domain.

3. Test Material

material	heat resistant structural steel 10CrMo9.10 (DIN)
chemical compo-	C: 0.06-0.15; Si: ≤0.50; Mn: 0.40-0.70; P: 0.035; S: 0.030; Cr:
microstructure	ferritic-bainitic
specimen design	Charpy-V, 20% sidegrooved, pre-fatigued to $a_0/W=0.5$, CVN_{ps}
specimen and	T-L from rolled plate with 12 mm thickness,
impact properties	USE = 250 J ; $T_{68\,J}$ = - 45 °C

Table 1: Characterization of test material

The material which was used in the tests has strength and toughness properties that are similar to those of real RPV steel. Fracture mechanical CHARPY-type single ended notch bending specimens [SEN(B)] were machined from a commercial heat resistant steel with the specimen axis perpendicular and the crack growth direction parallel to the rolling direction of the plate. Some material properties are shown in table 1.

4. Results

A typical load curve with associated AE obtained at room temperature and for an initial

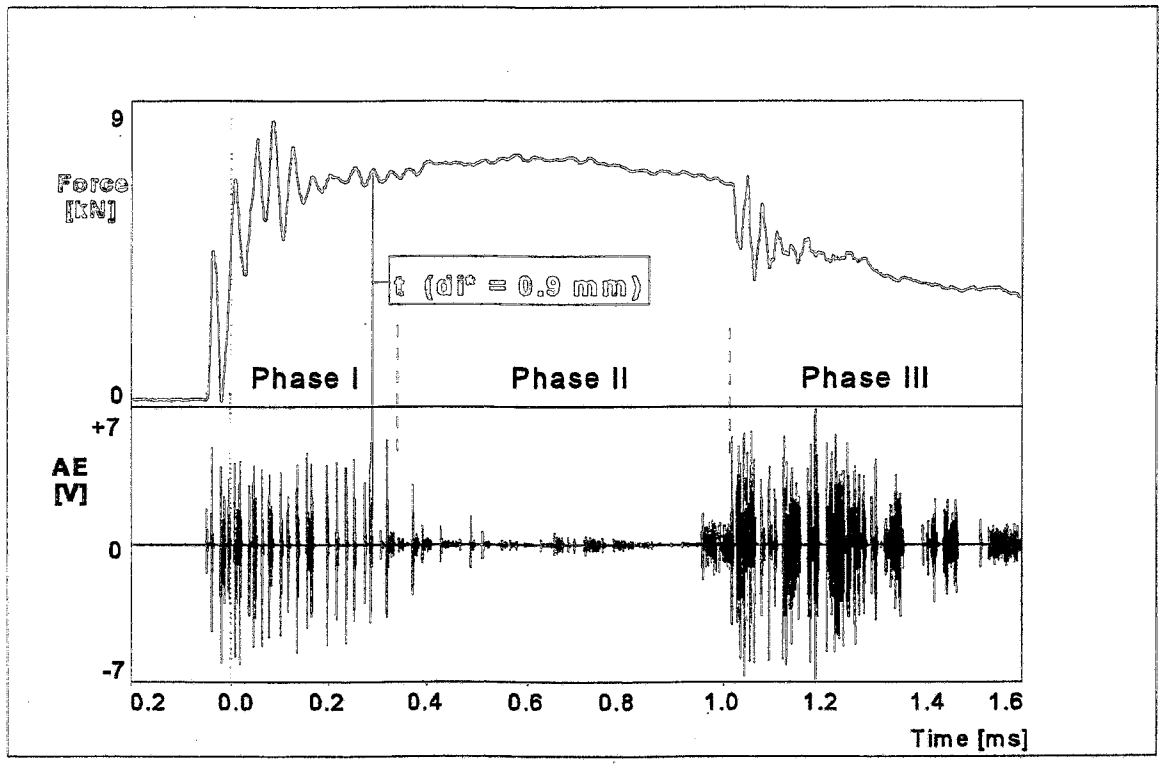

Fig.2: Typical load and AE curves in the transitition region at $v_0 = 2.8$ m/s

hammer velocity 2,8 ms^{-1} is shown in Fig.2.

It exhibits a typical loading and unloading part. From the load time trace three different phases can be recognized which are associated with typical acoustic behaviour. Phase 1 is marked by strong oscillations of the load and of the AE signal too. Phase 2 is characterised by small load oscillations and large plastic deformation, accompanied by lower acoustic intensity. The character of acoustic emission clearly differs from phase 1. After general yielding but before passing the load maximum first crack growth occurs. The third phase begins with a load drop caused by the begin of unstable crack growth. The sensitivity of the AE detector to acoustical events connected with unstable crack extension is clearly recognizable from the strong AE intensity in this phase. The phases of crack arrest and plastic deformation with repeated stable crack growth are also mapped in the rms-value of the AE-signal. The identification of the beginning stable crack growth from the load trace is not possible, but a special treatment of AE data can render this possible.

Two ways were chosen to find the point of stable crack growth initiation. At first the so called low blow test with varying blow angle (α_0=17° to 30°) was performed at room temperature to produce different lengths of stable crack growth. These lengths were determined by heat tinting and following breaking of the specimen in liquid nitrogen. The second way to extract a correlation between specimen deflection (i.e. load point displacement) and stable crack growth was the testing in the ductile to brittle transitition region by varying test temperature. The stable crack length can be seen in the SEM microscopical view of the fractured specimen surface. The results are presented in Fig.3.

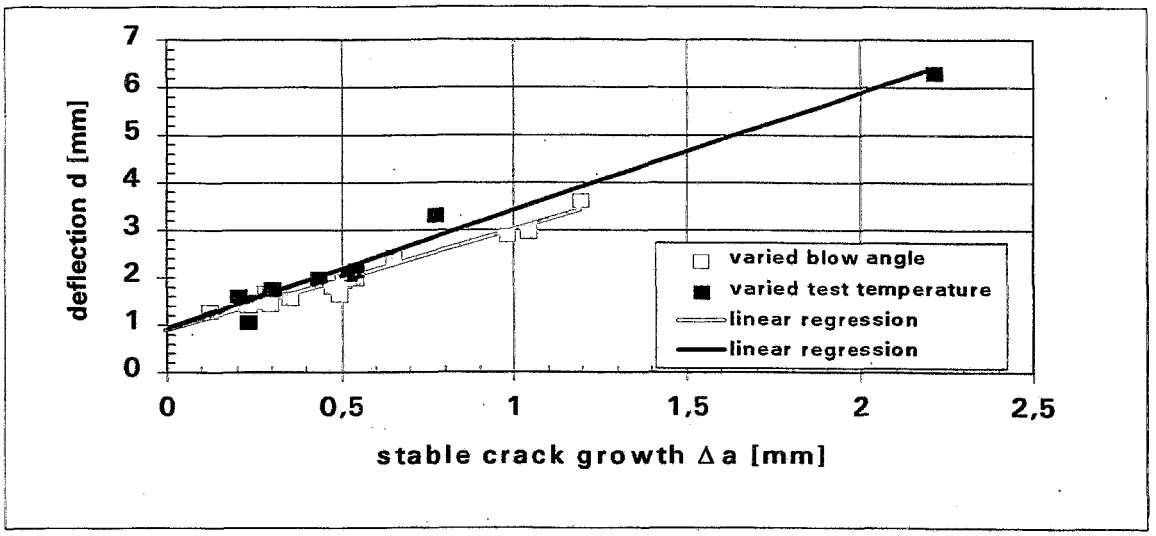

Fig.3: Correlation between stable crack growth and specimen deflection

Both ways provide a compareable initiation deflection d_i^* of 0.9 mm after extrapolation to zero crack growth. The time pertaining to initiation deflection $t(d_i^*)$ is marked in Fig. 2 and leads to J-integral $J_{di}(d_i^*)$=170 N/mm. This value corresponds with the J-integral computed from SZW measurements J_{di} (SZW=100 µm)=180 N/mm.

Four different AE signal types can be observed around the initiation deflection d_i^* (Fig. 2). These different AE types are shown in Fig. 4. Table 2 contains some main features of the different AE signals.

type of signal	amplitude [V]	duration [µs]
A	± 0,01	/
B	> ± 3	about 7
C	< ± 1	about 10
D	< ± 0,5	> 10

Table 2: Some features of the different AE signals

Type A AE is a result of the electronic properties due to the design of the whole measuring system. Mechanical events from the dynamic loading process cause the

type B signals. Signal types C and D can be associated with the crack initiation and growth process, because signal type C occurs very close to the estimated crack initiation time $t(d_i^*)$ in a lot of tests. Signal D type AE is distinguished by different signal

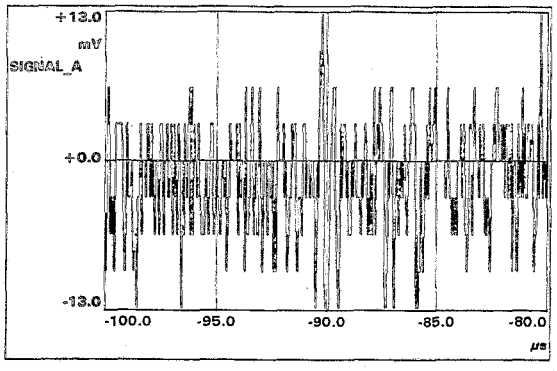

Fig. 4A: Noise due to the measuring channel

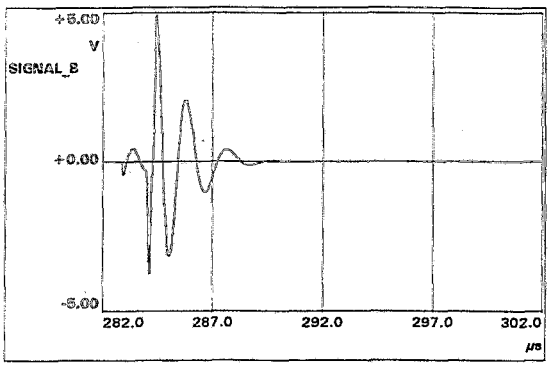

Fig. 4B: AE burst with high intensity

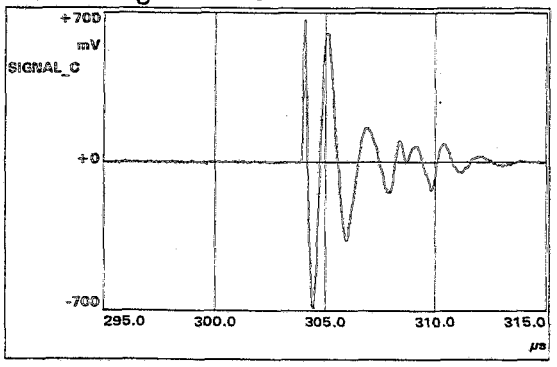

Fig. 4C: Low intensity AE burst

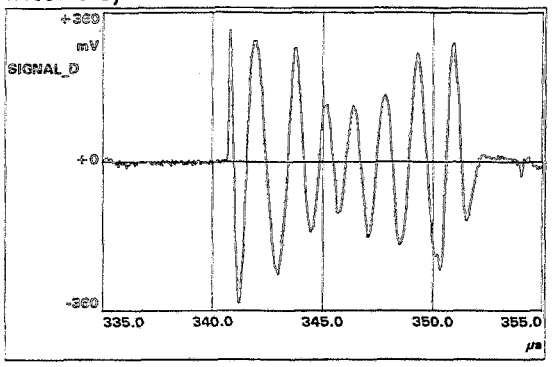

Fig. 4D: Quasicontinuous AE

Fig.4: Time traces of the observed four AE signal types obtained from AE in Fig.2

duration and is assumed to be connected with intensive plastic deformation processes. Signal D type AE starts later than type C AE. It is supposed that the plastic deformation before stable crack initiation in that material was too weak to be detected at the present sensor position. Furthermore, it was observed that the first separable type C signals were started after d_i^*. Type C and D are also present in the region of stable crack growth till the onset of unstable crack extension. Maybe the type D AE is an overlapped Type C signal under these impact conditions, because many superimposed transient type C events from activated AE sources near the crack tip contribute to type D signal with different duration. In agreement with results mentioned in literature [7,11,12] the occurrence of signal type C seems to be associated with the beginning stable crack growth.

5. Conclusions

AE during dynamic fracture toughness tests of a heat resistant steel was investigated by an AE analysis in combination with multiple specimen techniques. The results are summarised as follows:

(1) The two investigated multiple specimen methods, the variation of test temperature

and of initial blow angle, provide a comparable crack initiation deflection.

(2) The AE signals around the estimated stable crack initiation were classified into four types. AE type C seems to be a signal associated with the beginning of stable crack growth.

(3) It was found that type C AE starts in the transition region of phase I to phase II (see Fig.2), where this type is superimposed by intensive type B AE signals.

(4) The J-integral $J_{id\ szw}$ characterises the physical crack initiation toughness. The J-integral $J_{id\ AE}$ computed from the first occurrence of type C signal was verified with independent SZW measurement (based on J-integral $J_{id\ szw}$ using SEM) with good results.

However, the present impediment for the application of the AE method can be overcome and it seems to be possible to conclude the time of stable crack initiation from the AE signal.

References

[1] J. Heerens
"Rißabstumpfung, Spaltbruch im Übergangsbereich und stabiles Rißwachstum untersucht mit Methoden der nichtlinearen Bruchmechanik"
GKSS 90/E/31, GKSS-Forschungszentrum Geesthacht GmbH 1990

[2] E. Roos
"Grundlagen und notwendige Voraussetzungen zur Anwendung der Rißwiderstandskurve in der Sicherheitsanalyse angerissener Bauteile"
VDI-Fortschritt Berichte Reihe 18: Mechanik/Bruchmechanik; Nr.:122;
VDI-Verlag 1993

[3] K. H. Schwalbe
"Bruchmechanik metallischer Werkstoffe"
Carl Hanser Verlag, München - Wien ; 1980

[4] E. Roos
"Grundlagen, Anwendungsmöglichkeiten und -grenzen der Zähbruchkonzepte"
17. Technischer Bericht; Schriftenreihe Reaktorsicherheit und Strahlenschutz;
MPA Stuttgart; März 1985

[5] H. Blumenauer and G. Pusch
"Technische Bruchmechanik"
Verlag Grundstoffindustrie Leipzig, 3. Auflage, 1993

[6] H. Blumenauer, R. Ortmann and J. Ude
"Einfluß der Beanspruchungsgeschwindigkeit auf die Stretchzone und Rißinitiierung bei Feinkornbaustählen"
24. DVM-Vortragsveranstaltung des DVM-Arbeitskreises Bruchvorgänge: Bruchvorgänge unter hohen Beanspruchungsgeschwindigkeiten; Aachen; 18/19.Februar 1992; S.79-88

[7] D. Kalkhof
"Schallemissionsanalyse zur Bestimmmung der Rißinitiierung beim instrumentierten Kerbschlagbiegeversuch"
Materialprüfung 28(1986)9, S.267-271

[8] R. Rintamaa
"Single specimen fracture toughness determination procedure using instrumented impact test"
Espoo 1993, Technical Research Centre of Finland, VTT Publication No. 140

[9] S. Winkler
"Magnetische Emission - Ein neues Brucherkennungsverfahren"
IWM-Bericht T3/88, FhI für Werkstoffmechanik Freiburg, Februar 1988

[10] S. Winkler
"Brucherkennung mit elektrischer Emission"
IWM-Bericht T10/90, FhI für Werkstoffmechanik Freiburg, August 1990

[11] H. A. Crostack and A.H. Engelhardt
"Acoustic emission measurement during instrumented impact tests"
in Clough,R.B (ed.): Quantitative NDE in the nuclear industry Proc. of the fifth int. conference,San Diego/USA, 10-13 May 1982, Metals park, Ohio; Am. Soc. f. Metals, 1983

[12] H.W. Viehrig, K. Popp and R. Rintamaa
"Measurement of dynamic elastic- plastic fracture toughness parameters using various methods"
Int. J. Pres. Ves. & Piping 55(1993)233-241

[13] "Kerbschlagbiegeversuch mit Ermittlung von Kraft und Weg"
Stahl-Eisen-Prüfblatt 1315; Entwurf 7/86

[14] "Meßtechnische Anforderungen beim instrumentierten Kerbschlagbiegeversuch"
DVM Merkblatt 0001 Entwurf 3.86, Deutscher Verband für Materialprüfung, DVM

The project this report is based on was funded by BMBF (Bundesministerium für Bildung, Wissenschaft, Forschung und Technologie) and registered with No.1500919. The authors are responsible for the scientific content of the report.

THEORETICAL AND EXPERIMENTAL INVESTIGATIONS ON FLUID-STRUCTURE-INTERACTION IN CYLINDRICAL STRUCTURES

E. Altstadt, G. Grunwald, and J. Zoller

1. Introduction

The correct description of the mechanical vibrations e.g. of the reactor pressure vessel and its internals requires the fluid-structure-interaction in the downcomer region to be considered in the finite-element-model. For this purpose the coupled system of fluid equations and of structural equations of motion must be solved. To obtain a fluid-structure-element (FSE) that can be implemented in the finite-element-model, the system of equations can approximately be solved for the special case of a narrow annular gap geometry. To obtain the mass matrix and the damping matrix, the fluid equations can be reduced from 3D to 2D by averaging over the gap width [1], whereas the stiffness matrix will be obtained by an analytical approximate 3D-solution of the fluid equations for the stationary flow through the deformed annular gap.

2. Basic equations

The approximation applied to solve the system of coupled equations in order to get the FSE is specially taylored for incompressible fluids streaming through a narrow annular gap which is formed by two concentric cylinders A and B (Fig. 1). The fluid flow is driven by a pressure gradient $p_1 - p_2$. The cylinders can perform small motions according to Fig. 2 (two displacements and two rotations).

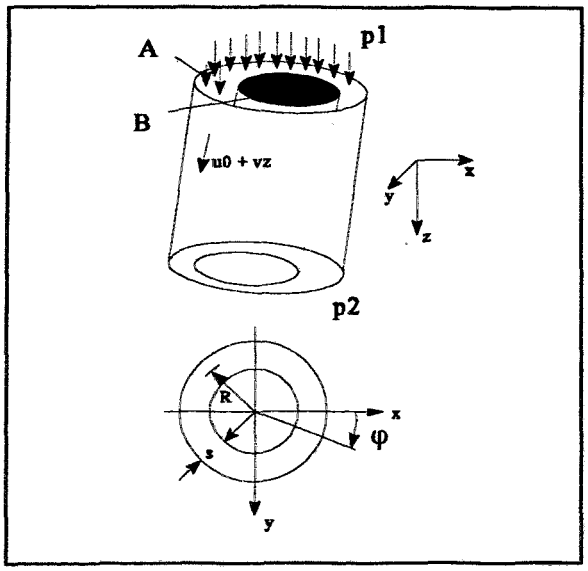

Fig. 1: Fluid-structure-system.

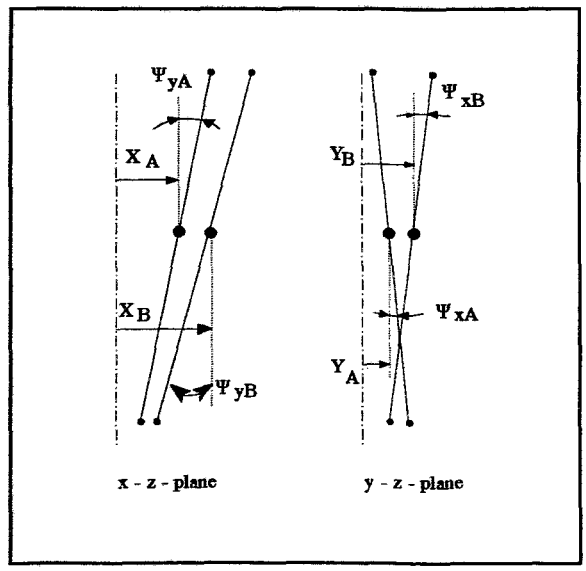

Fig. 2: Structural DOF of the FSE.

Thus the FSE has 8 structural degrees of freedom (DOF):

$$\underline{q}^T = [x_A, y_A, \psi_{xA}, \psi_{yA}, x_B, y_B, \psi_{xB}, \psi_{yB}] = [\underline{q}_A^T, \underline{q}_B^T] \quad . \tag{1}$$

According to this, the structural nodal forces and momenta are:

$$\underline{Q}^T = [F_{xA}, F_{yA}, M_{xA}, M_{yA}, F_{xB}, F_{yB}, M_{xB}, M_{yB}] = [\underline{Q}_A^T, \underline{Q}_B^T] \quad . \tag{2}$$

Fluid velocity **v** and pressure p are described in cylindrical coordinates {r, φ, z}. The basic fluid equations are the continuity equation (3) and the Navier-Stokes equation (4):

$$\nabla \cdot \vec{v} = 0 \quad , \tag{3}$$

$$\frac{\partial \vec{v}}{\partial t} + (\vec{v} \cdot \nabla)\vec{v} = \frac{\mu}{\rho} \Delta \vec{v} - \frac{1}{\rho} \nabla p \quad . \tag{4}$$

with μ being the fluid viscosity and ρ the fluid density. At the cylinder surfaces $\{r,\varphi,z\} \in \mathbf{S}$ the fluid velocity **v** and structural motion are coupled:

$$\vec{v}_s = \dot{\underline{q}}^T \underline{H}(S) \quad . \tag{5}$$

The components of $\underline{H}(S)$ are derived from the geometrical relations between the centers of gravity and the surfaces of the cylinders. The resulting forces and momenta which act on the structure can in turn be obtained from the pressure field:

$$Q_j = \int_S p(S; \underline{q}, \dot{\underline{q}}, \ddot{\underline{q}}) \cdot H_j(S) \, dS \quad . \tag{6}$$

After linearizing the pressure distribution with respect to q and its time derivations the FSE mass matrix, the FSE damping matrix and the FSE stiffness matrix can be obtained from:

$$m_{jk} = \frac{\partial Q_j}{\partial \ddot{q}_k} \quad , \qquad b_{jk} = \frac{\partial Q_j}{\partial \dot{q}_k} \quad \text{and} \quad c_{jk} = \frac{\partial Q_j}{\partial q_k} \quad . \tag{7}$$

3. Determination of mass and damping matrix from a 2-D solution

Starting from a linear formulation for the radial component of the fluid velocity

$$v_r(r,\varphi,z) = \sum_{j=1}^{8} \dot{q}_j \cdot \left(\frac{1}{2} - \frac{r - R}{s}\right) \cdot g_j(\varphi, z) \tag{8}$$

with g_j being the shape functions relating **v** with dq/dt, and presuming that the components v_φ and v_z do not depend on r but on φ and z only, the continuity equation can be averaged over the gap width [2]:

$$\int_{R-s/2}^{R+s/2} \nabla \cdot \boldsymbol{v}\, dr = 0 \quad . \tag{9}$$

This 2D equation can be solved analytically. The potential solution for the velocity field is applied to calculate the pressure distribution in dependence on the structural motion using the Navier-Stokes-Equation (4) with a simplified friction term [1]. Experimental investigations at a laboratory set-up were performed to validate the analytical 2D solution [1]. These experiments proved the FSE to be applicable to laminar fluid flow in the annular gap as well as to turbulent fluid flow. The mass and damping matrix can be obtained according to equation (7). As the fluid velocity and thus the pressure distribution depend on $d\underline{q}/dt$ only but not on $\underline{q}$ itself (eq. 8), a stiffness matrix cannot be derived. However, the experimental results have shown that the flowing fluid also causes a stiffness, i.e. forces and momenta which are proportional to $\underline{q}$ (chapter 5). Therefore the stiffness matrix has to be obtained by an analytical approximate 3D-solution of the fluid equations for the stationary flow through the deformed annular gap.

4. Determination of the stiffness matrix from an approximate 3-D solution (C-correction)

To get a stiffness correction for the FSE, a stationary 3-D fluid flow through the deformed gap is considered ($\underline{q} = \underline{q}_0$, $d\underline{q}/dt = \underline{0}$). The displacements of the cylinders are presumed to be small. Hence terms being quadratic in the components of $\underline{q}$ will be neglected. According to the geometry the dependence of the pressure and the fluid velocity on the angle φ will be expanded in a Fourier series. Terms of sum with period smaller than 2π are omitted in the Fourier expansion, because they are quadratic in the displacements. In addition, the values of v_r and v_φ averaged over the circumference are set equal to zero. In order to describe the boundaries of the deformed gap with constant radial coordinates, the following coordinate transformation is introduced:

$$\begin{aligned} \xi &:= r - \underline{q}^T \underline{N}(r,\varphi,z) \\ \phi &:= \varphi \\ \zeta &:= z \end{aligned} \tag{10}$$

with

$$N_I = h_I(r) \cdot g_I(\varphi,z)$$

$$\begin{aligned} h_I(r=A) &= 1\,, \quad h_I(r=B) = 0 \quad \text{for} \quad q_I \in \underline{q}_A \\ h_I(r=A) &= 0\,, \quad h_I(r=B) = 1 \quad \text{for} \quad q_I \in \underline{q}_B \end{aligned} \tag{11}$$

$$g_I(\varphi,z) = (a_{I0} + a_{I1} z)\cdot\cos\varphi + (b_{I0} + b_{I1} z)\cdot\sin\varphi$$

where A and B stand for the radia of outer and inner cylinder. The $\{\xi,\phi,\zeta\}$ - system corresponds to the reference system of an Arbitrary-Langrange-Euler (ALE) representation of the transient problem [3]. The g_i are the same as in eq. (8), whereas the interpolation functions h_i can arbitrarily be chosen.

It should be noted that velocity and pressure are expressed in $\{\xi,\phi,\zeta\}$, but the vector components remain in the spatially fixed directions $\{r, \varphi, z\}$.

Due to the assumption that the annular gap is narrow (s << A, B), all expressions with 1/r or $1/r^2$ are neglected in the friction part and in the convection part of eq. (4). In the continuity equation (3) v_r/r is neglected. Thus the Fourier expansion provides a solution of (3) and (4) in three main steps: At first from the z-component of the momentum equation (4) the basic flow velocity is obtained:

$$u_o(\xi) = \left[1 - \left(\frac{\xi - R}{s/2}\right)^2\right] \cdot \frac{(p_1 - p_2)s^2}{8\mu L} \quad . \tag{12}$$

This basic flow is similar to a plane Poiseuille flow between two parallel, broad plates with distance s. Secondly the z-derivation of the circumferential momentum equation is compared with the axial momentum equation. From the resulting differential equation the Fourier coefficients of v_z can be determined after the coefficients of v have been eliminated by the z-derivative of the continuity equation. In the third step the ξ-derivative of the circumferential momentum equation is compared with the radial momentum equation. This provides the coefficients of v_r and in turn the coefficients of ψ and the pressure. The result of this procedure is the pressure distribution in dependence on the displacement $\underline{q}$ of the structure.

$$\begin{aligned} p(\xi,\phi,\zeta;\underline{q}) &= p_1 + \frac{p_1 - p_2}{L}\zeta + \frac{3R^2(p_1 - p_2)}{s \cdot L}\left[\underline{c}_p(\zeta)\cdot\cos\phi + \underline{s}_p(\zeta)\cdot\sin\phi\right]^T \underline{q} \quad , \\ \textit{with} \quad \underline{c}_p^T &= (1 - e^{(\zeta - L)/R}) \cdot [0,0,0,-1,0,0,0,1]; \\ \underline{s}_p^T &= (1 - e^{(\zeta - L)/R}) \cdot [0,0,1,0,0,0,-1,0] \quad . \end{aligned} \tag{13}$$

Finally the stiffness matrix follows from eqs. (6) and (7-3). Small radial pressure gradients are neglected in eq. (13).

5. Application to a simple pendulum and experimental investigations

To validate the above theory, it is applied to a pendulum being a rather simple system from the structural point of view. The mechanical system is shown in Fig. 3. There is one structural degree of freedom ψ_y which is the plane pendular elongation of the inner cylinder. The equation of motion is:

$$(J_S + J_F)\ddot{\psi}_y + d_F\dot{\psi}_y + (m^* gL/2 + cL^2 + c_F)\psi_y = 0 \quad . \tag{14}$$

J_S is the mass inertia momentum of the pendulum body related to the rotation point and m^*g its weight reduced by the buoyancy. The parameters J_F, d_F and c_F representing the influence of the fluid are calculated from eq. (7).

$$J_F = \pi\rho\frac{L^3R^3}{s}\left\{\frac{1}{3} - \alpha\frac{R}{L}\left[\frac{\cosh(\frac{L}{R})}{\sinh(\frac{L}{R})} - \frac{R}{L}\right]\right\} . \tag{15}$$

The factor α ($0 \le \alpha \le 1$) has to be chosen in such a way that the boundary condition p = const. at the outlet is fulfilled [1].

$$d_F = u_0 \pi \rho \frac{L^2 R^3}{s} \{\frac{1}{2} - \alpha[1 - \frac{R}{L} \frac{\cosh(\frac{L}{R}) - 1}{\sinh(\frac{L}{R})}]\}$$

$$+ u_0 \lambda \pi \rho \frac{L^3 R^3}{4 s^2} \{\frac{1}{3} - \alpha \frac{R}{L}[\frac{\cosh(\frac{L}{R})}{\sinh(\frac{L}{R})} - \frac{R}{L}]\} . \qquad (16)$$

λ is an empirical friction parameter depending on the Reynolds number [1].

$$c_F = 3\pi \frac{R^3}{S} \cdot (p_1 - p_2) \cdot \{\frac{L}{2} - R + \frac{R^2}{L}(1 - \exp(\frac{-L}{R}))\} ; \quad \textit{for} \quad p_1 \geq p_2 . \qquad (17)$$

According to this model, a laboratory set-up was constructed consisting of a fixed outer pipe and an exchangeable inner cylinder as pendulum body. Using pendulum bodies of several diameters the gap width can be varied. The set-up can be operated with water or air. If air is used the flow direction can even be reversed, i.e. the air streams from the bottom to the top of the gap ($p_2 > p_1$). For experiments with water an additional spring c (Fig. 3) was mounted to increase the eigenfrequency and to avoid an overcritical damping. The pendulum elongation can be measured by a HALL probe near the bottom of the pendulum cylinder. From the measured time series the eigenfrequency and the dimensionless damping degree of free pendulum vibrations can be estimated. These experimental values are compared with the theoretical ones which follow from the equation of motion of the pendulum in a fluid (14).

In Fig. 4 the measured and the calculated eigenfrequencies are compared. The results were obtained for a s/R ratio of 0.06. The lower curve results if the fluid mass and damping from the 2D-solution are considered only (chapter 3), whereas the upper curve additionally takes the fluid stiffness from the stationary 3D-solution (chapter 4) into account. This leads to good agreement between measurement and theory. The downward flow direction is connected with a positive stiffness resulting in a higher eigenfrequency.

Fig. 5 depicts the dimensionless damping.

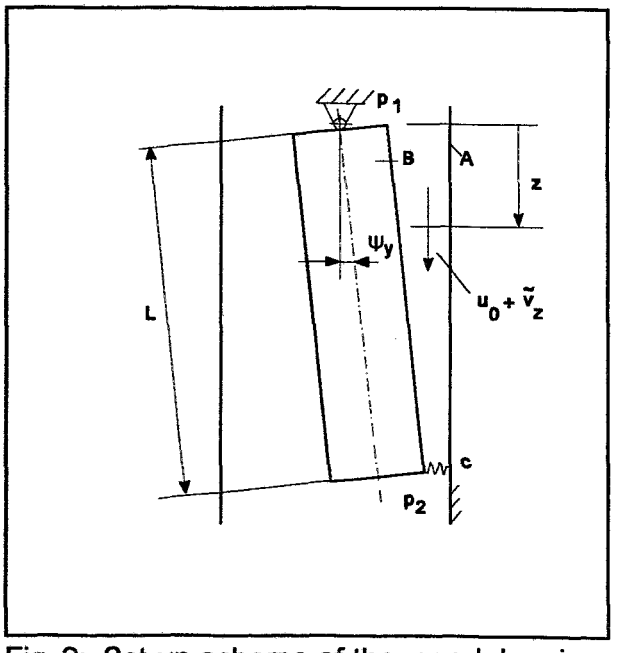

Fig. 3: Set-up scheme of the pendulum in a streaming fluid.

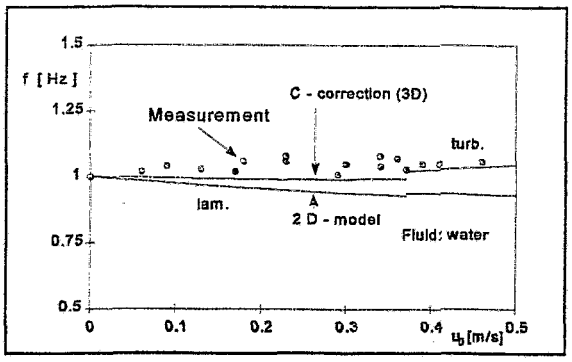

Fig. 4: Eigenfrequencies of a pendulum in water for different average axial flow velocities.

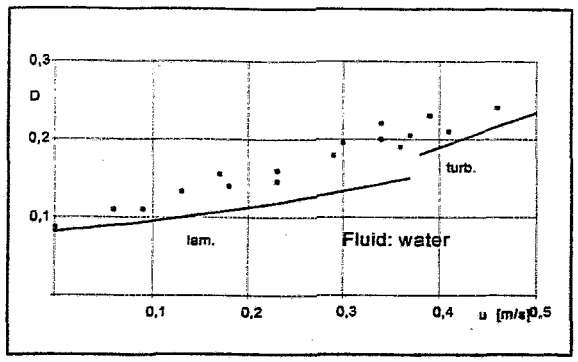

Fig. 5: Damping degrees of a pendulum in water for different average axial flow velocities.

Another experiment was carried out with air streaming from the bottom to the top (against positve z-direction). Fig. 6 depicts the pendulums eigenfrequency in dependence on the axial flow velocity. The eigenfrequency decreases with increasing velocity, so there is a negative stiffness effect for upward flow direction. During the performance of this experiment the displacement of the pendulum was not small in comparison with the gap width. So one precondition of the theory was fulfilled badly.

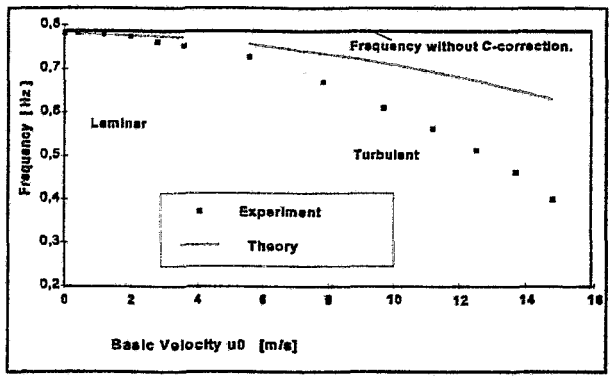

Fig. 6: Eigenfrequencies of a pendulum in air for different upward directed axial flow velocities.

6. Final Remarks

The presented FSE (eq.(7)) is based on approximate analytical solutions of the continuity equation and the Navier-Stokes equation considering the structural motion. Due to the linearization with respect to the structural DOFs a mass and a damping matrix can be obtained from the instationary 2D-solution, and a stiffness matrix is derived from the stationary 3D-solution. Experimental investigations have proved the FSE to be applicable for narrow annular gaps in the laminar as well as in the turbulent flow range.

The FSE can be used to integrate the fluid-structure-interaction (FSIA) into large finite element (FE) models. It has already been used within a FE based vibration model of the VVER-440 type pressurized water reactor.

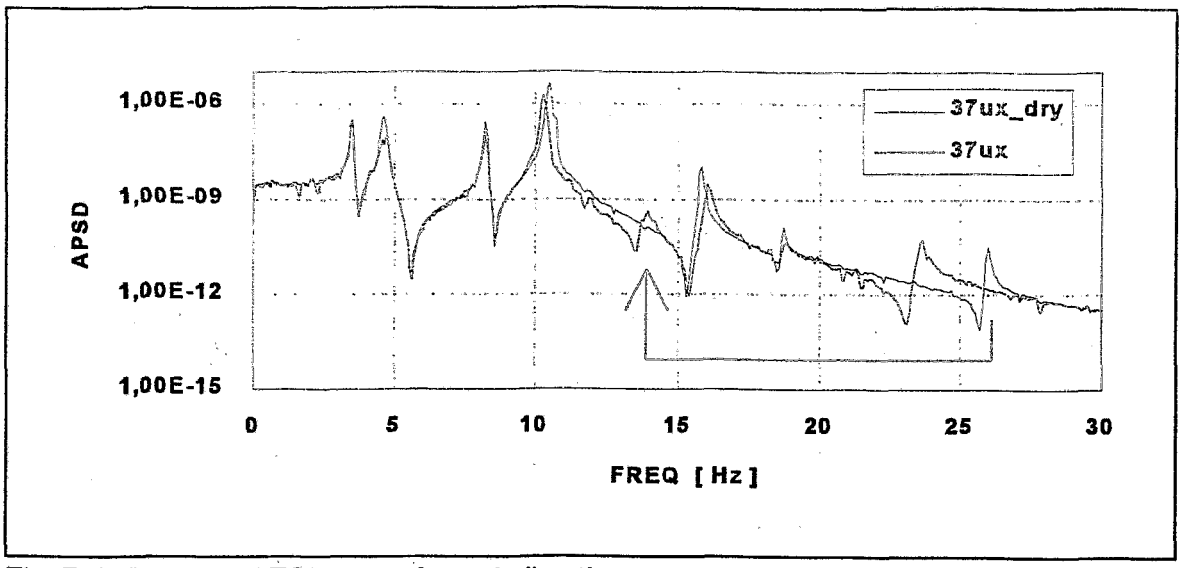

Fig. 7: Influence of FSIA on a forced vibration spectrum of RPV bottom displacement.

To demonstrate the strong influence of the FSIA on the vibration behaviour of the reactor pressure vessel (RPV) internals, Fig. 7 depicts a forced vibration spectrum of the reactor vessel bottom displacement with and without consideration of FSIA. The first mode exhibiting a relative displacement between RPV and core barrel is calculated to 26 Hz without FSEs. Consideration of FSIA shifts that frequency down to 13.8 Hz.

References

[1] G. Grunwald, and E. Altstadt
"Analytical and Experimental Investigations for Modelling the Fluid-Structure-Interaction in Annular Gaps."
Preprints of the IFAC-Symposium on Fault Detection Supervision and Safety for Technical Processes (SAFEPROCESS '94) 147-152, 1994.

[2] P. Schulz
"Theoretische und experimentelle Untersuchungen zur Fluid-Struktur-Wechselwirkung am Schwingungsmodell eines Druckwasserreaktors."
Ph. D. thesis at University of Erlangen-Nürnberg, 1982.

[3] T. Nomura, and T.J.R. Hughes
"An Arbitrary Lagrangian-Eulerian Finite Element Method for Interaction of Fluid and a Rigid Body."
Computer Methods in Applied Mechanics and Engineering 95 (1992) 115-138.

INVESTIGATIONS FOR GENERALIZATION CAPABILITY OF THE PATTERN RECOGNITION BASED LEAK LOCALIZATION METHOD

G. Hessel, W. Schmitt, and F.-P. Weiß

1. Introduction

After having experimentally proved the efficiency of neural networks and fuzzy pattern classifiers for acoustic leak localization at complicated three-dimensional structures [1], the further work has been focused on improving the generalization capability of the used pattern classifiers. In particular, the assignment of patterns of untrained leak locations, which could not be learned during the training of the classifier, is to be improved because normally they are misclassified or rejected by the trained classifier. However, their assignment is important for the practical value of this leak localization approach since it is impossible to train all possible leak positions, e.g. positions are not accessible during training or a flaw occurs in the base material (not in the welding or at a flange).

It must be remarked that in this context the term "generalization" is used in an extended sense here while in the literature it mainly describes the ability of a classifier to handle so-called testing data which were not presented during training although they belong to the set of the trained classes. Here the possibilities for improving the generalization capability of the neural network approach are described and then for comparison this ability of a fuzzy pattern classifier is presented. For better understanding the generalization problem, the leak localization method will be briefly described in the following.

2. Description of the Method

By combining the pattern recognition with the acoustic method, a new approach has been developed for detecting and localizing leaks at a complicated three-dimensional topology. The working principle is shown in Fig. 1. A neural network was used as pattern classifier. However, a leak can only be localized after having trained the neural network by the leak induced sound patterns of possible leak positions. The neural network is trained using a mobile simulator for leaks, e.g. a transmitting AE (acoustic emission)-sensor, which simulates leak induced structure-borne sound.

Training of the neural network also requires characteristic features for the different leak positions. They are extracted from the sound patterns measured by an array of AE-sensors directly mounted at the structure. A transient recorder was used to measure and process the high frequency sound signals (50-500 kHz) simultaneously. Mostly two types of feature vectors were used. One of them contained the broad band, short-time-RMS-values over 65 milliseconds for all AE-sensor signals and the other one consisted of RMS-values in three different frequency ranges. These feature vectors are fed into the input layer of the neural network.

The topology of a neural network is represented on the right side of Fig. 1. It consists of one input layer, in general one or more hidden layers, and one output layer. The number of input neurons corresponds to the number of the elements of the feature vector, while the number of neurons in the output layer depends on the number of leak positions (classes) which have to be localized. The training of a neural network means adjusting the connection strengths between the neurons in the different layers. To adjust these connection strengths, the neural network is learned by pairs of feature vectors at the input layer and classification vectors (classification results) at the output layer. This supervised learning procedure has to be continued till the trained neural network attains correct classification results for the training data.

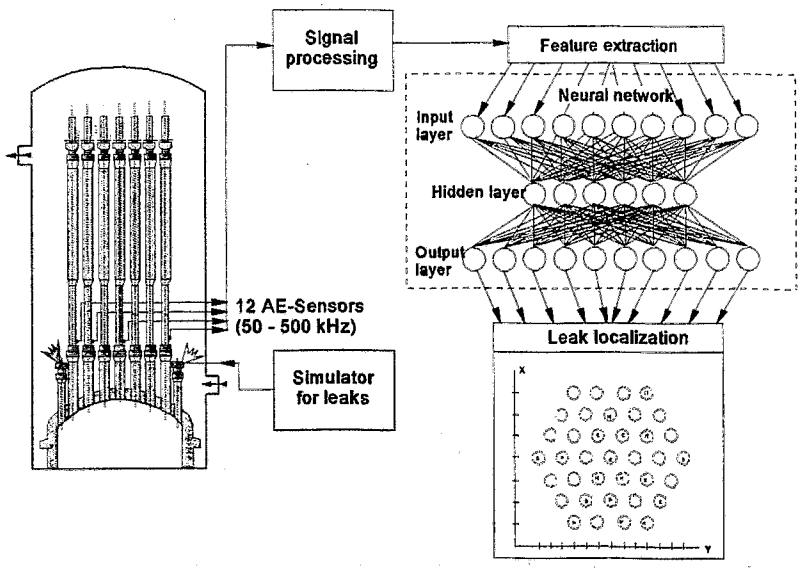

Fig. 1 Working principle - leak localization using neural networks

3. Improving the Generalization Capability of the Neural Network

After training the neural network must also be capable of correctly classifying the testing data which were not presented during training. If feature vectors of untrained classes are offered, such a neural network will misclassify or reject them in general.

To improve the generalization also for untrained leak locations, first, different types of neural networks such as perceptron networks and radial basis function networks were optimized regarding the number of neurons in the hidden layer. Experimental investigations showed that with the optimized three-layer perceptron network an improved generalization was achieved when the shapes of the decision boundaries between different classes in the high dimensional feature space are appropriately formed by the nonlinear transfer functions of hidden neurons. Due to the optimization, this perceptron network was capable of assigning untrained leak patterns to neighbouring leak positions which were learned during training [2].

To overcome the deficiency that only discrete leak positions, represented by their pertaining output neurons, can be recognized, neural networks with continuously valued

outputs were investigated. In particular, neural networks with two continuous output neurons corresponding to the x-and-y coordinates of the leak position were used. Improved generalization was tested for the upper unit of a PWR with 37 standpipes at the callotte which contain the control element drives (see also left part of Fig. 1). The input vector was formed by RMS-values of AE-sensors.

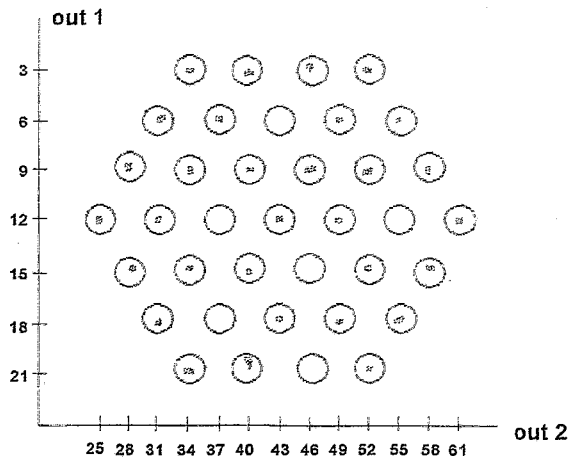

Fig. 2 Assignment of testing data (31 trained leak positions)
° net output— deviation ○ diameter of standpipe

All the used neural networks were trained with the same set of measuring data. It was found that the three-layer perceptron network (12-20-2) with a hyperbolic tangent as transfer function in the hidden and output neurons was best suited for this problem. A second hidden layer did not improve the generalization but it made the training slower.

The classification results of the optimized perceptron network are shown in Fig. 2 and Fig. 3 as a projection of the two output-neuron activities upon the topology of the standpipe positions. It must be mentioned that the perceptron network was trained using only 31 of the 37 leak positions. The activities of both the output neurons for each feature vector (sound pattern) are represented by a single point in the out1-and-out2 plane. So there are totally 310 points in Fig. 2, ten for each of the leak positions. As can be seen all locations are correctly classified.

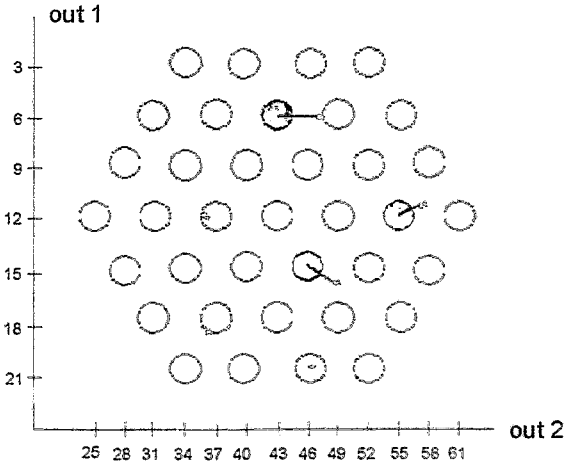

Fig. 3 Assignment of six untrained leak positions

The classification of the six untrained leak positions is shown in Fig. 3. It can be seen that three untrained leaks are correctly recognized (yellow-marked leak positions 12-37, 18-37, 21-46), two leaks are assigned near to the real leak position (blue-marked 15-46, 12-55), and only one untrained leak (red-marked 6-43) is misclassified to a neighbouring standpipe. This shows that the perceptron network might be suited even to recognize untrained leak positions. Certainly, improvements are possible by using modified feature vectors. A disadvantage is that a neural network with continuous outputs cannot give any information about the reliability of the classification when patterns of untrained leak positions are assigned.

4. Generalization Capability of the Fuzzy Pattern Classifier

4.1 The Used Fuzzy Pattern Classifier

The base of this application of fuzzy pattern classification is the PC-code micro-FUCS [3]. The peculiarity of this type of pattern recognition is connected with the fuzziness of the membership $\mu_k(x_i)$ of a feature x_i to a certain class k. This fuzziness comes from fluctuations of the leak sound amplitude, from variations of the leak sound spectrum over the time and from disturbances during the measurement. Fuzziness is expressed by membership values between zero and one.

The membership functions are generated in the training phase by adjusting parameters of predefined membership functions with the training patterns or by parameter estimation. As parametric membership functions for one feature, potential functions are used as defined by Eq. (1) and as represented in Fig. 4.

$$\mu_k(x_i) = \frac{1}{1 + \left| \frac{x_i - x_{ik}}{c_{ik\pm}} \right|^{d_{ik\pm}}} \qquad (1)$$

where the parameters mean

- x_{ik} component i of the domain centre k
- $c_{ik\pm}$ "distance" of the left (-) and right (+) margin from the centre x_{ik} of domain k in direction i
- $d_{ik\pm}$ exponent defining the slope of the drop at the left (-) and right (+) side of the potential function for direction i and domain k.

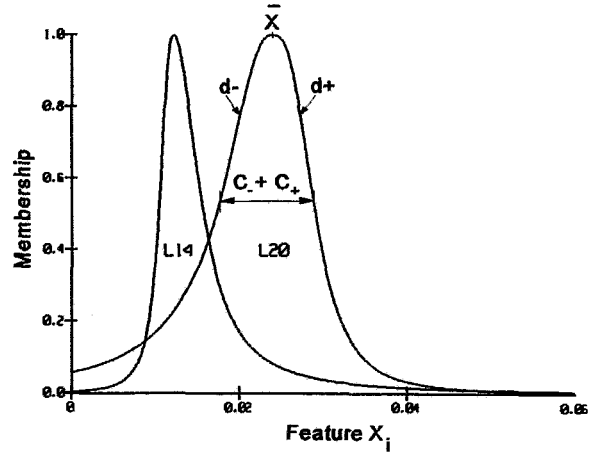

Fig. 4 Typical trained membership functions of two leak positions for one feature showing the parameters of Eq. (1)

Fuzzy logic performs classification by determining the so-called sympathy from the membership of all features to the class considered.

$$\mu_k(\underline{X}) = \frac{1}{1 + \sum_i \left| \frac{x_i - x_{ik}}{c_{ik\pm}} \right|^{d_{ik\pm}}} \qquad (2)$$

The whole set $\mu_k(\underline{X})$ (k=1,2..K) forms the sympathy vector $\underline{\mu}(\underline{X})$ which contains the membership of the current feature vector $\underline{X}$ to all classes (Eq. (2)). In case of an unambiguous classification the elements of the sympathy vector would be zero except one.

Through comparing the training and (re)classification capabilities for a great number of leak positions (44), it was found that the fuzzy classifier learned considerably faster than the neural networks (5s to 15min, e.g. for the three-layer perceptron network) and it also

provided a correct reclassification (100%) for the training data. However, the fuzzy classifier offers only a classification accuracy of 98.6% concerning the testing data whereas the three-layer perceptron network also attained a classification rate of 100% [2].

4.2 Classification of Untrained Leak Positions by the Fuzzy Pattern Classifier

Leaks were only simulated at those positions where AE-sensors were available that could be operated in the transmitting mode. So in the concrete experiment, see Fig. 5, only 12 from 37 potential leak positions could be trained. The other 25 positions could therefore be used to test the generalization capability of the fuzzy pattern classifier. To achieve a generalization capability, the fuzziness $c_{ik\pm}$ of the 12 trained membership functions were artificially increased from about 1% to 30% of the maximum value of all features x_i occurring in the training data. To display the classifications, the sympathy vectors were mapped into the two-dimensional scheme of the leak positions.

The coordinates (y,z) associated with the current sympathy vector in the scheme are calculated by the weighted mean:

$$y = \frac{\sum_k \mu_k(\underline{X}) \cdot y_k}{\sum_k \mu_k(\underline{X})} \quad and \quad z = \frac{\sum_k \mu_k(\underline{X}) \cdot z_k}{\sum_k \mu_k(\underline{X})} \tag{3}$$

where y_k and z_k are the coordinates of the trained leak positions.

In the left part of Fig. 5, the localizations obtained with this modified classifier are shown. All leak positions, even the trained one, are localized at places shifted to the centre of the AE-sensor array. This is due to the fact that even small sympathy values, which are obtained far from the domain centre and which only come from the artificial modifications, are fully considered when the sympathy vector is mapped into the two-dimensional space. The influence of this "sympathy noise" can be reduced by a sympathy threshold level. All sympathies smaller than this threshold are set zero. The right part of Fig. 5 shows the localization results using a sympathy level of 0.07. The localization is much better, but it is not sufficient for exact leak localization. If there are great distances between trained leak positions, as it is the case in the centre of the scheme (Fig. 5), serious misclassifica-

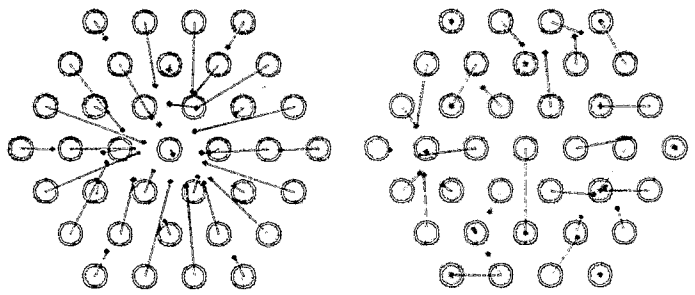

Fig. 5 The capabilty of leak localization of a fuzzy pattern classifier for untrained leak positions

tions can occur. By increasing the threshold level, the results become better, but more and more feature vectors cannot be localized because all elements of the sympathy vector are lower than the level.

Obviously the training of only 12 leak positions does not generate sufficient generalization capability. However, this approach is useful to get an overview in which region of the AE-sensor array the detected leak may be suited.

5. Conclusions

The generalization capability of neural networks and a fuzzy classifier was experimentally proved for leak localization at complicated structures. The tests showed that the three-layer perceptron network which was optimized regarding the number of hidden neurons offers a better generalization capability than the fuzzy classifier, especially when two output neurons are used the activities of which correspond to the coordinates of the leak positions.

Though the multilayer perceptron network has a promising generalization, further work is necessary to improve the reliability of the classification results when a great number of patterns of untrained classes have to be classified.

References

[1] W. Schmitt, G. Hessel, and F.-P. Weiß
Acoustic Leak Detection at Complicated Topologies Using Fuzzy Classifiers and Neural Networks,
Proc. of IMEKO XIII World Congress, September 5-9, 1994, Torino, Italy, pp. 1259-1264, (1994)

[2] G. Hessel, W. Schmitt, and F.-P. Weiss
Leckdetektion an komplizierten dreidimensionalen Topologien,
Forschungszentrum Rossendorf e. V., Bericht FZR-67, Januar 1995

[3] W. Kretzschmar
Programmbeschreibung MICRO FUCS - Fuzzy Classification System,
Institut für Mechanik, Chemnitz, (1991)

The project this report is based on is partially funded by the SMWK (Sächsisches Staatsministerium für Wissenschaft und Kunst) and registered with No. 7541.83-FZR/2. The authors are responsible for the scientific content of the report.

CALCULATION AND SPECTRUM ADJUSTMENT RESULTS FOR THE RHEINSBERG PRESSURE VESSEL STEEL IRRADIATION PROGRAM

H.-U. Barz, B. Böhmer

1. Introduction

The presented investigations are related to the Rheinsberg irradiation program which was performed in three reactor cycles between 1984 and 1988. More than a thousand steel specimens of different compositions were irradiated at a large number of positions and up to different fluences. At a selected number of positions the irradiation was monitored by activation probes. To establish the correlation between irradiation and degradation of the mechanical properties the irradiation conditions and related fluences are needed for all specimens. Since only a limited number of activation detectors was available, which cannot exactly be located at the positions of the specimens and which do not cover the appropriate range of neutron energy, this goal can exclusively be achieved by detailed transport calculations. In that context the monitoring results are used to substantiate the calculations by methods of spectrum adjustment. The methodical background was described in [1,3-6] while here selected results and some essential conclusions shall be presented. All this work was sponsored by the BMBF.

2. Fluences within the target channels

The correlation between neutron exposure and the specimens mechanical properties is mainly influenced by fast neutrons. For the determination of the correlation between the neutron exposure of the specimens and their mechanical properties the neutron fluences beyond 0.5 MeV and 1.0 MeV respectively and the number of displacements of atoms per

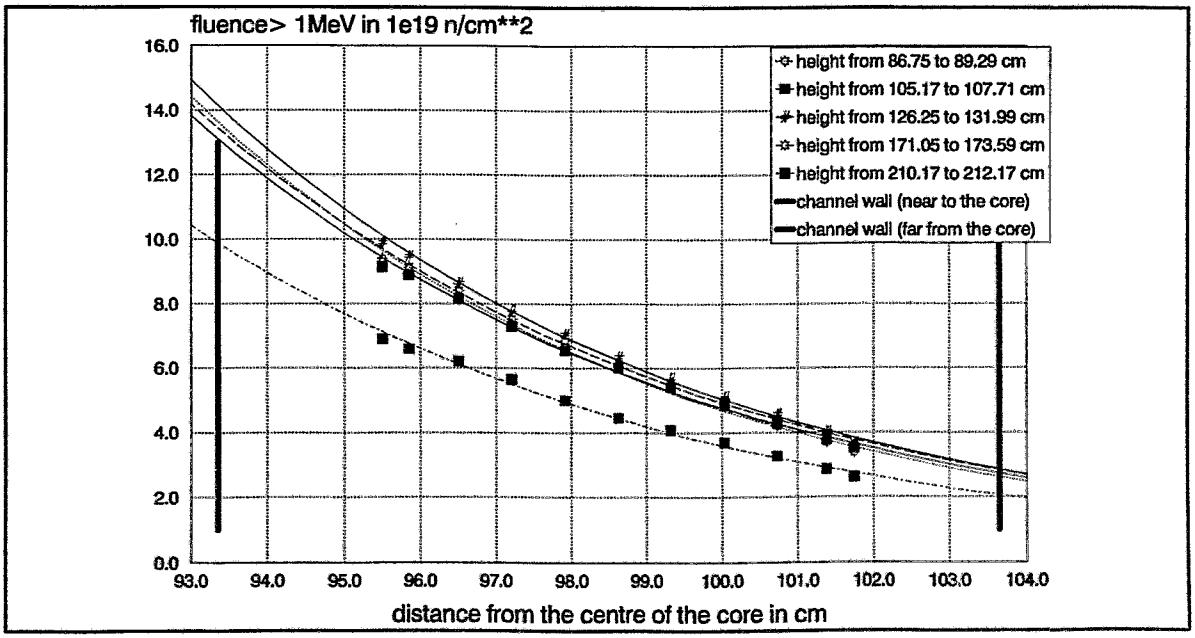

Fig.1: Neutron fluences within the Target channels

cm^3 (dose) were calculated. All these quantities are internationally used for the determination of the correlation mentioned above. Nevertheless, for each specimen and each irradiation series the full group spectra down to 21.5 keV were calculated. Below 21.5 keV the displacement cross section can be neglected. Though calculations were performed for almost 1000 specimens, only general results demonstrated by some examples can be discussed here.

The neutron fluences exhibited considerable radial gradients in the target channels (see Fig. 1 and 2). This situation causes the necessity of additional calculation efforts, especially extensive error and influence estimations had to be performed. But above all, it makes the recognition of fluence - embrittlement correlations much more complicated because there are strongly differing neutron loads even over a single specimen. On the other hand the fluence changes over the specimens in vertical direction can in general be neglected.

Fig. 1 shows some typical fluence curves within a target channel. Different calculations proved the observed gradient itself to be widely independent on the special fuel cycle conditions (fuel element loading, reactor power, fuel cycle time) and on the azimuthal position of the target channel. The fuel cycle conditions mainly influence the absolute fluence level. Even the arrangement of the specimens in the channel does not significantly affect the fluence curves. Fig. 2 gives fitted curves of equal relative fluence in a large size (6.35x6.09x2.54cm^3) CT-1 specimen.

Combining Fig. 1 and 2 it becomes possible to provide fluences for each location in the specimen even if one only disposes of mean fluence values in a certain region of the specimen.

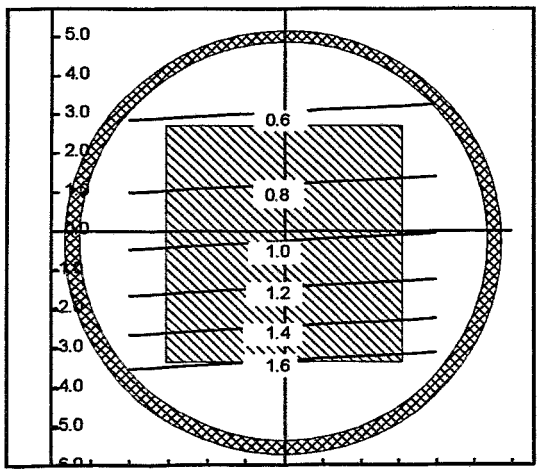

Fig.2: Neutron fluences for CT1-specimens

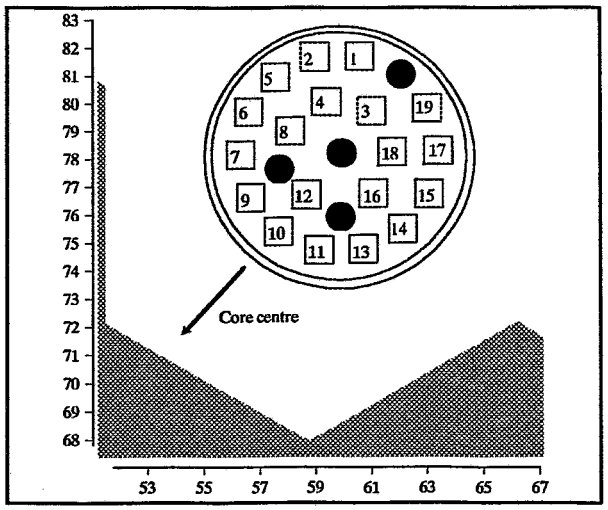

Fig.3:Arrangement of Charpy specimens

3. Fluences in special specimens

On Table 1 are given as example the needed results mentioned before for 2 of 19 selected Charpy specimens (1cmx1cmx5.5cm sizes in x,y,z-directions). Their location (number 1 and 10) in the target channel is shown in Fig.3. The extension of Charpy specimens in

the x-y plane is so small and the vertical dependence of fluences is so weak, that it is sufficient to calculate mean values for the whole specimen. As outlined in [1] and [2] by using improved Monte Carlo methods it was possible to achieve reasonable small statistical errors though the specimens sizes are rather small in comparison to the reactors structural components. The values written in brackets (Table 1) indicate the statistical error. In detail the results are presented in [2]. The application of time efficient calculation procedures (e.g. improved "weight window method") permitted to provide fluences for such a great number of locations without waiving of the exact 3-dimensional description.

Table 1: Reactor period 84/85 target channel 1 (Charpy specimens)
height from 60.75 to 68.00 cm

specimen 1:	
dose	= 3.401E+21 (±0.110E+21)
total fluence(>21.5 keV)	= 6.793E+19 (±0.261E+19)
cum. fluence > 1.0 MeV	= 2.952E+19 (±0.100E+19)
cum. fluence > 0.5 MeV	= 4.142E+19 (±0.126E+19)
specimen 10:	
dose	= 9.175E+21 (±0.307E+21)
total fluence(>21.5 keV)	= 1.878E+20 (±0.089E+20)
cum. fluence > 1.0 MeV	= 7.875E+19 (±0.282E+19)
cum. fluence > 0.5 MeV	= 1.112E+20 (±0.036E+20)

4. Assessment of accuracy

The sources of errors with respect to the inaccuracy of the geometrical measures and of the composition of materials are difficult to estimate. Detailed studies were accomplished to assess the influence of different neutron cross section data upon the results.

It was found that the errors due to different applied neutron cross section libraries amount to some percents as far as fluences in the target channels are concerned but increase significantly when regions far from the core are considered (near to the pressure vessel). The main contribution to the error is related to the distribution of fission sources that was made available by burn up and power distribution calculations of the utilities. As input for the Monte Carlo calculation this fission source distribution is needed for the whole fuel cycle. Unfortunately the inaccuracy of the fission source distribution is maximal in fuel elements at the core edge where the influence upon the calculated fluences is strongest. These errors are estimated to be about 10%. Test calculations with large artificial changes revealed the source distributions mainly to affect the absolute fluence level and to be of minor importance for gradients and neutron flux spectra.

5. Comparison with experimental data

While a relatively rough structure of neutron group data is sufficient to calculate the fluences, a comparison with the measured activities of the fluence monitors requires a more detailed description of the group structure. Therefore, the corresponding calculations were based on a 123-group data set derived from the JEF-1 library. Besides they took into account the real positions of the detectors more effectively. To obtain smaller

statistical errors the 123-group results are condensed to a 29-group structure beyond the energy of 21.5 keV. Due to the finite half-life of the detectors they are virtually more sensitive to radiation in time intervals near to the end of the irradiation period.

To cope with this effect the time, space and energy dependent flux distribution had to be calculated for the whole fuel cycle. If the number of activation reactions that have to be considered is small, another procedure can be more effective. Then for each reaction an effective neutron source distribution is calculated by weighting the time dependent source with a decay factor of the corresponding activation. This procedure provides effective, i.e. weighted and time integrated fluences for all detectors and all activation reactions. Actually an even simpler method was used which exclusively considered the integrated source for the most important spatial source region near the target channel [6].

6. Spectrum Adjustment

The measured activation reaction rates of those detectors, irradiated during the fuel cycle 1984/1985 in target channels 1 and 5 of the Rheinsberg reactor were compared with reaction rates determined by means of fluence spectra calculated with the TRAMO code. The ratios of theoretical and measured reaction rates are listed in Table 2 for some of the detectors irradiated in channel 1.

Table 2: Relations between calculated and measured reaction rates (C/E-values) for 8 detector positions

No.	Name	$^{54}Fe(n,p)^{54}Mn$	$^{63}Cu(n,\alpha)^{60}Co$	$^{93}Nb(n,n')^{93m}Nb$	$^{93}Nb(n,\gamma)^{94}Nb$
1	2111	1.083	0.766	1.075	1.354
2	1811	1.074	0.828	1.073	1.393
3	0712	1.088	0.726	1.053	1.485
4	2013	1.107	0.949	1.191	1.699
5	1913	1.063	0.713	1.080	1.563
6	2831	1.080	0.744	1.109	1.588
7	0932	1.073	0.434	1.073	1.807
8	2933	1.087	0.610	1.123	1.882

The calculation was based on a 26-group neutron data set. There is reasonable agreement for the $^{54}Fe(n,p)^{54}Mn$ and $^{93}Nb(n,n')^{93m}Nb$ reactions. But for the other two reactions considerable deviations have to be stated. In case of $^{93}Nb(n,\gamma)^{94}Nb$ the reasons are clear, because due to their small contribution to radiation embrittlement low energy neutrons have not been treated with energetic and spatial resolution adequate to that activation reaction.

Since the discrepancy for $^{63}Cu(n,\alpha)^{60}Co$ could not be explained by realistic changes of the spectra, in order to exclude possible error sources several improvements were implemented in the calculation of spectra and in the evaluation of experiments, such as:

- increase of the number of groups in the energy region beyond 21.5 keV from 10 to 29
- application of the latest version of the IRDF-90 dosimetry data file (from March 1994)

and of IRDF-90 covariance data
- improvement of the detector decay correction by taking into account the spatial changes of the flux distribution over the fuel cycle (see chpt. 5).

However, all these measures did not decisively improve the agreement between calculation and experiment. In particular, the increased energy resolution did not significantly influence the shape and absolute level of the theoretical spectra when adjusted with experimental data (see Fig. 4).

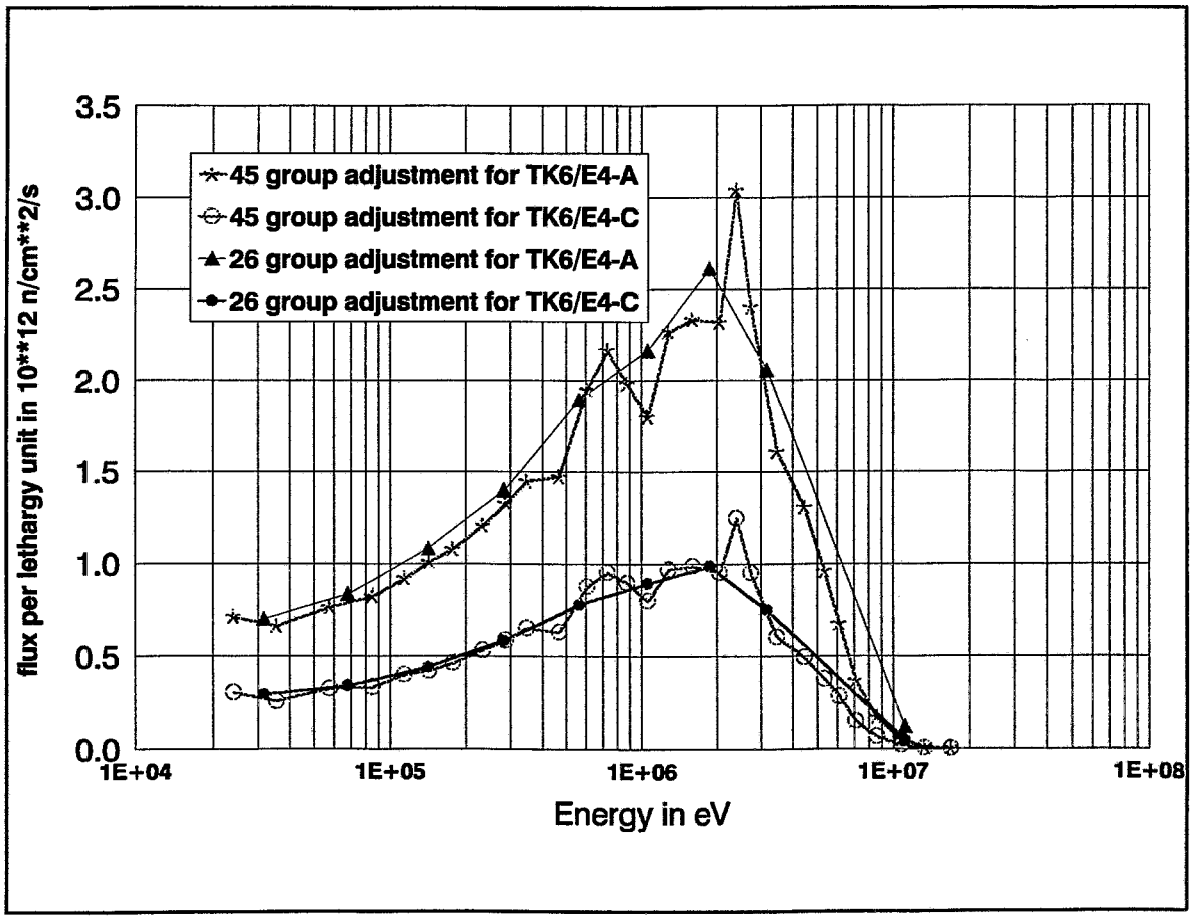

Fig.4: Comparison of adjustment results with 26 and 45 energy groups (only high energy region)

Accordingly it was concluded that there must be unidentified errors in the experimental results gained from channels 1 and 5 (1984/85).
Nevertheless, the spectrum adjustments based on these experimental data gave reasonable results for parameters relevant for embrittlement, as fluence integrals over relevant energy regions and displacement rates. Usually the adjusted integral parameters and the pure theoretical values only differed in their error limits.

An example for the case presented in Table 2 is shown in Table 3.

Table 3: Fluence integrals in units of 10^{19} neutrons/cm^2 before and after adjustment for an irradiation time of 273.0 days for channel 1 (1984/85)

Position No.	Name	Fluence (E>0.1Mev) before	Fluence (E>0.1Mev) after	Fluence (E>0.5Mev) before	Fluence (E>0.5Mev) after	Fluence (E>1.0Mev) before	Fluence (E>1.0Mev) after
1	2111	14.41±20%	14.06±10%	10.07±20%	9.93± 9%	6.66±20%	6.69± 8%
2	1811	14.41±20%	14.23±10%	10.07±20%	10.04± 9%	6.66±20%	6.74± 8%
3	0712	11.88±20%	11.32±10%	8.29±20%	7.99± 9%	5.45±20%	5.35± 8%
4	2013	9.57±20%	8.98±10%	6.66±20%	6.29± 9%	4.37±20%	4.17± 8%
5	1913	9.57±20%	9.18±10%	6.66±20%	6.46± 9%	4.37±20%	4.32± 8%
6	2831	14.74±20%	14.04±10%	10.37±20%	10.00± 9%	6.95±20%	6.83± 8%
7	0932	12.04±20%	10.71±11%	8.40±20%	7.61± 9%	5.51±20%	5.16± 8%
8	2933	9.66±20%	8.94±10%	6.72±20%	6.31± 9%	4.40±20%	4.24± 8%

7. Conclusions

Fluences and displacement values could be determined with satisfying accuracy for a huge number of specimens of the Rheinsberg irradiation program accomplished between 1984 and 1988.

When planning future irradiation programs attention should be paid to the following items:
1. Specimens should not be situated in positions where high flux gradients have to be expected.
2. The orientation of the specimens in the target channel must be documented and be reproducible.
3. The detectors must be protected against contamination but the protection capsules should allow an ease recovery of the detector.
4. The detector materials should stand temperature and pressure and keep their mechanical integrity. Pulverization has to be avoided.

The discrepancy between measured and calculated activation rates of the Cu-detectors could not be clarified.

8. REFERENCES

[1] F.-P. Weiß, U.Rindelhardt
Annual Report 1993 (Institute for Safety Research), FZR-68, June 1994

[2] H.-U.Barz, J.Konheiser
Fluenzberechnungen für das Bestrahlungsprogramm Rheinsberg von Material proben im Rheinsberger Reaktor im Zeitraum 1984-1988, FZR-51, August 1994

[3] H.-U. Barz
Problems of Weight Determination for the Multigroup Monte Carlo code TRAMO for Neutron Flux Calculation, Progress in Nuclear Energy, Vol. 24,
pp. 69-75, 1990

[4] H.-U.Barz, B.Böhmer, J.Konheiser, I.Stephan
High Precision Neutron Fluence Calculations, Activation Measurements and Spectrum Adjustment for the Rheinsberg Pressure Vessel Steel Irradiation Program, Presentation to the EWGRD,WGRD-VVER Meeting, April 18-22, 1994, Rez,

Czech Republic
[5] H.-U.Barz, B.Böhmer, J.Konheiser
Neutron Fluence Calculations and Spectrum Adjustments for the Rheinsberg Pressure Vessel Steel Irradiation Program, Proc.Jahrestagung Kerntechnik´94, 17-19 Mai 1994, S.19-22
[6] H.-U. Barz, B.Böhmer, J.Konheiser, I.Stephan
Aufgaben und Probleme bei der Bestimmung der Neutronenbelastung für den WWER-1000, Beitrag zum 5. Deutsch-Russischen WTZ-Seminar der Arbeitsgruppe Komponentensicherheit und Qualitätssicherung vom 3.-5.Oktober 1994 in Stuttgart

The project this report is based on is funded by the BMBF (Bundesministerium für Bildung, Wissenschaft, Forschung und Technologie) and is registered with Nr. 1500917. The authors are responsible for the scientific content of the report.

APPLIED DECISION ANALYSIS AND RISK EVALUATION

W. Ferse, S. Kruber[1]

1. Introduction

During 1994 the workgroup 'Applied Decision Analysis and Risk Evaluation' continued the work on the knowledge based decision support system XUMA-GEFA [1] for the evaluation of the hazard potential of contaminated sites.

Additionally a new research direction was started which aims at the support of a later stage of the treatment of contaminated sites: the clean-up decision. For the support of decisions arising at this stage, the methods of decision analysis [2] will be used. Computational aids for evaluation and decision support were implemented and a case study at a waste disposal site in Saxony which turns out to be a danger for the surrounding groundwater ressource was initiated.

2. The flow chart for the treatment of contaminated sites in Saxony

Fig. 1. shows the steps which are performed during the investigation and clean-up of contaminated sites in Saxony [3].

The second up to the fourth step are supported by the knowledge based system XUMA-GEFA. After the detailled, technical investigation of the site, a final decision is made about the necessity of clean-up actions. This is the starting point for the decision analysis related steps.

The first two steps consist of the choice of technically feasible remediation techniques and a call for clean- up concepts from remediation companies. The offered concepts are checked against the technically feasible techniques and are if necessary revised. Finally a decision is made, which concepts are worth of further investigation.

The two steps concept and company preselection are to be developed by external research institutes and are currently not part of our current research.

Starting with a set of technically feasible remediation concepts together with a set of companies which offer them, it is the task of decision analysis to guide the responsible authorities to the final selection of the most prefered clean-up concept.

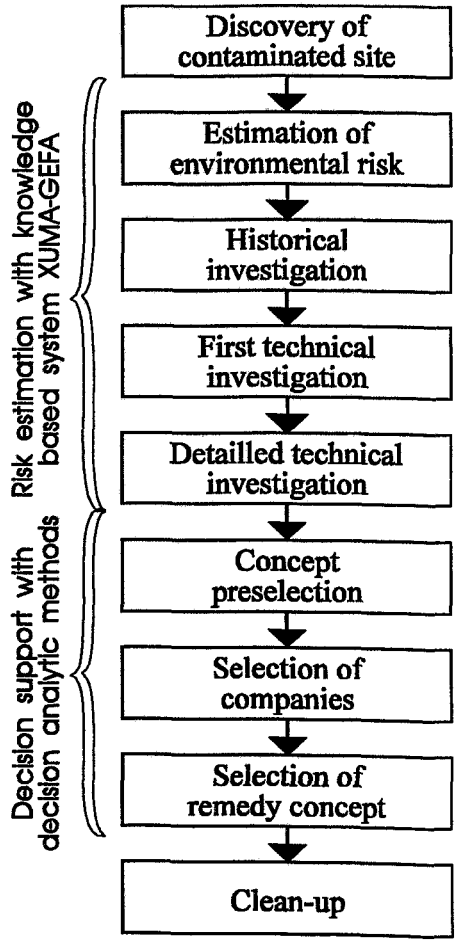

Fig. 1. Flow-chart for the processing of contaminated sites in Saxony.

[1] Nuclear Analytics and Engineering Rossendorf Inc.

3. Decision analytic methods

The main problems of the decision about the optimal remediation technique are the comparison of strategically different remediation actions, multiple, conflicting objectives, uncertainty about the actual outcomes of a remediation action and the participation of several agents with diverging opinions.

Decision analysis is based on an axiomatic system, developed by the German mathematicians vonNeumann and Morgenstern [4]. During the 1970s the theory was extended by American scientists (Keeney [5], Raiffa, Fishburn, Howard) for the support of decisions with multiple, conflicting objectives. Since then decision analysis has found many applications in various areas (energy, militar, research, politics, economics) [6].

The main intention of decision analysis is not to determine and dictate the optimal action but rather to guide the decision maker through a complex decision problem and to give him insight in the relevant aspects of his situation.

Decision analysis subdivides complex decisions into small ones which can be understood easily and uses the answers of the decision maker to these small problems in a rational and defensible manner for the solution of the complex problem.

The main steps of the application of decision analysis are sketched in figure 2.

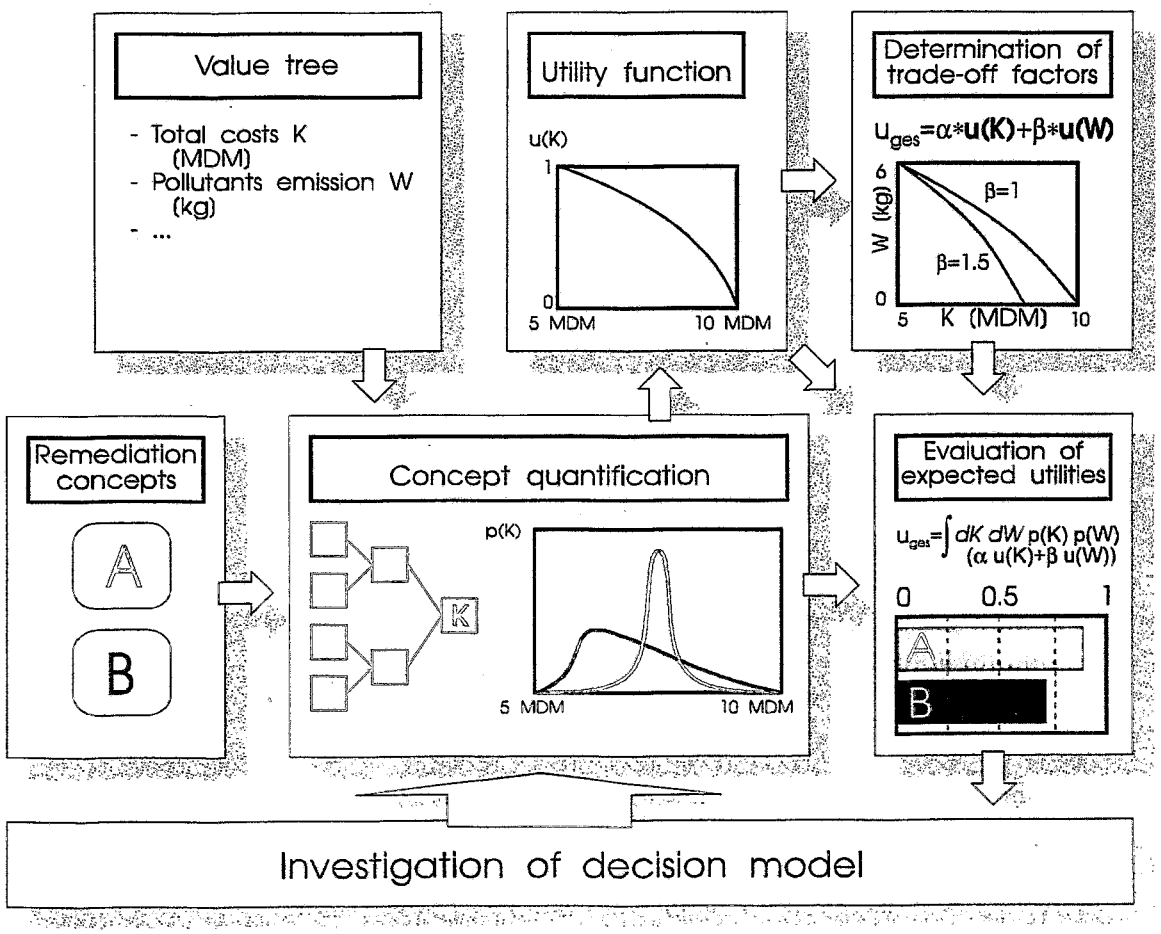

Fig. 2. Methodology of Decision Analysis

First it is necessary to define a list of objectives (value system) together with appropriate attributes to fix the necessary information which must be determined for every concept under investigation.

Generally the outcomes of the concepts can only be roughly estimated. Therefore, it is important to encode the uncertainty involved. This is done by means of subjective probability distributions. Often the distributions of the decision relevant information depend in a very complex manner on known input parameters. Therefore, easily usable computational aids are required for representing the functional dependencies and for the calculation of the relevant distributions.

When all decision relevant objectives have been quantified for every concept, the decision maker must define his attitude towards risky decisions. The decisions he makes in simple situations are encoded in one-dimensional utility functions.

Furthermore he must define how the different objectives are weighted against each other. It is our opinion, that this weighting process is of paramount importance for the final decision. Therefore, great care should be taken, not to use abstract weighting factors, but always to visualize and explain to the decision-maker the meaning and consequences of the selected numerical values of the trade-off coefficients.

When the aggregation function has been defined completly, numbers indicating the performance of the concepts can be calculated: the expected utilities. The concept with the maximum expected utility should be best.

Calculating the utility for every concept is just the first step in the solution of a decision problem. As the aim of decision analysis is insight and not numbers the following investigations should always be performed:

- Identification of specific strengthes and weaknesses of the concepts. This step is crucial for an explanation of the result.
- Search for the most and least important objectives and coefficients. These investigations show, which parts of the decision model are important and should be reinforced and where simplifications are possible.
- Sensitivity analysis of the trade-off coefficients helps identifying important aspects and defending subjective opinions.
- The sources of uncertainty should be identified and the value of additional information should be calculated. This information can be used to guide further expertise.
- The influence of input parameters on the concept ranking has to be investigated. So robust and flexible concepts are discovered.

4. Computational aids for the application of decision analysis

Computational tools are required to support the application of decison analytic methods for remedy selection. These tools have been implemented during 1994 and provide the user with the following services:

- Input and editing of function networks to encode the functional dependency of the decision relevant information on the input parameters. The networks are also used for the definition of utility functions and the weighted aggregation of the objectives.
- Calculation of probability distributions of the depending variables based on the distributions of the input parameters.

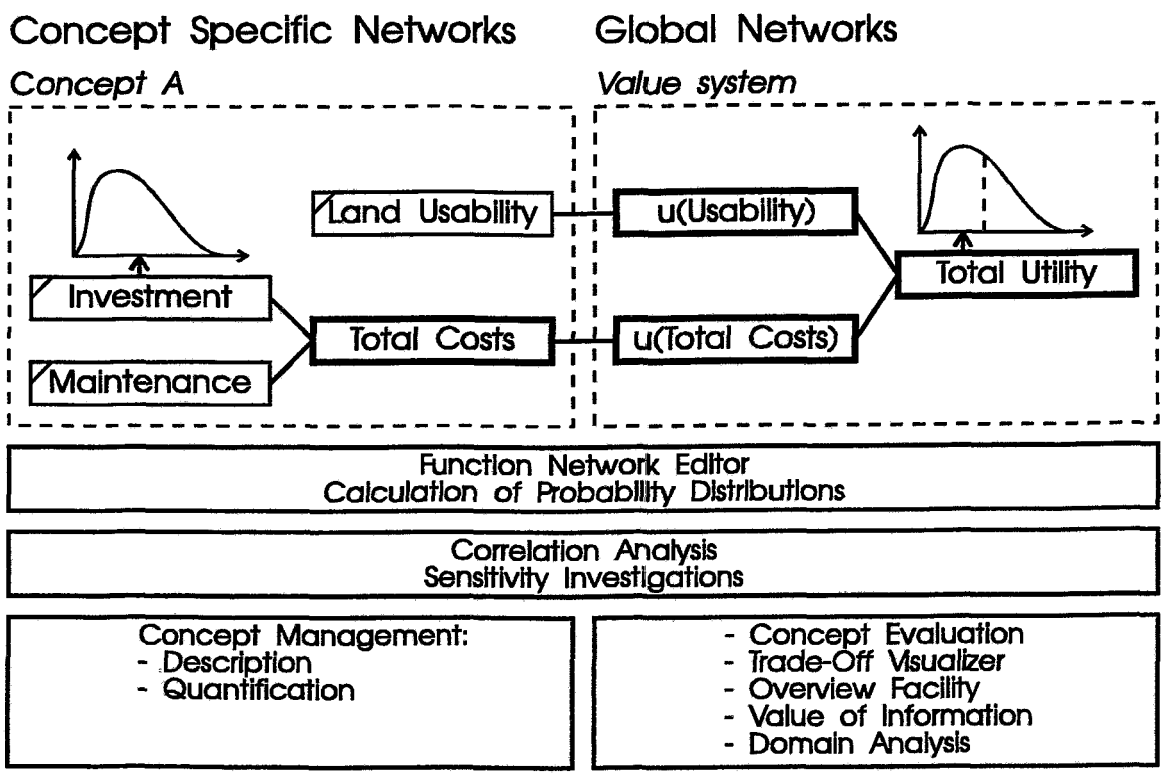

Fig. 3. Structure of the Program System 'Decision Analysis for Remedy Selection'

- Management tools for remediation concepts and value systems
- Tools to perform sensitivity investigations and correlation analysis.
- Aids to adjust and visualize trade-off coefficients.
- Tools to investigate the results of a decision model and to find relevant and irrelevant parts.

The principal structure of the program system is shown in fig. 3.

5. A case study

In order to investigate the applicability of decision analytic methods for remedy selection a case study was initiated in conjunction with the Saxonian Ministry of the Environment and the Saxonian State Institute for Environmental Protection.

The test object is a large waste disposal site located near Hoyerswerda. The open cast coal mining in this region created large holes and lowered the groundwater level about 50m. Such a hole was filled with municipal waste during the 70s and 80s. After the closure of the coal mines, the groundwater level raised again, so large parts of the waste disposal site are now under the water level. This results in a large emission of pollutants into the groundwater (Fig. 4.).

This site is especially interesting because of its huge size, which makes extensive investigations acceptable, because of the specific problem situation, which is found quite often in Saxony and Brandenburg, and because of several plausible, but strategically different remediation concepts which have to be compared.

Currently investigations about the value system to be used and for the definition and quantification of remediation concepts are under way.

6. Conclusions

Our research in the field of decision analysis for remedy selection is a logical extension of previously started work on hazard estimation. It is planned to continue the successful work in both fields and to join them as close as possible.

Although decision analysis has a great potential for supporting the responsible authorities in the environmental sector, still a lot of work has to be done. Our current investigations are just intended to show the applicability of decision analytic methods for remedy selection and to give hints for necessary extension of decision analysis. It is not the purpose of our current work, to provide a system which can assist any decision-maker in the selection of an optimal remediation concept, although such a system would be a great aid in the remediation sector. If the test case is successful, it is possible, that such a project is initiated by the governmental agencies.

Furthermore efforts are necessary to connect the current hazard assessment system XUMA-GEFA to decision analytic tools. It is even possible to strive for a totally integrated computer system which supports all processing steps of a contaminated site.

The next activities will aim at the completion of the above-mentioned case study. Its results will help us to draw conclusions about the application of decision analytic techniques in the public domain. This knowledge will facilitate the support of decisions in other fields.

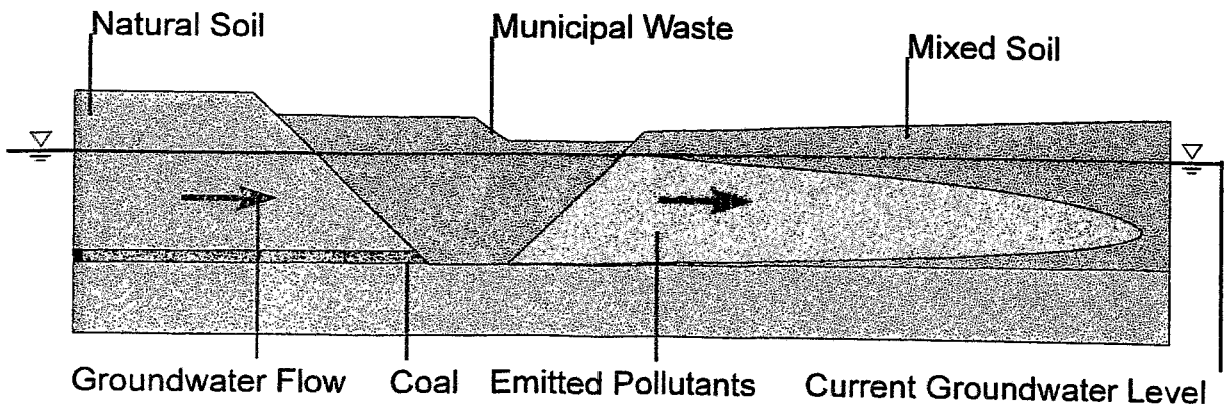

Fig. 4. Waste Disposal Site under Investigation

References

[1] W. Ferse and F. Schröder
"Applied Decision Analysis and Risk Evaluation"
Report FZR 94-68, 65-69

[2] F. Eisenführ and M. Weber
"Rationales Entscheiden"
2nd ed., Springer, Berlin, 1993

[3] Landesamt für Umwelt und Geologie Sachsen
"Handbuch zur Altlastenbehandlung, Teil 3"

[4] J. vonNeumann and O. Morgenstern
"Theory of games and economic behaviour"
2nd ed., University Press, Princeton, 1947

[5] R.L. Keeney and H. Raiffa
"Decisions with multiple objectives"
Cambridge University Press, Cambridge, 1993

[6] J.L. Corner and C.W. Kirkwood
"Decision analysis applications in the operations research literature, 1970-1989"
Op. Res. 39 (1991) 206-219

COMBINED USE OF SOLAR HEAT FOR DOMESTIC HOT WATER AND FEEDING INTO A DISTRICT HEATING NETWORK - DEMONSTRATION FACILITY WALDBLICKSCHULE FREITAL -

D. Brünig and U. Rindelhardt

1. Introduction

In Germany 44 % of the primary energy is used for room heating and for hot water preparing. According to different investigations [1] the use of solar heat is of high potential for heat supply. Today small solar systems are more and more used in one or two family houses. These systems need quite big buffer units for compensating the temporal shift between solar heat delivery and domestic heat demands. This results in high solar energy costs and low system efficiency, respectively. A way to improve the energetic balances consists in connecting large solar thermal systems (of collector areas with more then 100 m^2) to conventional district heating systems of residential settlements. In Saxony for the first time systematic investigations on solar heat feeding into a gas-fuelled district heating system were possible at the demonstration facility Waldblickschule Freital. This pilot solar system was put into operation in June 1994. In this paper the system design is shortly described (see also [2]) and a summary of the first results is given.

The project was funded by the Sächsisches Staatsministerium für Umwelt und Landesentwicklung and has been jointly realised with the township of Freital and the muncipal heat supplier Technische Werke Freital. To optimize solar heat systems and to transfer the gathered experience Forschungszentrum Rossendorf e.V. carries out a long-termed data acquisition and analysing programme.

2. System Design

The collector array of 100 m^2 overall surface was integrated into the roof of the school Waldblickschule directed to S.S.W. and inclined by 36° with respect to the horizontal position. The solar heat output is used for the domestic hot water demand of the school as well as to increase the return flow temperature of the conventional district heating system. The power station of the newly installed system is located in the cellar of the school. It delivers heat for room heating and domestic hot water for the school (including a nursery school) and a residential area with 256 flats.

The solar system consists of four heat circuits connected by heat exchangers. If the solar insolation G exceeds a threshold sufficient for a minimum heat gain the **collector circuit** is activated by the collector pump. The selected low flow of the heat carrier fluid through the collector array, i.e. 1.2 m^3/h, offers a large temperature enhancement. The first heat exchanger transfers the gathered solar heat (Q1) to the **storage circuit**. The storage circuit contains four buffer tanks, each 0.75 m^3 in volume, coupled in series and equipped with devices for automatic thermal layer loading to reduce temperature layer mixing in the store. An example of the resulting temperature layering in the buffer tanks starting from thermometer T6 in the warmest tank PS4 and ending at thermometer T2 in the coldest tank PS1 is shown in Fig. 1.

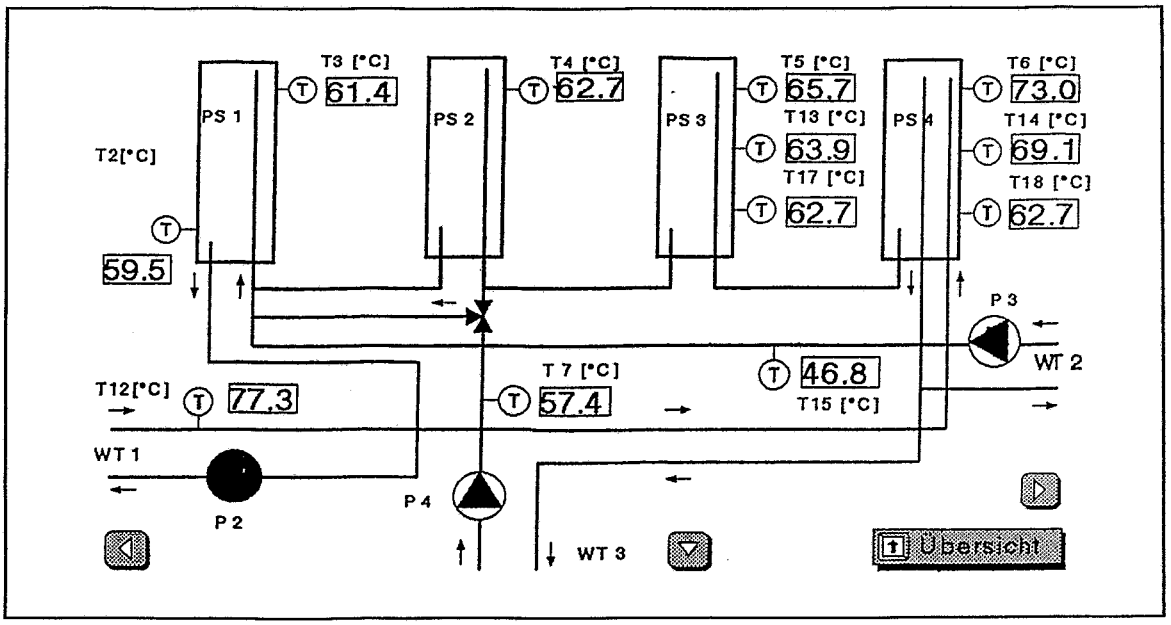

Fig. 1. Temperature layering in the buffer tanks

The stored heat is distributed on two ways:

1.**Preheating of the domestic water for the school:** Via the second heat exchanger the domestic water in the preceding store (Domestic Hot Water Store) 0.4 m³ in size is heated by the solar buffer tanks. The two domestic hot water boilers of the non-solar system, each of 0.5 m³ volume, are fed with the solar preheated water (solar heat Q2) of this preceding store and, if needed, are up-heated by the district network to the final temperature of 60 °C.

2.**Temperature enhancement of the district heating return flow:** The residential area provided by the district heating network has a very high heat demand (approximately 2,1 MW). The flow temperature is higher than the preheating temperature of domestic hot water. Especially during the summer and the weekends the solar collectors produce more heat than needed for the daily demand of the school (60 kWh). Temperatures up to 100 °C may be reached. At a third heat exchanger the solar surplus heat is transferred to the district heating system by raising its return flow temperature (heat Q3).

The solar system is controlled by a freely programmable operation control. It additionally handles the data acquisition and storage as well as the data transmission via modem to Rossendorf. This data link enables also the direct changing of the system control parameters for investigating the resulting effects on the system efficiency.

3. Results

During summertime approx. 80 % of the generated solar energy has been fed into the district heating network. Fig. 2 shows the time dependence of different system temperatures and of the insolation G during a sunny day in July (compare [3]).

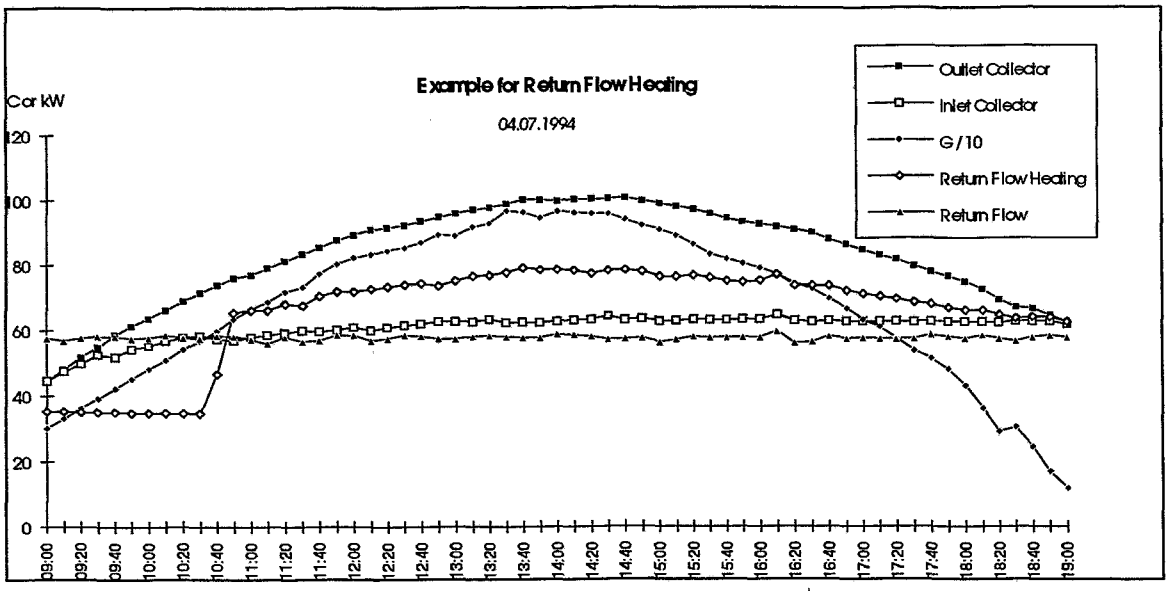

Fig. 2: Return flow heating during a sunny day

The energetic results of this day can be characterised by the following values:

•Total irradiance on the absorber surface:	G = 647 kWh
•Heat carried by the collector circuit:	Q1 = 273 kWh
•Solar efficiency of the collector array:	42 %
•Maximum temperature difference in the collector circuit:	37°C
•Domestic water preheating:	Q2 = 18 kWh
•District network feeding:	Q3 = 235 kWh

The collector gain decreases if the system temperature is rising. Therefore, the level of the district heating return flow temperature is the most important factor for the reachable system efficiency. During summer a temperature of 58 °C was measured in the return flow, that is 20 K above the designed value of the system. At the beginning of the flat heating in autumn the return flow temperature lowered, therefore about 55 % of the gathered solar energy in September and October have been fed into the district heating network. The results of the first half year of system operation is displayed in Table 1, that is the period between June and November 1994.

The total efficiency of the collector array during this time was measured to be 31%, the system efficiency (which includes all the energy losses in the buffers and pipes) was measured to be 26 %. Both values are related to the solar insolation on the absorber area.

To reach the projected solar gain of 35 to 40 MWh per year technical changes are needed to lower the return flow temperature. On the base of the gathered system data the real system behaviour can be modelled, and thereby the system control may be optimised. On this way further reserves for a higher system efficiency may be activated.

Month	Collector-gains Q1 kWh	Used for School Q2 kWh	Feeded into District heating net Q3 kWh	Part Q2/Q1 %	Part Q3/Q1 %	Total Solar Insola-tion G kWh	Degree of use Q1/G %	Degree of use $\frac{Q2+Q3}{G}$ %
June	3878	819	2259	27	73	12926	30	24
July	6100	545	4837	10	90	16390	37	33
Aug.	3903	837	2388	26	74	12117	32	27
Sept.	2403	928	1093	46	54	8997	27	22
Oct.	1962	650	907	42	58	7393	27	21
Nov.	752	552	115	83	17	3130	24	21
Sum	18998	4331	11635			60953	31	26

Table 1: First Results from June to November 1994

The projected solar heat prize is about 0.30 DM/kWh without any financial support. This is approximtely 3 times the heat price of conventional systems. With the experiences of the investigated system a solar heat price below 0.20 DM/kWh seems to be possible in new designed systems with similar collector area.

References

[1] Deutscher Bundestag, Drucksache 11/8030, Mai 1990

[2] D.Brünig, F. Naehring, U. Rindelhardt
4. Symposium Thermische Solarenergie, Staffelstein 1994, Tagungsband S. 241

[3] D.Brünig, U. Rindelhardt
Terratec '95, Kongreß West-Ost-Transfer Umwelt, 1. - 3.3.1995 in Leipzig,
Tagungsband S. 156, B.G. Teubner Verlagsgesellschaft

MAGNETOHYDRODYNAMIC FLOW PHENOMENA

G.Gerbeth, G. Mutschke, S. Eckert

1. Introduction

The MHD group of the Institute of Safety Research performs basic studies on fluid dynamics and heat/mass transfer in fluids, particularly for electrically conducting fluids (liquid metals) exposed to external magnetic fields (Magnetohydrodynamics - MHD). Such a contactless influence on transport phenomena is of principal importance for a variety of applied problems including safety and design aspects in liquid metal cooled fusion reactors, fast reactors, and chemical systems. Any electrically conducting flow can be influenced without any contact by means of an external electromagnetic field. This, of course, can change the known hydromechanically flow patterns considerably. In the following two examples of such magnetic field influence are presented.

2. MHD Flow around a Cylinder

Fluid flows around obstacles determine in many applied cases the heat/mass transfer rates. The fluiddynamic standard problem of the flow around a circular cylinder serves as the generic problem for any studies in that field. This flow problem is extensively documented in literature. However, the relevance of 3d-effects along the cylinder axis was only recently detected and analysed.

We study this type of flow for the case of a liquid metal flow exposed to an external magnetic field [1]. In this situation there is besides the usual Reynolds number a second control parameter for the flow dynamics: The interaction parameter which is proportional to the square of the magnetic field strength. Depending on the magnetic field direction a variety of specific influences arises due to the magnetic field action. If the magnetic field is parallel to the oncoming flow a stabilization, i.e. the suppression of the Karman vortex street (Fig. 1a), is produced by the magnetic forces [2]. However, the magnetic field is not able to fully relaminarize the flow, standing eddies are always present how strong the magnetic field might be. This result is shown in Fig.1b. Only in the case of a magnetic field directed perpendicular to the flow and to the cylinder axis a full relaminarization is posssible as shown in Fig.1c. The results shown in Fig.1 were obtained by a 2d numerical simulation. They correct considerably the simulations available in literature up to now [2,4]. The most interesting aspects, however, are connected with a full 3d view on the problem [4]. In this case a list of interesting phenomena must be expected from general MHD principles:

- 3d-instabilities before 2d due to the break of the hydrodynamic Squire theorem,
- suppression of 3d instabilities if the magnetic field is parallel to the cylinder axis,
- occurence of new instabilities for a growing magnetic field strength in strong contradiction to the usually assumed damping action of steady magnetic fields transverse to cylinder axis.

The extension of the present 2d code to the general 3d case is the logical next step but requires huge calculating ressources.

In addition first MHD wake flow measurements were performed at the mercury facility of IMG Grenoble showing clearly the Karman vortex street suppression, but also an unexpected tendency for longwave instabilities [3].

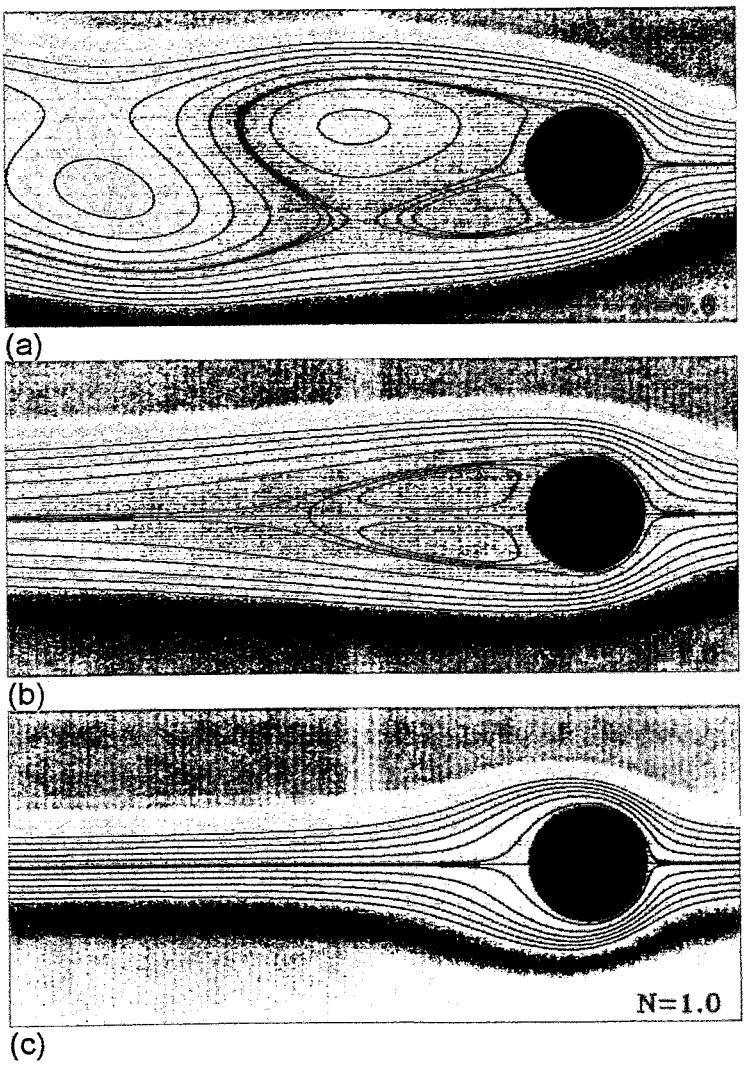

Fig. 1: 2d MHD flow around a circular cylinder at Re = 100
(a) unsteady flow, N = 0
(b) steady flow, aligned field, N = 1
(c) steady flow, transverse field, N = 1

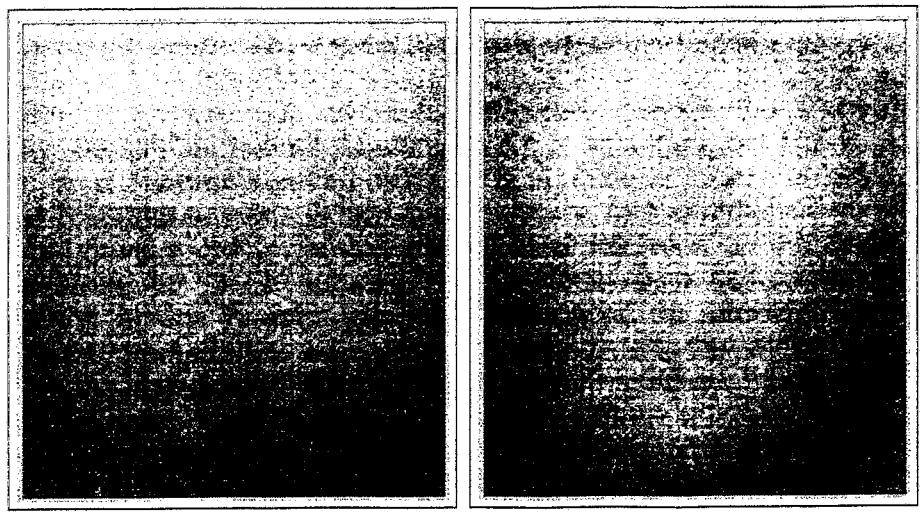

(a) Ha = 0, N = 0

(b) Ha = 600, N = 19

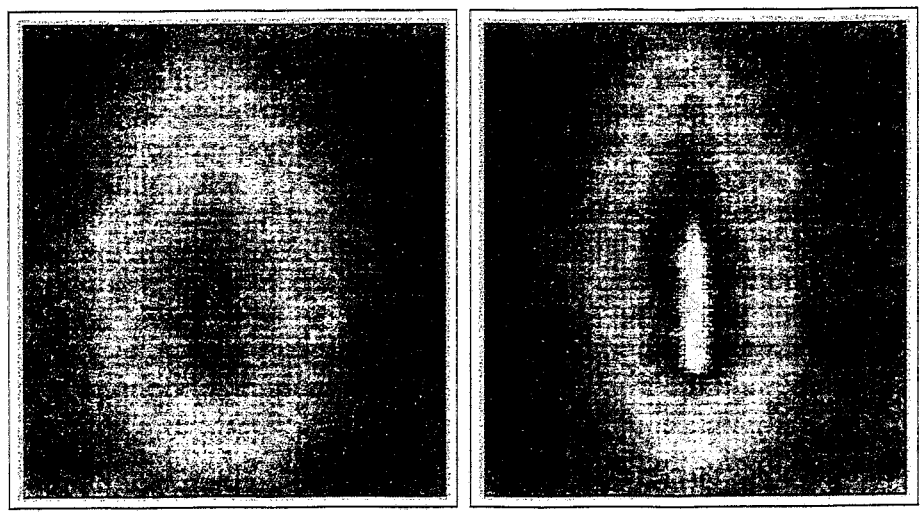

(c) Ha = 1200, N = 78

(d) Ha = 1505, N = 122

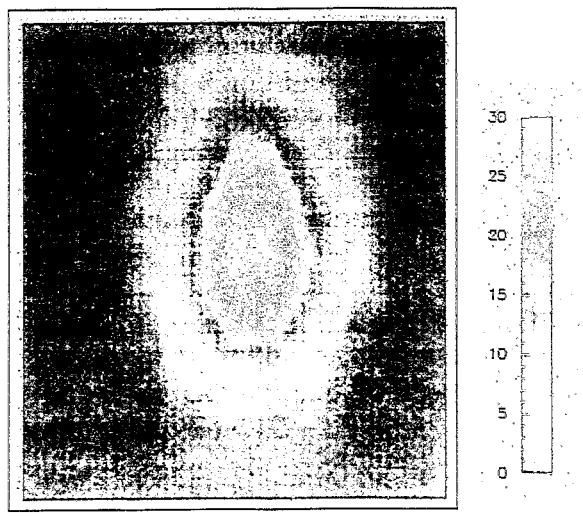

(e) Ha = 2110, N = 239

→ direction of the B-field →

Fig. 2:
Meas. void fraction distributions in a vertical sodium/argon flow at Re =18600,
strong anisotropic dispersion due to the magnetic field action

3. Anisotropic transport in strong magnetic fields

Application of an external magnetic field can change the transport mechanism drastically. Usually an overall damping effect is assumed, but this is not correct. The magnetic field redistributes the vortices leading to a highly anisotropic turbulence structure. This phenomenon is known in literature as two-dimensional MHD turbulence [7]. It could have a distinctive and even crucial influence on the Blanket design of a liquid metal cooled fusion reactor. The possibility of a self-cooled liquid metal (Li) Blanket for a Fusion Reactor strongly depends on the problem which rate of heat transport away from the first wall can be realized. Due to the strong magnetic fields in a TOKAMAK the liquid metal Blanket design was based on the assumption of a fully relaminarized flow due to the turbulence damping of the magnetic forces. In that case a liquid metal Blanket is not possible since the required flow rates would lead to extraordinary pressure drops in the flow channels. However, this picture was not a correct one: Even in very strong magnetic fields turbulence can persist, namely, vortices parallel to the magnetic field direction. Based on a physical understanding of this remaining turbulence special means for its intensification can be proposed.

To measure these transport phenomena experiments were performed and prepared at the sodium test facility of the MHD group [5-7]. At one test section bubbles are injected through a single orifice into the center of the vertical test section. Local measurements of the void fraction appr. 30cm above the injection point give a clear picture of the magnetic field influence on the bubble dispersion. Fig. 2 shows such measuring results, particularly the anisotropic action of the magnetic field. A more sophisticated heat transport test section is in preparation now. The goal is to demonstrate that the heat transport rate away from a heated wall can be higher compared to the fully relaminarized case by a factor of 3...6. The bubble measurements are in accordance with such a transport enhancement.

References:

[1] G.Gerbeth, A.Alemany
"Magnetohydrodynamic flow around a circular cylinder"
H.Eckelmann, J.M.R.Graham, P.Huerre, P.A.Monkewitz (Eds): Bluff body wakes, dynamics and instabilities, Springer 1993, 51-54

[2] V.Shatrov, G.Mutschke, G.Gerbeth
"Numerical simulation of the two-dimensional MHD flow around a circular cylinder"
Proc. of: Int. Conference on "Energy Transfer in MHD Flows", Aussois (France), Sept. 1994, 745-756

[3] T.Weier, G.Mutschke, G.Gerbeth, A.Alemany, A.Pilaud
"Stability of MHD flow around a cylinder in an aligned magnetic field"
Proc. of: Int. Conference on "Energy Transfer in MHD Flows", Aussois (France), Sept. 1994, 561-570

[4] G.Mutschke, G.Gerbeth
"Control of the cylinder wake instabilities by an external magnetic field"
Lecture at: American Physical Society, 47th Annual Meeting of the Division of Fluid Dynamics, Atlanta, 1994; Bulletin of the American Physical Society, Series II, Vol.39, No.9, 1994, p. 1979

[5] G.Gerbeth, S.Eckert, H.Langenbrunner
"Dispersion of gas bubbles in a two-dimensional MHD turbulence"
Magnetohydrodynamics, No.4, 1994, 678-682

[6] S.Eckert, G.Gerbeth, G.Mihalache, J.-P.Thibault
"Influence of external magnetic fields on slip ratio in LMMHD two-phase flow"
Proc. of: Int. Conference on "Energy Transfer in MHD Flows", Aussois (France), Sept. 1994, 607-616; Magnetohydrodynamics No.3, 1995

[7] S.Eckert, G.Gerbeth, H.Langenbrunner, W.Witke, O.Lielausis, I.Platnieks
"Anisotropic transport in MHD turbulence: Experimental results using small gas bubbles as local tracers"
Proc. of: Int. Conference on "Energy Transfer in MHD Flows", Aussois (France), Sept. 1994, 787-799; Magnetohydrodynamics No.3, 1995

The projects this report are based on are funded by the DFG (Deutsche Forschungsgemeinschaft) and are registered with No. Ge 682/3-1 and No. Ge 682/4-1, and by the DAAD (Deutscher Akademischer Austauschdienst) in frame of the PROCOPE programme and from the European Fusion Technology Programme under KfK-BLMH-D.
The authors are responsible for the scientific content of the report.

CALCULATION OF NEUTRON NOISE DUE TO CONTROL ELEMENT VIBRATIONS USING NODAL METHODS FOR HEXAGONAL-Z-GEOMETRY

F. Hollstein

1. Introduction

In a NPP with VVER-440 type reactors, the control element vibrations are most important sources of neutron flux fluctuations [1]. There are 37 control elements in a VVER-440 core (Fig.1). The control elements essentially consist of absorber and fuel part connected by a hinge. The channel surrounding a control element is formed by the neighbouring fuel elements.

The source of the neutron noise is the varying water gap in the control element channel. The varying water gap can be provoked by core barrel motion, by random pressure fluctuation in the coolant and/or random impact forces. The impact frequencies can be used as an indicator for the mechanical integrity of the control elements [2].

To realize the interpretation of measured incore neutron detector signals the transfer functions of the reactor must be known. The purpose of the present work is to describe briefly a new 3D-model to calculate the transfer functions. Based on numerical investigations properties of the transfer functions are discussed.

2. Model

To study the properties of the transfer functions the code NOISE_3D has been developed. It is based on the modified one-group diffusion equation for the stationary neutron flux density and the so called prompt-response-approximation [3] of the one-group diffusion equation for the neutron flux noise (1) in standard notation:

$$div\ \delta\vec{j} - \Sigma^R \left(\frac{k_{00}}{k_{eff}} (1-\beta) - 1 \right) \delta\Phi = \delta Q \qquad (1)$$

The explanation of the noise sources δQ is given later. To solve the diffusion equations the reactor is divided into nodes with hexagonal cross sections [4] (Fig. 2). For a fuel node, the material distribution is space independent. All parameters are averaged over the node volume. The control elements are movable in their channels. Especially the varying water gap width causes the neutron noise. Thus, the water gap is taken into account for a control element node (Fig. 3).

$$\sum_{k=1}^{8} \frac{F_k}{V} \delta\bar{j}_k + \Sigma^R \left(1 - \frac{k_{00}}{k_{eff}} (1-\beta) \right) \delta\bar{\Phi} = \delta\bar{Q} \qquad (2)$$

The nodal balance equation (2) is obtained by integrating the diffusion equation over the volume V of a node where neutron current and flux are averaged values over volume and surface. F_k means the surface area of node side number k (k=1..6 refer to radial surfaces, k=7,8 stand for top and bottom of the node). The surface averaged neutron current is divided into partial currents δj^+ and δj^- (3,4). As usually the index "+" denotes the partial out-going and the index "-" the in-coming current respectively.

$$\delta \bar{j}_k = \delta j^+_k - \delta j^-_k \qquad (3)$$

$$\delta j^{\pm}_k = \frac{1}{4F_k} \int df_k \left(\delta\Phi \mp 2D \frac{\partial}{\partial n_k} \delta\Phi \right) \qquad (4)$$

It is necessary that the partial currents are smooth functions across the node surfaces. To obtain a relationship between in-coming and out-going currents the diffusion equations are solved approximately using Fick's law. First the space dependence of the flux inside the node is separated into the axial dependency and the radial dependency using cylindrical approximation [4]. After some mathematics the response relation is obtained by introducing the response matrix **R** and the source matix $\delta\mathbf{q}$ (5):

$$\delta j^+_k = \sum_{n=1}^{8} R_{kn} \, \delta j^-_n + \delta q_k \qquad (5)$$

Due to the special construction of a control element in VVER-440 type reactors, two different methods are developed to determine the noise sources. For the fuel part the noise source is described as a surface source induced by material fluctuation in the water gap (6):

$$\delta \bar{Q}_F = \delta R \sum_{k=1}^{6} c^k_F \cos\left((k-1)\frac{\Pi}{3} - \varphi \right) \bar{\Phi}_{0k} \qquad (6)$$

δR is the distance and φ is the direction of random control element motion according to Fig. 4. The factor c^k_F depends on the different macroscopic cross sections in the fuel region and the water gap of the node. It should be noticed that both the radial surfaces of the control element nodes and the common radial surfaces of the adjacent fuel element nodes are sources of the neutron noise in the reactor. If the control element node and an adjacent fuel node consist of different fuel, the perturbation of the neutron current is discontinuous across the common surface.

The absorber part of a control element is considered to be a black absorber for thermal neutrons and to be transparent for fast neutrons [5,6]. The noise source will be induced by random displacement of the "black absorber" surface.In (7) L_H^0 holds for the modified one-group extrapolation length for the stationary flux.

$$\delta\bar{Q}_A = \delta j^- - \frac{L_H^0 - 2D}{L_H^0 + 2D}\delta j^+ - \frac{c_A}{L_H^0 + 2D}\, j\, \delta x_s \qquad (7)$$

The constant coefficient c_A only depends on the material properties in the (water filled) absorber node. δx_s is the varying water gap width. It should be noted that the noise source appears in the balance equations for adjacent nodes only. The source can be interpreted as a perturbation of the thermal back scattering due to random displacements of the common node surface.

The neutron noise $\delta\Phi$ in a special node with the co-ordinates $d=(d_x,d_y,d_z)$ is determined by eq. (8):

$$\frac{\delta\phi(d,s)}{\phi_0(d)} = h_x(d,s)\,\delta x + h_y(d,s)\,\delta y \qquad (8)$$

$h_x(d,s)$ and $h_y(d,s)$ mean the transfer functions for the mechanical displacements δx and δy at the source node located at $s=(s_x,s_y,s_z)$.

3. Numerical Results and Conclusions

To study the properties of the transfer functions and the stationary flux distribution for a given fuel assembly the code NOISE_3D has been used for many test calculations. Three different kinds of fuel nodes are considered, denoted in following by numbers „1" to „3" which refer to different enrichments (k_{00}=0.94, 1.08 and 1.2). Nodes of the (water filled) absorber part and nodes of the reflector are denoted by „4" and „r" respectively. Two kinds of fuel loadings are considered: the homogeneous loading where all fuel nodes consist of material of kind „2" and the heterogeneous loading with enrichments according to Fig. 5. It is assumed that only control elements of the group number 6 are inserted. Insertion depth is indicated by n_T.

As an example for stationary calculations the control element worth was calculated for the homogeneous loading (Fig. 6). The result corresponds very well with the known estimation for the homogeneous cylindrical reactor [7].

To estimate neutron noise, the transfer functions h_x and h_y were calculated for many possible combinations of „source node" and „detector node" positions. Examples are represented in Figs. 7 and 8. Summarizing the results the following conclusions can be drawn:

- The influence of the non homogeneous fuel loading on the transfer functions is very complex. As in the 2D case of stochastic fuel part vibrations [8] for this kind of noise sources the transfer functions can change their sign depending on boronconcentration. For stochastic absorber part vibrations no changes of the sign of transfer functions occur. This is due to the independence of the noise sources on changes of material properties in the water gap.

- Normally the reactivity changes generated by control or fuel element vibrations can by neglected against the space dependent dipol term of the transfer functions. This is at least valid in the frequency range 0.1 .. 10 Hz.

- At first look the dependence of the transfer functions from the axial co-ordinate is almost the same as for a 1D calculation. However, an independent treatment of the „axial" and the „radial" problem is not possible because of the strong space dependence of axial and radial buckling in the one-group consideration.

References

[1] E. Altstadt, G. Grunwald, P. Liewers, P. Schumann and F.-P. Weiß
Proc. JAHRESTAGUNG KERNTECHNIK '94, 159-162, Stuttgart 16.-19.5.1994

[2] G. Hessel, P. Liewers, W. Schmitt, P. Schumann and F.-P. Weiß
Nuclear Safety 29(1988)3 293-306

[3] E. Kleiss and H. van Dam
Annals of Nuclear Energy 6(1979) 385-398

[4] U. Grundmann and U. Rohde
Report FZR 93-01, 1993

[5] R. Barthel
Kernenergie 25(1982)4 163-166

[6] F. Hollstein
Report FZR-52, 1994

[7] K. Meyer
Introduction to Reactor Physics, unpublished

[8] D. Lucas
Kerntechnik 57(1992)5 317-321

[9] F. Hollstein and K. Meyer
Proc. SMORN VII, Vol. II-12.1, Avignon 19.-23.6.1995

The project this report is based on is funded by SMWK (Sächsisches Staatsministerium für Wissenschaft und Kunst) and is registered with No. 4-7541.83 FZR/307. The author is responsible for the scientific content of the report.

Appendix

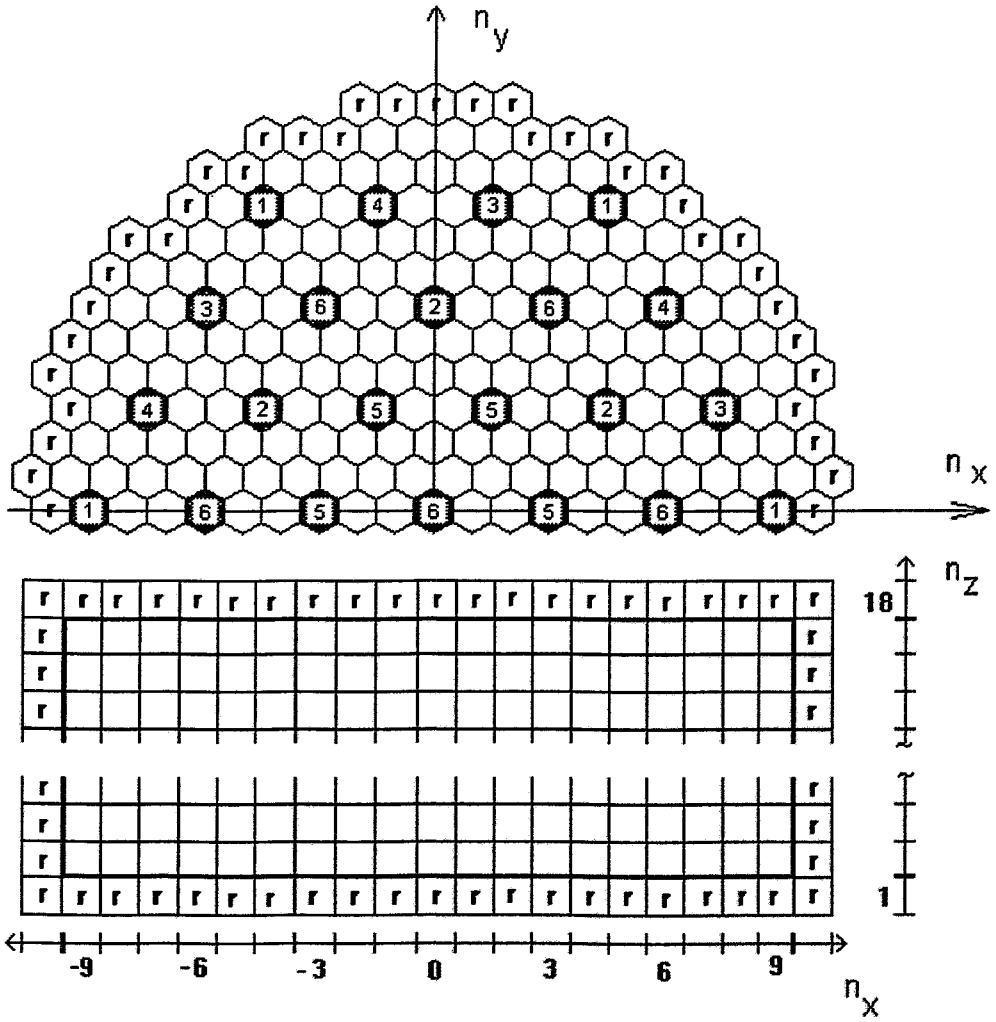

Fig. 1: Scheme of (half) cross-section of VVER-440 type reactor ; r denotes reflector nodes; n_x, n_y and n_z refer to co-ordinates of a node and 1 ..6 hold for number of control element group respectively

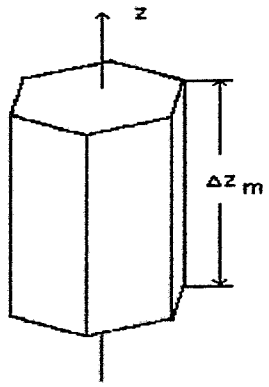

Fig. 2: Hexagonal node

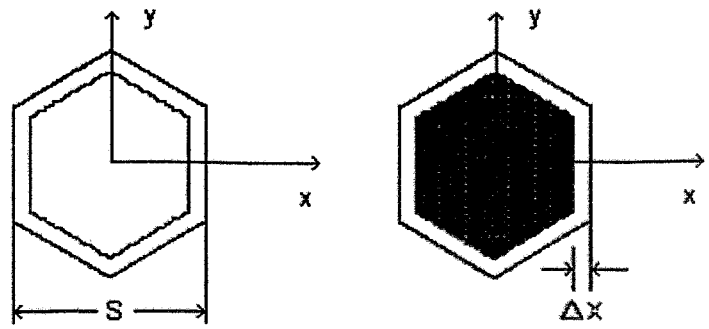

Fig. 3: Scheme of cross section of an absorber node with water gap; Δx refers to the gap width

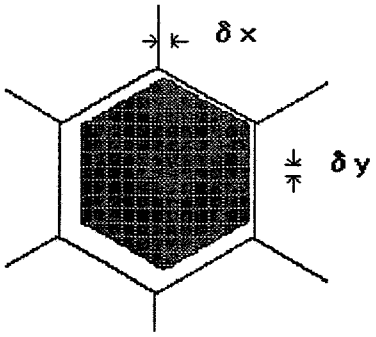

Fig. 4: Scheme of random displacement of a control element

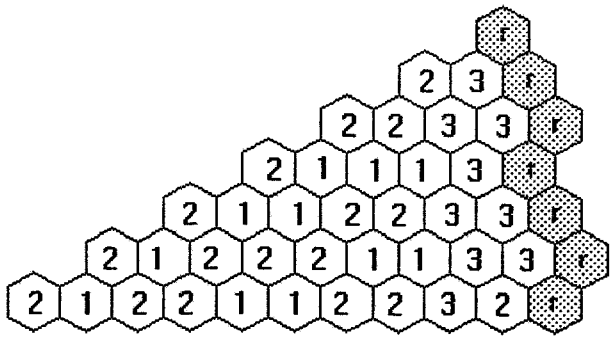

Fig. 5: Heterogeneous test fuel assembly (1/12 anti-symmetric)

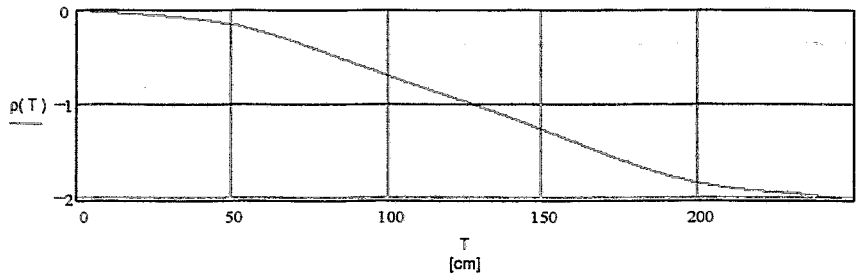

Fig. 6: Reactivity in $ as function of control element inserting length T (group number 6)

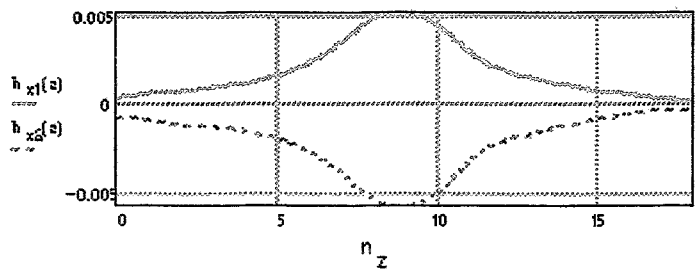

Fig. 7:

Transfer function h_x as function of source position (n_T =0):

h_{x1}: s=(0,0, 1 .. 18) d=(1,0,9)
h_{x2}: s=(6,0, 1 .. 18) d=(5,0,9)

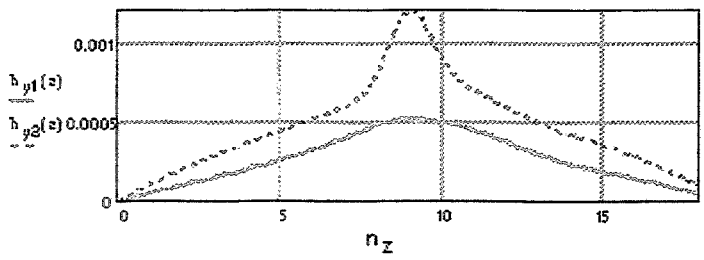

Fig. 8:

Transfer function h_y as function of source position (n_T =0):

h_{y1}: s =(0,0, 1 .. 18) d=(5,3,9)
h_{y2}: s =(6,0, 1 .. 18) d=(5,3,9)

Abstracts of Publications

PUBLICATIONS IN SCIENTIFIC AND TECHNICAL JOURNALS AND IN CONFERENCE PROCEEDINGS

Altstadt, E.; G. Grunwald
Analytical and Experimental Investigations for Modelling the Fluid-Structure-Interaction in Annular Gaps
Proc. Jahrestagung Kerntechnik 1994
Stuttgart, 17. - 19. Mai 1994

Modelling the mechanical vibrations of pressurized water reactor internals the fluid-structure-interaction is to be taken into account. Especially at VVER-440 reactors there is a strong influence of the fluid due to the specific geometry. The intention of the presentation is to provide a solution of the continuity and the Navier-Stokes equations for the special case of a narrow annular gap geometry considering the fluid friction.
To obtain an analytical solution for these coupled 3D partial differential equations further assumptions and simplifications must be made:
- the width of the annular gap is small compared with the diameter,
- displacements of the mechanical structure are small compared with the gap width
- the fluid flow velocity components are independent on the radius.

Keeping these assumptions in mind one can reduce the dimension of the continuity equation from 3D to 2D by averaging over the gap width.
Two elementary types of motion of the cylinder are considered: parallel displacement and pendular motion. By superimposing these elementary types even more general motions can be described.
In practice the application could be meaningful for core barrel motion at LWRs in general and for flow induced vibrations of control elements at VVER-440 reactors.
The analytical results are compared with experimental ones from a cylindrical pendulum setup. The criteria of comparison are the eigenfrequency and the damping of the pendulum in the static and flowing fluid. There is a good agreement between analytical and experimental results. Especially the strong influence of the chosen boundary condition upon the pressure equations can be shown.

Altstadt, E.; M. Scheffler, F.-P. Weiß
Component Vibration of VVER-Reactors - Diagnostics and Modelling
In: Progress in Nuclear Energy 1994

Flow induced vibrations of reactor pressure vessel (RPV) internals (control element and core barrel motions) at VVER-440 reactors have lead to the development of dedicated methods for on-line monitoring. These methods need a certain developed stage of the faults to be detected. To achieve a real sensitive early detection of mechanical faults of RPV internals, a theoretical vibration model was developed based on finite elements. The model comprises the whole primary circuit including the steam generators (SG). By means of that model all eigenfrequencies up to 30 Hz and the corresponding mode shapes were calculated for the normal vibration behaviour. Moreover the shift of eigenfrequencies and of amplitudes due to the degrada-

tion or to the failure of internal clamping and spring elements could be investigated, showing that a recognition of such degradations even inside the RPV is possible by pure excore vibration measurements. A true diagnostics, that is the identification of the failed component, might become possible because different faults influence different and well separated eigenfrequencies.

Barz, H.-U; B. Böhmer, J. Kohnheiser
Neutron Fluence Calculations and Spectrum Adjustments for the Rheinsberg Pressure Vessel Steel Irradiation Program
Proc. Jahrestagung Kerntechnik 1994
Stuttgart, 17. - 19.Mai 1994

The starting point of these investigations is the performed irradiation program for the Rheinsberg reactor for 3 different reactor periods during 1984 to 1988. In this program a great number of steel specimens were irradiated at different positions. Additionally a certain number of activation monitors were installed. For the planned mechanical testing of these specimens information about the irradiation condition is needed. Therefore the neutron fluences at the different irradiation points have to be calculated for all relevant reactor periods. Spectrum adjustment is used to check and correct calculational results taking activation measurements into consideration.

Block, F.R.; R. Dittmer, G. Gerbeth
Electromagnetic Detection of Nonconducting Inclusions in a Liquid Metal Flow
Electromagnetic Processing of Materials Conference EPM 94,
Nagoya (Japan), Oct. 1994, Proceedings published by ISIJ Japan, 1994
pp. 61 - 67

The paper describes a first experimental test of a new electromagnetically based bubble detection method in an electrically conducting fluid. A reliable and continuous bubble detection method is important for a lot of liquid metal flows, in particular, flows of reactive liquid metals like sodium or lithium. Moreover, the method is suitable for the detection of any inhomogeneity having different electrical conductivity compared to the bulk flow.
The experimental approach for the detection of inhomogeneities was developed at RWTH Aachen for an early slag detection in steel production. The method is based on the fact that a primary electromagnetic field is changed by the motion of an electrically conducting fluid. This change is very sensitive to any inhomogeneities in the flow which have a different electrical conductivity compared to that of the fluid. The signals of suitably arranged secondary coils are evaluated in order to separate the influence of the inhomogeneity. In the experiments performed at the sodium facility of RCR it was possible to detect single bubbles which were of diameters in the range 0.5 - 2 mm.
Compared to usual, mainly acoustically based detection methods the following advantages of the electromagnetic approach are obvious:
- No time delay between bubble occurence in the coil region and the signal.
- High sensitivity up to single bubble detection.
- Contactless method. No need to install sensors at hot walls, even a thermal isolation between the coils and the channel is possible.

- Every flowing bubble is detected whereas acoustic methods are able to detect acoustically active bubbles only.

The results of the experiment convincingly show the efficiency of such an electromagnetic detection method.

Böhmert, J.; H.-W. Viehrig
Irradiation Programme in the Rheinsberg VVER-2 Reactor to Evaluate the Susceptibility of Russian Reactor Pressure Vessel Steels against Neutron Embrittlement
Jahrestagung Kerntechnik, Stuttgart, 17. - 19. Mai 1994, Proc. p. 388 - 391

An extensive irradiation programme was performed in the Rheinsberg VVER-2 reactor from 1984 to 1988. The programme comprised 25 different heats from base and weld metal of VVER-440- and 1000-type reactor pressure vessel steels using specimens of various geometry (CT, COD, tension, Charpy-V). It was focused on validating of the safety assessment procedure and on determining of fracture mechanics parameters in their dependence on fluence and thermal annealing.
At present the investigation of the irradiated specimens is still mainly outstanding. In the unirradiated state all investigated VVER-type steels show good toughness and strength properties and are comparable with A 533 class 1 and A 508 class 3 steels. The scattering between the different heats of the same material is partly large and does not correlate with the chemical composition or the heat treatment. The results of irradiated specimens tested up to now do not always confirm the conservativeness of the values which are obtained on the base of the valid safety assessment procedure. That supports the urgency to extend the data base for irradiated VVER-type pressure vessel steels.

Bojarevics, A.; Yu Gelfgat, G. Gerbeth
Thermocapillary Connection in a Liquid Metal under Influence of the Magnetic Field - Experimental Techniques and Results of the Tests
Proc. Energy Transfer in MHD Flows, Aussois France, Sept. 1994
pp. 117 - 126

Thermocapillary convection in low-Prandtl-number fluids up to now remains insufficiently experimentally studied due to difficulties to realize free surface conditions on liquid metals. A novel technique has been developed to produce small sized easily transportable deep vacuum containers filled with a thin layer of gallium under a transparent glass window. The first tests showed that the free surface of the liquid gallium did not deteriorate during a period of up to 45 days. The flow pattern on the free surface, while point heating the bottom of the container, has been demonstrated. The temperature gradient on the free surface of the liquid gallium caused surface relief deformations of an order up to 10 - 100 microns. Video recordings of the tracer particle motion on the free surface of liquid gallium due to thermal convection and surface relief deformations due to changes in heating conditions has been made. The presence of the thermocapillary convection has been demonstrated.

Brünig, D.; F. Naehring, U. Rindelhardt
Feeding Solar Heat into Conventional District Heating Networks
Energieanwendung, Energie- und Umwelttechnik 43, 1994, S. 445 - 448

Solar heat from large-scale solar collector plants will be effectively used by feeding it into existing or planned district heating networks, particularly if the feeder point is at low temperature. The ways towards high solar energy gain by such systems are outlined and illustrated by newly built plants.

Brünig, D.; F. Naehring, U. Rindelhardt
Solar Warm Water Heating and Feeding Solar Surplus into the Return Flow of a District Heating System
Proc. 4. Symposium Thermische Solarenergie, Kloster Banz, 09. - 10. Juni 1994, S. 241 - 245

A model project for integrating a large-scale solar heating plant into a district heating system is presented. This project includes the installation of a solar heating plant with 100 m² collector area and the realization of a measurement programm. The measured temperatures and other parameters will be used for improving the controling system and the enhancement of the solar energy generation. The plant consists of four solar buffer tanks, the low flow principle is used in the collector field.

Brünig, D.; U. Rindelhardt
Solarwärme - Einbindung ins Fernwärmenetz wird in Sachsen erprobt
In: Sonnenergie und Wärmetechnik, 5/19/94, S. 21 - 22

Die im Juni 1994 in Betrieb genommene solarthermische Anlage mit 100 m² Kollektorfläche ist ein sächsisches Modellvorhaben. Neben der üblichen solaren Trinkwarmwasserbereitung - hier für die Schule - steht die Einspeisung von Solarwärme in ein neugeschaffenes gasbeheiztes Fernwärmenetz im Mittelpunkt eines Langzeitmeß- und analyseprogramms des Forschungszentrums Rossendorf. Die Solaranlage arbeitet nach dem Low-Flow-Prinzip der Kollektordurchströmung in Verbindung mit einer selbstregelnden Speicherschichtbeladung. Regelung und Meßdatenerfassung werden durch eine DDC-Anlage realisiert.

Daniels, W.; J. Kuntzsch, U. Rindelhardt
Wind Energy Ressources in Saxony: An Experimental Approach
Proc. European Wind Energy Association Conference, Thessaloniki, Greece, 10. - 14. Oktober 1994, pp. 238 - 243

In 1991 a special programme was initiated by the Saxonian Environmental Ministry to estimate the wind energy potential in Saxony and to identify sites for economic operation of wind energy converters.
In the frame of the programme 16 wind measuring stations were installed, more concentrated in orographically complicated regions. The wind speed was measured at two heights between 10 m and 36 m above ground level. Ten-minutes-averaging-values of wind velocity and direction were recorded over a time of minimally one

year.
The Danish Wind-Atlas Program WASP was applied to calculate wind atlas libraries from the measured wind data. The atlas library represents the regional wind climate of the measuring station. Since WASP was developed mainly for coast and lowland regions far from mountains, special efforts were necessary to estimate the region of representance in Saxony. It could be shown, that in lowland regions the area of representance regions in some cases was comparable with WASP results from coast regions. Especially in the mountain region of the "Erzgebirge" the representance regions were found to be very small. By means of atlas libraries the wind power density in the northern part of Saxony was calculated.
On the basis of these investigations the wind energy potential of Saxony could be estimated. Totally 500 usable sites were identified with an average number of 5 500-kW-wind turbines at each site. Using this capacity a yearly energy production of 2200 GWh seems to be possible.

Eckert, S.; G. Gerbeth, H. Langenbrunner, W. Witke, O. Lielausis, I. Platnieks
Anisotropic Transport in MHD Turbulence: Experimental Results Using Small Gas Bubbles as Local Tracers
Proc. Energy Transfer in MHD Flows, Conference, Aussois Frankreich, Sept. 1994, pp. 787 - 799
Publication in: Magnetohydrodynamics

It is well known now that in a liquid metal duct flow exposed to a strong transverse magnetic field turbulent fluctuations can persist even when the mean flow can be regarded as laminar with respect to the overall pressure drop. It was also found, that these fluctuations can even be increased under distinct conditions. This effect is in line with the model of two-dimensional MHD turbulence. While 3D turbulence elements are effectively damped by the magnetic field, 2D eddies with axes in the direction of the B-field are not influenced by this damping mechanism. The use of this 2D turbulence allows an enhancement of the heat/mass transport perpendicular to the flow direction without a significant influence on the overall pressure drop.
There is an ongoing research in the FZR MHD group on local transport phenomena in a turbulent LM duct flow exposed to a transverse magnetic field. Measurements were performed at the FZR sodium facility. The advantage of sodium is that high MHD parameters (Ha = 3000, N = 800) can be reached with moderate values of the magnetic field (B = 0.5 T). On the other hand the properties of sodium cause considerable difficulties with respect to any local measurements in such a flow (velocity, fluctuation intensities). Thus the idea was created to use small gas bubbles (argon) as local tracers for the investigation of local transport mechanisms. In the case of our experimental conditions a volumetric gas flow ratio lower than 0.09 clearly indicates a pure bubbly flow regime. The bubbles are injected by means of a single injector in the center of the channel cross section or in the vicinity of a channel wall. The injector was located in the region where the flow enters into the magnetic field. A traversing mechanism allows to move the B-field-region. Single wire resistivity probes are used for measuring the local void fraction and the number of bubbles.
The measured local dispersion of bubbles shows a significant anisotropy which clearly corresponds to the model of 2D MHD turbulence. A special turbulence

promotor (a system of bars) was installed in the magnetic field entrance region. The axis of the bars can be continuously changed between a parallel and a perpendicular orientation compared to the direction of the external magnetic field. Experimental results on anisotropic MHD turbulence will be presented and analysed in terms of 2D MHD turbulence in a duct.

Eckert, S.; G. Gerbeth, G. Mihalache, J.-P. Thibault
Influence of External Magnetic Fields on Slip Ratio in LMMHD Two-Phase Flow
Proc. Energy Transfer in MHD Flows, Conference, Aussois Frankreich, Sept. 1994, pp. 607 - 616
Publication in: Magnetohydrodynamics

LMMHD two-phase flow modelling strongly depends on the accuracy of the constitutive equations and the corresponding closure laws. Several questions rise from various attempts to model these flows. They are mainly connected with the modification of two-phase flow (interfacial dragging, wall friction, apparent electrical conductivity, etc.) due to the electromagnetic forces.
The paper presents a comprehensive survey of the LMMHD two-phase investigations performed at the Rossendorf laboratories using different liquid systems, mercury-air (LEGI-IMG) and sodium-argon (FZR), with quite different properties. The remarkable difference in the material properties allow to reach a wide range of nondimensional parameters.
For theoretical predictions a two fluid model (LEGI-IMG) and a bubbly flow model (FZR) have been developed in order to meet the requirements of the corresponding facilities.
The experiments have been realized in rectangular vertical test sections immersed into a transverse magnetic field. The gas is injected in the entrance region of the magnetic field. The distribution of the local void fraction over the channel cross section was measured by means of single wire resistivity probes. The electrical boundary conditions of the test sections are rather different. While the FZR test section consists of a simple stainless steel channel (thickness of the walls: 5 mm), the LEGI-IMG configuration, which includes segmented copper electrodes and an external load resistance, is more similar to a MHD generator. In the FZR experiment a volumetric quality in the range of 0.06 - 0.09 leads to a pure bubbly flow regime. In contrast to this the LEGI-IMG facility usually is operated with considerably higher gas flow rates.
Experimental results are presented showing the dependence of the mean values of the void fraction, the slip ratio and the gas velocity on the magnetic field strength as well as on the mean sodium velocity. These results are compared with the theoretical curves obtained by the models. One of the main results obtained is a verification of the effect that the slip ratio shows a minimum if the magnetic field is increased from zero to higher values. The second main result is that a theoretical overestimation of the interfacial dragging constitutive law was always identified for the mercury/air pair.

Ferse, W.
The Application of the Expert System XUMA in the State of Saxony
Proceedings of 4th Workshop on Information Management in Nuclear Safety, Radiation Protection and Environmental Protection, GRS-105
Köln, Januar 1994

In the last years contaminated sites have become a relevant problem in the Federal Republic of Germany because there exist a large number of these sites. That's why in Germany more intensive efforts are undertaken in order to start necessary remediations. Basic initial conditions for an effective execution of these works are on the one side a systematic registration of these sites and on the other side the creation of a uniform evaluation capability for the assessment of environmental hazards.

Regarding this background the Research Centre Rossendorf (FZR) together with Nuclear Engineering and Analytics, Inc. Rossendorf apply and modify the computer code system XUMA (German synonym for expert system on environmental hazards of contaminated sites) which is a joint project of the Institute for Applied Information Science of the Karlsruhe Nuclear Research Centre and the State Institute for Environmental Protection of Baden-Württemberg. XUMA is a knowledge based computer system, which shall support the staff of the responsible governmental offices in the uniform evaluation of the hazard potential, the preparation of analysis plans, and the assessment of contaminated sites and mines.

To enable the registration and evaluation of contaminated sites at engineering offices FZR developes an interface program which can be generated automatically from the knowledge base of the expert system XUMA. This interface program can be executed at each IBM-compatible PC without any additional runtime environment.

Futterschneider, H.; H. Morgenstern, U. Rindelhardt
Solar betriebene netzunabhängige Meßstation - Energiebilanzen eines einjährigen Betriebes
Proc. 9. Internationales Sonnenforum
Stuttgart, 28. 06. - 01.07. 1994, S. 1243 - 1250

Für die dosimetrische Umgebungsüberwachung des Forschungsstandortes Rossendorf wurden zwei solar betriebene netzunabhängige Meßsysteme konzipiert und in einem einjährigen Meßzyklus erprobt. Eine wesentliche Forderung bestand in der Gewährleistung einer 100%igen Versorgungssicherheit der Meßsonden.
Die energetisch relevanten Ergebnisse dieser Langzeiterprobung werden diskutiert. Zur Analyse der Energiebilanzen wurden die 10-Minuten-Mittelwerte von Mudolstrom und -spannung, Batteriestrom und -spannung, der jeweilige Laststrom und die solare Einstrahlung gemessen. Beide Systeme liefen auch im sehr einstrahlungsarmen Winter 1993/94 ohne Ausfall. Die vollständige Jahresbilanz des Systems 1 ergab einen reinen Solarbetrieb während 3022 h, einen Batteriebetrieb während 4686 h und in der restlichen Zeit einen Mischbetrieb.
Die gewählte Dimensionierung der beiden photovoltaischen Energieversorgungssysteme erwies sich als ausreichend für einen sicheren Betrieb. Die der Auslegung zugrunde liegenden Parameter (spezifische Modulgröße 33 - 41 W_p/W, spezifische

Batteriegröße 33 d) können für Systeme mit beliebig großen Lasten verallgemeinert werden.

Galindo, V., G. Gerbeth, D. Langbein, M. Treuner
Unsteady Thermocapillary Drop Migration in a Uniform Temperature Gradient
Proc. Drop Tower Days'94, Bremen, July 1994, pp. 90 - 94

A theoretical analysis of liquid drop unsteady migration under microgravity conditions is presented, for the case of an interfacial tension gradient on the drop surface generated by a uniform temperature gradient in the surrounding liquid. The effect of buoyancy due to a residual gravity vector aligned parallel to the temperature gradient is included. The relevant equations are solved in the creeping flow limit where in the convective transport of momentum as well as that of the energy is neglected, i.e. at low Reynolds and Marangoni numbers. The flow and the temperature field within and around the drop are obtained after transforming the results from the Laplace domain, in which they are derived, to the time domain. The time transient behaviour of the migration speed depends strongly on the choice of the initial flow and temperature fields. The comparison with other initial conditions from the literature is performed.

Galindo, V., G. Gerbeth, D. Langbein, M. Treuner
Unsteady Thermocapillary Migration of Isolated Spherical Drops in a Uniform Temperature Gradient
Microgravity Sci. & Technol. 7 (1994) 3, pp. 234 - 241
München: Carl Hanser Verlag, 1994

A theoretical analysis of liquid drop unsteady migration under microgravity conditions is presented, for the case of an interfacial tension gradient on the drop surface generated by a uniform temperature gradient in the surrounding liquid. The effect of buoyancy due to a residual gravity vector aligned parallel to the temperature gradient is included. The relevant equations are solved in the creeping flow limit where in the convective transport of momentum as well as that of the energy is neglected, i.e. at low Reynolds and Marangoni numbers. The flow and the temperature field within and around the drop are obtained after transforming the results from the Laplace domain, in which they are derived, to the time domain. The time transient behaviour of the migration speed depends strongly on the choice of the initial flow and temperature fields.

Gerbeth, G.; Galindo, V. u.a.
Thermocapillary Bubble Migration at Higher Marangoni Numbers
- Theory and Experiment
1994 Meeting of the Division of Fluid Dynamics, Atlanta, 20. - 22. Nov. 1994, Bulletin of the American Physical Society, Series II, 39 (1994) 9, p. 1841

Single bubble motion driven purely by thermocapillarity (i.e. a linear temperature gradient in the surrounding liquid) is analyzed theoretically with the following steps: A full numerical simulation up to Reynolds numbers of several hundreds depending on the Prandtl-number of the liquid, and a simple analytical treatment describing the asymptotic migration at high Reynolds numbers. Results of short-term microgravity

experiments performed at drop Tower Bremen will be reported for $20 < Re < 160$. The theoretical migration velocities are slightly higher than the experimental values which might be due to the short-time nature of the experiments. An unsteady theoretical analysis will be given explaining, at least in part, the remaining discrepancy between theory and experiment.

Große, M.; J. Böhmert, F. Eichhorn et. al.
ASAXS and SANS Investigations of the Chemical Composition of Irradiation-Induced Precipitates in Nuclear Pressure Vessel Steels
1st European Conference on Synchrotron Radiation in Material Science Chester (UK), 02. - 08. Juli 1994, Nucl. Instr. and Methods, B 97 (1995) S. 487 - 490

The deterioration of the mechanical properties of reactor pressure vessel (RPV) steels during their irradiation in a nuclear power plant is known as neutron embrittlement. The structural reason of the neutron embrittlement of low alloyed RPV steel is the radiation-induced formation of precipitates. Up to now the chemical composition of these precipitates in the VVER 440 type RPV steel 15Kh2MFA are not clarified.
A combination of small angle neutron scattering (SANS) and small angle X-ray scattering (SAXS) using methods of contrast variation were employed to determine the chemical composition of the irradiation-induced precipitates in the 15Kh2MFA steel.
The difference between the scattering intensities from irradiated and unirradiated specimens gives the small angle scattering effect of the radiation damages. Irradiation-induced precipitates were found with a mean diameter of $D = 1...2$ nm. The defect volume fraction is depending on the neutron fluence and amounts 0.1 - 0.35 %.
Information about the chemical composition was obtained by using the magnetic scattering contrast in the SANS experiment and the anomalous scattering contrast in the SAXS measurements.
A scan of the X-ray energy in the range of the V-, Cr-, Mn-, and Fe-K-absorption edges proves that the precipitates are vanadium rich. The scattering density of the precipitates is lower than the scattering density of the matrix.
These facts and the results of the magnetic contrast variation in the SANS experiments are in agreement with the assumption that the irradiation-induced precipitates are vanadium carbides.

Große, M.; F. Eichhorn, J. Böhmert, G. Brauer
Characterization of Irradiation-Induced Precipitates by Small Angle Scattering Experiments
Proc. of the 17th International Symposium on Effects of Radiation on Materials, Sun Valley, 20 - 23. Juli 1994, ASTM-STP

The nature of the irradiation-induced precipitates in the VVER-440-type steel 15Kh2MFA has been investigated by the combination of small angle neutron scattering and anomalous small angle X-ray scattering. By the method of contrast variation information about the chemical composition of the irradiation-induced precipitates was obtained. ASAXS experiments with variation of the X-ray energy near to the

energy of the vanadium K-absorption edge prove the content of vanadium within the irradiation-induced precipitates. The scattering density of the precipitates is lower than the scattering density of the iron matrix. The chemical shift of the vanadium-K_α-absorption-edge and the results of the variation of the contribution of the magnetic scattering in the SANS experiment show, that vanadium does not precipitate in an elementary state. By assuming the precipitates being vanadium carbide these results can be explained in the best way.

Große, M.; F. Eichhorn, J. Böhmert u.a.
Characterization of Nanoscale Precipitates in Reactor Pressure Vessel Steel 15Kh2MFA by Small Angle Scattering Experiments
Proc. EUROMAT'94, Balatonszeplak, Hungaria, 30.Mai.bis 01.Juni 1994
p. 448

The deterioration of the mechanical properties of reactor pressure vessel (RPV) steels during their irradiation in a nuclear power plant is known as neutron embrittlement. The microscopic mechanisms of the neutron embrittlement of low alloy RPV steel are not fully understood.
These mechanisms were investigated at the RPV steel of Russian and Czech type 15Kh2MFA. This steel differs from ASTM type A503 or A533 steels mainly in its contents of the carbide forming elements Cr and V. Neutron small angle scattering (SANS) using the SANS-2 facility at the FRG-1 reactor in Geesthacht and anomalous X-ray small angle scattering (ASAXS) using the JUSIFA facility at the HASYLAB in Hamburg were employed.
The difference between the scattering intensities from irradiated and unirradiated specimens give the small angle scattering effect of the radiation damages. Irradiation induced precipitates were found with a mean diameter of D = 1...2 nm. The defect volume fraction depends on the neutron fluence.
From the magnetic scattering contrast (SANS) and the anomalous scattering contrast (ASAXS) information about the chemical composition were got. These results are compared with the idea that the irradiation induced precipitates in 15Kh2MFA steel are carbides.

Große, M.; J. Böhmert, H.-W.Viehrig
Correlation Between Volume Fraction of Radiation-Induced Precipitates and Toughness of VVER Pressure Vessel Steel 15Kh2MFA
Journal of Nuclear Materials 211 (1994), pp. 177 - 180

The deterioration of mechanical properties of reactor pressure vessel (RPV) steel during its irradiation in a nuclear power plant is known as neutron embrittlement. It is for instance manifested as a shift of the ductile - brittle transition temperature toward higher values. The microscopic mechnisms of neutron embrittlement of low alloy RPV steel are not yet fully understood. It is known that dislocation loops, vacancy clusters (voids) and precipitates are formed during irradiation.
The dimensions of radiation induced precipitates are less than 5 nm, in RPV steel 15Kh2MFA they are about 1 - 3 nm. One of the objectives of present research in this field is to throw light on the nature of these precipitates.
In this article the correlation between the results of small angle neutron scattering

(SANS) and the ductile - brittle transition temperature are studied and possible mechanisms of neutron embrittlement are discussed.

Große, M.; G. Schuster, K. Teske u.a.
Neutron and X-ray Investigations on the Oxygen Bonding in $YBa_2Cu_3O_{7-x}$ Combined With Physico-Chemical Methods
Fresenius J Anal Chem (1994) 349, pp. 231-233, Springer-Verlag 1994

The occupancy of the oxygen lattice positions at different annealing conditions in $Yba_2Cu_3O_{(7-x)}$ were determined by Rietveld refinements using neutron and X-ray diffraction data. The occupation density for the oxygen positions O1 to O4 were ascertained. The values of the oxygen content of the samples from this method were compared with those measured by thermoanalysis. The O1 and O4 oxygen atoms are exchangeable by thermal treatment. The oxygen in the planes is fixed and cannot be removed by thermal treatment up to 935°C. The binding strength of O1 in the lattice is stronger than that of O4 atoms; this is demonstrated by a higher temperature of dissociation of the O1 atoms. The amount of the oxygen taken up is not exactly equal to the oxygen actually in the lattice positions. In the temperature region below 400°C adsorption and chemisorption processes become dominant.

Große, M.; J. Böhmert, H.-W. Viehrig
Structural Reasons of the Through-Thickness Variation of Mechanical Properties in Large Forgings of Nuclear Reactor Pressure Vessel Steel
Proc. EUROMAT'94, Balatonszeplak, Hungaria, 30.Mai.bis 01.Juni 1994
p. 570

The ductile-brittle transition temperature is the usual reference parameter for the safety assessment of the reactor pressure vessel. In large forgings this parameter can change with the distance from the surface. Thus, the safety assessment must consider the effect. To evaluate the significance for the VVER 440-type pressure vessel the relationship between mechanical properties, through-the-thickness position and microstructure was investigated for a forging of 15Kh2MFA steel. The change of the mechanical properties (hardness, strength, transition temperature) are relatively low. The surface-near position is harder and tougher than the deeper range. Both ranges differ in the content of preeutectoid ferrite and in the arrangement, but not in the content of carbides. The Orowan model for the mechanism of precipitation hardening can describe quantitatively the dependence of the yield strength and the number of $M_{23}C_7$ carbides per unit area of section plane found experimentally on the through-the-thickness position.

Grundmann, U.; U. Rohde
3-Dimensional Analysis of a Boron Dilution Accident by Using the Code DYN3D/M2
Proc. Jahrestagung Kerntechnik 1994, pp. 15 - 18
Stuttgart, 17. - 19. Mai 1994

An incorrect startup of a pump in an isolated loop containing a plug of diluted absorber can initiate a reactivity accident in a VVER-440. It is assumed that the main gate valve is opened after starting the main coolant pump. When the plug enters the

core, it gives rise to positive reactivity. An asymmetric distribution of diluted water in the core is expected which requires a 3-dimensional analysis for a more correct description of this accident.
The code DYN3D/M2 developed for investigations of reactivity initiated accidents in thermal reactors with hexagonal fuel elements is used for analysis. A model describing the mixing of water from the different loops in the lower plenum of a VVER-440 reactor gives the boron concentration at the inlet of each fuel element. The two limiting cases, ideal mixing and no mixing, are investigated for comparisons.

Grundmann, U.; U. Rohde
Investigations on a Boron Dilution Accident for a VVER-440 Type Reactor by the Help of the Code DYN3D
Proc. ANS Topical Meeting on Advances in Reactor Physics: Reactor Physics Faces the 21st Century, Knoxville (Tennessee), 11. - 15. April 1994
Vol. 3, pp. 464 - 471

A reactivity initiated transient caused by entering a plug of water with reduced boron concentration into the core during incorrect loop startup in a VVER-440/W-213 reactor is analyzed . Due to the asymmetric distribution of the boron dilution, significant space-dependent effects are expected. That requires the use of a three-dimensional reactor core model. The analysis was carried out with the help of the code DYN3D/M2 developed for investigations on reactivity initiated accidents in thermal reactors with hexagonal fuel elements. A semi-analytical model adjusted to experimental data on coolant mixing in VVER-440 type reactors is used for the estimation of boron concentration distribution at core inlet. For comparisons, the two limiting cases, ideal mixing and no mixing, are investigated.

Grundmann, U.
Results of the Second Kinetic AER-Benchmark
Proc. 4th AER Symposium, Sozopol, Bulgaria, October 10 - 13, 1994, pp. 397 - 415

Mathematical benchmarks are widely used and accepted means of verifying the reliability of numerical simulations. The present benchmark is aimed at assessing the discrepancies between three-dimensional core models used for transient calculations in VVER-reactor cores.
The second AER benchmark problem was defined at the 3nd AER Symposium in Pieštany (1993). The problem and the complete set of input data for a control rod ejection accident in a VVER-440 was described. An asymmetric control rod with a worth approximately 2 $ß_{eff}$ was ejected at hot zero power (HZP). The Doppler effect being the main feedback effect for this type of transients is the only feedback taken into account by an adiabatic model of fuel temperature. Therefore, it was possible to calculate this type of transient with codes which do not contain a complete thermo-hydraulic model.
Results of the four codes BIPR-8 (RRI Moskau), DYN3D/M2 (RCR Rossendorf), HEXTRAN (VVT Espoo) and KOKO3D (KFKI-AERI Budapest) were obtained and analyzed by comparisons. The agreement of the results is quite satisfactory, however there exist some discrepancies.

Hessel, G.; W. Schmitt, F.-P. Weiß
A New Method for Acoustic Leak Detection at Complicated Geometrical Structures
Proc. IFAC Symposium on Fault Detection, Supervision and Safety for Technical Processes - SAFEPROCESS'94, Helsinki, Finland, June 13 - 16, 1994,
Vol. 1, pp. 153 - 158

A method for detecting and localizing leaks at complicated three-dimensional topologies by measuring the leak induced structure-borne and airborne sound and by applying pattern recognition procedures is being developed. The sound patterns necessary to train fuzzy logic classifiers and neural networks are generated with simulated leaks at the original structure. As features for characterizing the occurrence and the location of a leak, coherence values between high-frequency microphone signals and RMS-values of acoustic emission sensors are used. The method is even applicable when localization based on propagation time differences or sound attenuation differences fail. The method is prototypically developed for a soviet-type pressurized VVER-reactor.

Hessel, G.; W. Schmitt, F.-P. Weiß
Anwendung neuronaler Netze zur akustischen Leckortung an komplizierten Strukturen
Preprint VDI/GVC Düsseldorf - Fachtagung Prozeß- und Anlagensicherheit
November 1994, S. 135 - 146

Eine Methode zur Erkennung und Ortung von Lecks an Druckanlagen komplizierter 3-dimensionaler Topologie ist entwickelt worden. Sie basiert auf der Merkmalsextraktion aus dem leckinduzierten Körper- und Luftschall und wendet neuronale Netze zur Mustererkennung an. Die zum Anlernen der neuronalen Netze notwendigen Schallmuster werden mit Hilfe von simulierten Lecks an einer Originalstruktur erzeugt. Als Merkmale zur Charakterisierung des Leckortes werden Kohärenzwerte zwischen hochfrequenten Mikrofonsignalen und RMS-Werte von Schallemissionssensoren angewendet. Die Methode ist sogar einsatzfähig, wenn die Leckortung auf der Basis von Laufzeit- oder Dämpfungsdifferenzen versagt. Die Methode wird prototypisch für einen russischen WWER-Druckwasserreaktor entwickelt. Die Anwendung neuronaler Netze ermöglicht eine Adaption der Leckortungsmethode an Druckanlagen unterschiedlicher Topologie.

Hirsch, W.; R. Lischke, J. Matthäi, U. Rindelhardt
Untersuchungen zur Windenergienutzung in Sachsen
Proc. "TERRATEC"-Fachmesse und Kongreß
Leipzig, 08.- 12. März 1994, S. 144 - 156

Im Rahmen eines umfangreichen Programmes wurden Untersuchungen zur Anwendbarkeit der Windatlas-Methode (WASP) zur Ermittlung des Windenergiepotentials in Sachsen durchgeführt. Das Ziel der Untersuchungen bestand darin, die erwarteten Grenzen bei der Nutzung von WASP in orografisch gegliedertem Gelände genauer zu ermitteln. Grundlage der Berechnungen waren Messungen von vier Stationen des sächsischen Windmeßprogrammes. Es konnte gezeigt werden, daß in großen Gebieten der Oberlausitz die Windatlas-Methode genutzt werden kann. In den Kammregionen des Erzgebirges wurden widersprüchliche Ergebnisse gefunden, so daß eine

Nutzung hier praktisch nur in sehr kleinen Repräsentationsgebieten in der Umgebung einer Meßstation möglich ist.

Jahn, U.; I. Grochovsky, T. Tegtmeyer, U. Rindelhardt, G. Teichmann
Detailed Monitoring Results and Operating Experiences from 250 Grid Connected Photovoltaic Systems in Germany
Proc. 12th European Photovoltaic Solar Energy Conference and Exhibition
Amsterdam, 11. - 15. April 1994, Vol. I, pp. 919 - 922

The German 1000 Roofs Programme includes more than 2000 grid connected photovoltaic (PV) plants, which are being supported by the Federal Ministry for Research and Technology and the governments of the Federal States. Monitoring data, which are continuously gained from the installed PV plants, are now availabe. This paper presents some recently obtained performance data from 250 installed PV systems in Saxony and Lower Saxony together with operating experiences gathered from technical inspections of the projects.

Krepper, E.; U. Rohde
Natural Circulation Instabilities During a Loca of VVER-Type Reactors
Proc. International Conference New Trends in Nuclear System Thermohydraulics, Pisa, May 30th - June 2nd, 1994, pp. 793 - 797

In the Research Centre Rossendorf pre- and posttest calculations to the OECD/NEA/-CSNI International Standard Problem No. 33 were carried out with the GRS code ATHLET. This Problem was based on a natural circulation experiment with stepwise reduced primary coolant inventory. In the ATHLET calculations after a drainage of about 50% of the primary inventory cyclic oscillations of the mass flows and the void fractions were observed. These are found in the experimental results too. A simple analytical model was developed to distinguish physically caused oscillations from numerically caused ones. The oscillations could be interpreted as density wave instability in the local recirculation loop core-bypass.

Krepper, E.; F. Schäfer
Post-Test Calculation of the IAEA-SPE4
Proc. 2. SPE-4 Workshop, Budapest Mai 1994

In the Research Center Rossendorf post test calculations of the SPE4 were performed using the thermohydraulic code ATHLET. The SPE-4 experiment was a small break loss of coolant accident in the cold leg with unavailable high pressure injection system. For the prevention of core damage the secondary side bleed and feed was used. The experiment was performed at the Hungarian PMK-2 test facility, modelling the Paks VVER-440 reactor. In the calulations different nodalizations were tested for modelling the hydroaccumulators and the horizontal steam generator. Deviations between calculation and experiment were observed especially in the primary pressure decay and consequently in the behaviour of accumulator injection. It was found, that the prediction of observed core dry out depends on the correct calculation of the low pressure injection setpoint.

Krepper, E.
Rechnungen zum Naturumlaufexperiment ISP-33 an der Anlage Pactel mit dem Code ATHLET
Proc. Jahrestagung Kerntechnik 1994
Stuttgart, 17. - 19. Mai 1994

Due to the low geodetic height differences and the presence of loop seals in VVER-reactors, the behaviour of natural circulation is an important safety feature. The experiment pertaining to the OECD/NEA/CSNI International Standard Problem No. 33 was dedicated to the investigation of this phenomenon. During the test, defined quantities of primary coolant were drained, while the facility was operated at 10% of nominal power and without pumps. The test was stopped at increasing temperatures of the fuel rod simulator.
In RC Rossendorf pre- and posttest calculations were performed by the code ATHLET, which was developed by the "Gesellschaft für Anlagen- und Reaktorsicherheit". The main events of the experiment could be predicted, shown and explained by the ATHLET calculations:
- After draining of about 20% of the primary inventory, the mass flow in the loops stagnates. Simultaneously, the primary pressure increases and the pressurizer is partly refilled.
- In later periods the mass flow through the three loops is nonequally distributed, which could be reproduced by the ATHLET calculations at least qualitatively.

Mittag, S.
Solution of AER Benchmark Problem on Control Rod worth of Paks VVER-440 by the Code DYN3D
Proc. 4th AER Symposium, Sozopol, Bulgaria, October 10 - 13, 1994, pp. 443 - 461

This paper presents a solution of the AER benchmark problem specified for the 7th cycle of the Paks-2 VVER-440 reactor. The problem concerns control rod worth for both the beginning and the end of burnup cycle states. The burnup distribution of cycle 7 was calculated starting from the burnup values of the third cycle. The calculations were carried out by using the burnup option of the DNYN3D code and a MAGRU group data library. The results are compared with calculations published by other authors on AER meetings. Furthermore the influence of the special control element construction in VVER-440s (absorber, fuel follower) on reactivity worth was studied.

Mutschke, G.; G. Gerbeth
Control of Cylinder Wake Instabilities by an External Magnetic Field
Proc. 1994 Meeting of the Division of Fluid Dynamics,
Atlanta, 20. - 22. Nov. 1994, Bulletin of the American Physical Society,
Series II, 39 (1994) 9, p. 1979

The standard cylinder wake is considered for the magnetohydrodynamic (MHD) case: The fluid is electrically conducting and exposed to an external uniform magnetic field of different directions. In general, the magnetic field stabilizes the flow, the vortex street can be suppressed at all Reynolds numbers. A numerical simulation of the

time-dependent flow as well as a simple analytical stability analysis will be presented and compared with available and own experiments. The experimentally found tendency of an increasing level of low-frequency perturbations for an increasing magnetic field will be discussed and compared with the analytical stability analysis. Typical features of the MHD case will be presented: Drag increase, up- and downstream wakes, surface pressure redistribution, recirculation bubbles at high Re, etc.

Noack, K.
Neutron-Physical Development of Reflectors for the Pulsed Reactor IBR-2
Kerntechnik 59 (1994) 6, S. 291 - 297
München: Hanser Verlag, 1994

The pulsed fast reactor IBR-2, Dubna, is at present the most powerful pulsed neutron source used for condensed matter research. The neutron pulses are generated periodically by reactivity modulation, which is accomplished by a rotating two-reflector system. The neutron physics which has been involved in the development of various reflectors is analysed with respect to the neutron pulse length. Two new reflectors are proposed.

Prasser, H.-M.; W. Zippe, D. Baldauf, L. Szabados, Ezsöl, Gy u.a.
Tow-Phase Flow Behaviour During a Medium Size Cold Leg LOCA Test on PMK-II (SPE-4)
Proc. Jahrestagung Kerntechnik 1994
Stuttgart, 17. - 19. Mai 1994

The Hungarian integral test rig PMK of the KFKI Atomic Energy Research Institute was used as a source of experimental data for the IAEA Standard Problem Exercise SPE-4, a medium size cold leg LOCA with secondary bleed-and-feed procedure. The needle shaped conductivity probes developed by the Research Center Rossendorf have been applied in order to obtain information about the void fraction and the structure of the two-phase flow. The primary circuit of the PMK-II test facility was practically fully equipped with probes (with exception of the core simulator and the downcomer). An overview of the signals of all probes and the general chronology of characteristic events are discussed. As a main result the mechanism of the hot leg loop-seal clearing was clarified in detail.

Prasser, H.-M.; F. Hensel, P. Schütz
Ultrasonic Two-Phase Flow Measurements Based on Pattern Recognition Techniques
Proc. IMEKO, Torino, September 5-9, 1994

The state-of art of ultrasonic two-phase flow measurements is characterised by a number of different approaches commonly based on the identification and characterisation of individual voids (bubbles, plugs etc.) applying the techniques of ultrasonic testing. The recorded individual events are integrated to extract parameters as void fraction or volume flow rates. The main limitation of these methods arises from the complicated structure of two-phase flow at higher void fractions which leads to multiple diffractions of the sound beam. The measurement is therefore limited to low void fractions or a simple flow structure.

The main idea of the present work was to overcome these limitations by means of pattern recognition. An ultrasonic beam crossing the two-phase flow is modulated by the changing structure of the voids passing by and therefore the through-transmission signal must contain information about the parameters of the two-phase flow even if information about individual flow effects cannot be derived. Therefore it was supposed that a pattern recognition algorithm trained with signals obtained at known conditions is able to identify the set of the flow parameters (flow rates, void fraction etc.) in an unknown situation.

Priede, J.; G. Gerbeth
Hydrothermal Wave Instability of Thermocapillary Driven Convection in a Plane Layer Subjected to a Uniform Magnetic Field
Advances in Space Research, Vol. 16, No. 7, pp. 55 - 58, Pergamon Press, 1995

Thermocapillary driven motion is considered in a horizontal electrically conducting fluid layer heated from the side and exposed to a magnetic field coplanar to the layer. The hydrothermal wave instability and its control by the magnetic field is studied by a linear stability analysis. The special assumption of disturbances traveling crosswise the basic flow allows an analytical solution of the problem. For a particular class of perturbations considered here, the critical Marangoni number and the wavelength of the most unstable mode increase directly with the strength of the applied magnetic field.

Priede, J.; A. Thess, G. Gerbeth
Theoretical Aspects of Thermocapillary Convection in Liquid Metals under Magnetic Field Influence
Electromagnetic Processing of Materials, Conference, EPM 94
Nagoya (Japan), Oct. 1994, Proceedings published by ISIJ Japan, 1994,
pp. 97 - 102

Magnetic fields provide the possibility to influence the convective flow pattern in an predefined contactless way, in particular, to suppress and control oscillatory instabilities. Therefore, there is increasing interest now in the use of magnetic fields in a variety of materials processing technologies like crystal growth from the melt or directional solidification.
Available knowledge is rather limited on the influence of a steady magnetic field (described by the Hartmann number Ha) on convective motions, described by the Grashoff number Gr (buoyancy), and by the Marangoni number Ma (thermocapillarity at free surfaces) in low Prandtl number fluids like liquid metals. Therefore, the paper presents theoretical results on the prototype problem of an infinitely extended fluid layer heated either from the side or from the bottom, and exposed to a steady external magnetic field.
In the first part the stability is considered of an unidirectional thermocapillary flow set up by a temperature gradient parallel to the free surface. The magnetic field is supposed to be parallel to the free surface. In this case the magnetic field has no influence on the basic flow, the stability of which is well known without magnetic field. The restriction to disturbances propagating in the same direction as the magnetic field allows to obtain an analytical solution of the stability problem and an

explicit expression for the dispersion relation. The hydrothermal wave instability is suppressed by the magnetic field, the critical Marangoni number grows proportionally to Ha. The most unstable wave pattern is stretched along the field lines. The wave number of the most unstable mode decreases as $Ha^{-4/5}$ for $Ha >> 1$.
The second part of this communication is devoted to the analysis of the thermocapillary instability in a layer with both temperature gradient and magnetic field being perpendicular to the free surface. Although this problem has been extensively treated in the past, the important limit of strong magnetic fields (Ha - $>\infty$) is still poorly understood. The asymptotic theory of thermocapillary instability is formulated in the limit of high Hartmann number, and a conceptually simple explanation is derived of the scaling laws of the critical parameters and of the hydrodynamic fields in terms of Hartmann boundary layers. The theory can be used as a tool to analyze more complicated problems that are not usually amenable to fully analytic treatment. The usual concept in convective problems of a constant Biot number will be critically analyzed.

Priede, J.; A. Thess, G. Gerbeth
Thermocapillary Instabilities in Liquid Metals: Hartmann-Number Versus Prandtl-Number
Proc. Energy Transfer in MHD Flows, Conference, Aussois Frankreich, Sept. 1994, pp. 571 - 580
Publication in: Magnetohydrodynamics

The technical need for instability postponement, turbulence suppression and flow control in material processing as well as the seek for low-cost alternatives to space-technologies for crystal growth are currently leading to an increased interest in the interaction between thermocapillary flows in electrically conducting fluids and magnetic fields. While the interplay between isothermal flows and magnetic fields is well understood, the physical understanding of the influence of magnetic fields on thermocapillary flow phenomena, i.e. flows driven by surface tension gradients, is lacking.
The goal of the present efforts is to demonstrate that a magnetic field acting on the thermocapillary flow of a low Prandtl number fluid causes the fluid to behave like a high Prandtl number fluid. This important feature is exemplified by considering the linear stability of an unidirectional thermocapillary flow set up by a temperature gradient parallel to the free surface of an unbounded planar fluid layer. The magnetic field is supposed to be normal to the free surface. The discussed problem is the magnetic counterpart to the work of Smith & Davis. Results are reported of a comprehensive study of the critical Marangoni number for the onset of hydrothermal waves as a function of the Hartmann number and of the Prandtl number. For weak magnetic field the instability mechanism in liquid metals is found to be the same as in the nonmagnetic case for low Prandtl numbers. For sufficiently strong magnetic field the basic flow and the most unstable perturbation are confined to a thin Hartmann boundary layer below the free surface which leads to a decrease of the effective viscous diffusion time-scale as Ha^{-2}. Computations reveal that at a certain value of the Hartmann number, when the effective viscous time equals the thermal diffusion time, the character of the instability changes discontinously. The new type of instability is reminiscent of the instability mechanism which, until now, has been

exclusively observed in high Prandtl number fluids such as silicone oil. This physical picture is supported by an analysis of the spatial structure of the unstable modes. Although the change of instability mechanisms was identified in a simple prototype problem, quasi-high-Prandtl-number behaviour is likely to represent a robust feature of thermocapillary convection in the presence of a magnetic field. The implications of theoretical results are discussed on both experimental and fully numerical studies of thermocapillary flows.

Richter, H.; H.-W. Viehrig, S. Winkler
Ermittlung dynamischer Rißeinleitungszähigkeiten mit dem instrumentierten Kerbschlagbiegeversuch bei elastisch-plastischem Werkstoffverhalten
Proc. der 26. Vortragsveranstaltung des DVM-AK "Bruchvorgänge"
Magdeburg, 22. - 23. Februar 1994, S. 373 - 383

Rißwiderstandskurven sind zum unentbehrlichen Instrumentarium zur Beschreibung des Versagens rißbehafteter Komponenten bei elastisch-plastischem Werkstoffverhalten geworden. Die Abhängigkeit der R-Kurve von der Dicke der jeweiligen Proben gestattet aber nur bedingt die Übertragung der Versuchsergebnisse auf das Bauteilverhalten. In der Literatur wird gezeigt, daß der Beginn der stabilen Rißeinleitung einen echten, geometrieunabhängigen Werkstoffkennwert darstellt. Als anerkannte Methode zur Bestimmung kritischer Rißeinleitungsparameter wird die Messung der Stretchzonenbreite vor der Rißspitze (SZW) verwendet. In quasistatischen Einproben (EPT)- oder in Mehrprobentechniken (MPT) lassen sich mit Hilfe von kritschen SZW gültige Rißeinleitungszähigkeiten auf J-Integralbasis bestimmen.
Noch ungelöst ist das Problem der Ermittlung von dynamischen Rißeinleitungszähigkeiten in EPT mit Hilfe des instrumentierten Kerbschlagbiegeversuches. Hierfür muß durch Messung physikalischer Größen, die mit dem Rißeinleitungsprozeß in Verbindung stehen, der Zeitpunkt der Rißeinleitung detektiert werden. Derartige physikalische Detektionsverfahren sind beispielsweise akustische Emission, elektrische und magnetische Emission. Man erkennt, daß alle drei Verfahren nur indirekt auf Rißbildungsprozesse reagieren. Erste Experimente mit einer Instrumentierung des Kerbschlagbiegeversuchs werden vorgestellt, wobei neben der Schlagkraft gleichzeitig akustische, magnetische und elektrische Emission erfaßt werden.

Durch die simultane Erfassung der Signale verschiedener Methoden in Zusammenhang mit hochauflösender Meßtechnik und mathematisch-numerischen Verfahren der Signalauswertung kann erwartet werden, daß die charakteristischen Zeitpunkte für Rißeinleitung und stabilen Rißfortschritt zuverlässig detektiert werden können.

Rindelhardt, U.
Photovoltaics in the New German Federal States - Results of the 1000-Roofs Programme in Saxony
Proc. Deutsch-Russische Konferenz "Die erneuerbaren Energiequellen und ihre energiepolitische Bedeutung in Rußland und Deutschland", Freiburg/Br., 24. - 26. Oktober 1994, p. 44 - 48

About 140 small grid connected photovoltaic plants (power 1 to 5 kW_p) were installed on the roofs of single and two family houses since 1991 in Saxony.

The results are summarized as follows:
The system reliability mainly depends on the reliability of the used inverters. The inverters cause more than 60 % of the total system deficiency time, what clearly indicates the need of further technical improvements.
The synchronization of generation and consumption of solar energy can only be restrictedly influenced through an active behavior of the plant owner. The results show, that, as a rule, 50 % of the yearly produced solar energy can be consumed directly by the owner's household. This fraction decreases up to 30 % in energy saving households.
Commonly the energy production is discussed in terms of final yield and performance ratio. The final yield describes the mean daily energy production per installed peak power, its value varied in 1993 between 1.4 kWh/kW_pd and 2.4 kWh/kW_pd. The 43 saxonian plants reached a mean final yield of 1.88 kWh/kW_pd, which corresponds to a yearly energy production of 685 kWh/kW_p. Differences between the nominal and the real modules peak power seems to be the main reason for the strongly varying results. Compared to this the influence of generator orientation is small. The performance ratio of the investigated systems varied between 50 % and nearly 80 %.

Schmitt, W.; G. Hessel, F.-P. Weiß
Acoustic Leak Detection at Complicated Topologies Using Fuzzy Classifiers and Neural Networks
Proc. of the XIII IMEKO World Congress, Torino, September 05-09, 1994,
pp. 1259 - 1264

A method for detecting and localizing leaks at complicated three-dimensional topologies by measuring the leak induced structure-borne and airborne sound and by applying pattern recognition procedures is being developed. The sound patterns necessary to train fuzzy logic classifiers and neural networks are generated with simulated leaks at the original structure. As features for characterizing the occurrence and the location of a leak, coherence values between high-frequency microphone signals as well RMS-values of acoustic emission sensors are used. The method is even applicable when localization based on propagation time differences or sound attenuation differences fail. The method is prototypically developed for a soviet-type pressurized VVER-reactor.

Shatrov, V.; G. Mutschke, G. Gerbeth
Numerical Simulation of the Two-Dimensional MHD Flow Around a Circular Cylinder
Proc. Energy Transfer in MHD Flows, Conference, Aussois Frankreich, Sept. 1994,
pp. 745 - 756, Publication in: Magnetohydrodynamics

In the present paper the time-dependent, two-dimensional, incompressible MHD flow around a circular cylinder is investigated numerically using a finite difference method in stream function-vorticity formulation. The calculations are restricted to the typical situation of liquid metal flows under laboratory conditions where the magnetic Reynolds number is small. The flow is investigated in the parameter range of $Re < 10000$ and magnetic interaction parameter $N < 20$ ($N = Ha^2/Re$).
To validate the numerical method, a comparison with the few published numerical results (MOCHIMARU, TSINOBER) is performed, and a good agreement is found.

Furthermore, the influence of different outer boundary conditions is tested.
The two cases of a magnetic field aligned to the flow as well as perpendicular to it are investigated in detail. The influence of the magnetic forces on the flow is shown in stream function and vorticity isoline plots for different Reynolds numbers and interaction parameters. The vorticity and pressure distribution at the cylinder surface and the induced magnetic field are calculated and compared with experimental results. The occurrence of a large, but slow recirculation eddy behind the cylinder for a strong aligned magnetic field is discussed. The motion of the fluid becomes more and more stagnant in that region for increasing magnetic fields.
The downstream wake is characterized by the velocity profiles, and the farfield of the vorticity is discussed.
As expected, the influence of the magnetic field on the flow in general is a stabilizing one. In particular, the suppression of an instationary wake flow can be achieved by the magnetic forces. A stability line in the (Re,N)-plane is extracted from the numerical simulations. This result will be compared with a linear stability analysis based on a Galerkin approach.

Stephan, I.; D. Gawlik, W. Gatschke, M. Matthes
Bestimmung der Neutronenflüsse in der drehbaren Bestrahlungseinrichtung im BER-II des HMI Berlin
Proc. Jahrestagung Kerntechnik 1994
Stuttgart, 17. - 19. Mai 1994

Zur Aktualisierung der Neutronenparameter in der drehbaren Bestrahlungseinrichtung des rekonstruierten BER-II wurde der im Forschungszentrum Rossendorf entwickelte Mehrkomponentenaktivierungsdetektor eingesetzt.
Durch das umfangreiche Datenmaterial sind axiale und radiale Neutronenflußverläufe bestimmt und es gelingt ein eindeutiger Bezug von Meßwert zur Bestrahlungsprobe.

Treuner, M.; D. Langbein, H.-J. Rath, V. Galindo, G. Gerbeth
Thermocapillary Bubble Migration - Drop Tower Experiments
Proc. Drop Tower Days'94, Bremen, July 1994, pp. 95 - 97

Experiments on the thermocapillary bubble migration are presently carried out in the Drop Tower Bremen. After a heating period of about two hours, a sufficiently linear temperature gradient is established with paraffin liquids in a cavity. For the moment of drop of the capsule two bubbles with diameters of up to 2 mm are generated and the injection needles are retracted. During 4.74 s under strongly reduced gravity the speed of the bubble migration is observed with video camera, the temperature field by Pt 100 temperature gauges and the use of a differential interferometer. First experimental results with a liquid characterized by the Prandtl number $Pr = 10$ (n-decane) agree very well with theoretical data available both from literature as well as with numerical simulations. The correspoding Reynolds numbers are in the range between $20 < Re < 160$. The experimental setup, the measuring technique and the evaluation method will be presented as well as comparison between experimental and theoretical results.

Weber, P.; S. Kusch, H.-M. Prasser
Analysis of Two-Phase Flow Phenomena with Conductivity Probes in Integral Reactor Safety Experiments
European Two-Phase Flow Group Meeting, Piacenza, Italy, June 6 - 8, 1994
Erlangen: Siemens AG, Power Generation Group (KWU), Paper I.1, 1994

The thermalhydraulic behaviour of a PWR during beyond-design-basis accident scenarios is important for the verification and optimisation of accident management measures and code development. Analyses require integral experiments, such as PKL III at Siemens / KWU, which simulates a 1300 MWe KWU-design PWR with scaling factor of 1:145.
The paper presents PKL III results obtained by needle shaped conductivity probes developed in the Forschungszentrum Rossendorf [1]. The probes provided local void fractions and particle frequences within an averaging period of 2s. This time resolution is sufficient to characterize slow transients. A special flow pattern map developed for the probes enabled the calculation of the length of an average bubble. The measured information was used to determine the changing flow regimes.
At first, a secondary side feed-and-bleed procedure was investigated. Two probes were installed in the feed water line close to the steam generators. A depressurization of the secondary side caused flashing of the feed water and discharge of two-phase flow. A comparison of the measured void fraction with the density reading of a radiation densitometer installed next to the probes shows good agreement. The experimentally found flow regimes are also consistent with expected trends from flow regime maps developed by other researchers (e.g. [2]). Both show slug flow at the beginning of the secondary-side depressurization.
In the second experiment, a primary-side feed-and-bleed following steam generator tube rupture, four probes were installed at one location in the vertical part of the pressurizer surge-line, but at different radial positions. Another set of probes was installed in the horizontal pressurizer bleed-line. Two of them were used for time-of-flight measurements providing velocity values directly. Flow regimes such as stratified flow in the horizontal tube or annular flow in the vertical tube were found during the depressurization.

Weier, T.; G. Mutschke, G. Gerbeth, A. Alemany, A. Pilaud
Stability of MHD Flow Around a Cylinder in an Aligned Magnetic Field
Proc. Energy Transfer in MHD Flows, Conference, Aussois Frankreich, Sept. 1994, pp. 561 - 570
Publication in: Magnetohydrodynamics

The hydromagnetic stability of the flow of an incompressible conducting fluid around a circular cylinder in a uniform magnetic field parallel to the mean flow is investigated with different approaches:
- Experiments for $1000 < Re < 9000$
- a simple analytical model
- numerical simulation for $Re < 1000$.

Main goal of the investigations is to find the stability curve in the (Re, N)-plane, and to distinguish between 2D and 3D instabilities.

Experimental results will be presented based on hot-wire measurements in the downstream cylinder wake. The suppression of the vortex street by increasing magnetic fields is clearly identified.
Parallel to the disappearance of the typical Kármán frequency an increase of low frequency fluctuations is observed in the spectrum. This will be discussed in terms of theoretical predictions for long-wave MHD instabilities.
More physical insight into the stability behaviour is obtained by a simple Kolmogorov flow modelling of the cylinder wake and the corresponding stability analysis. Theoretical results will be presented for the 2D case: critical Reynolds number, wave number and Strouhal number as function of the magnetic field.
The critical wave number jumps from the region of the typical Kármán value to very low values at a certain magnetic field strength. The simple model is extended to include 3D instabilities in the flow. Limitations of the model and the comparison to experiments will be discussed.
Finally the 2D case for Re $<$ 1000 will be compared with results of a full numerical simulation.

Weiß, F.-P.; E. Altstadt, P. Liewers, M. Scheffler, P. Schumann
Komponentenschwingungen an WWER-Reaktoren - Diagnose und Modellierung
Proc. Jahrestagung Kerntechnik 1994
Stuttgart, 17. - 19. Mai 1994

Seit Anfang der 70er Jahre sind an WWER-440-Reaktoren mehrfach anomale Schwingungen von Einbauten des RDB beobachtet worden, die teilweise zu Komponentenschäden führten.
Daher wurden speziell für den WWER-Typ zugeschnittene Diagnoseverfahren entwikkelt, die auf der Korrelationsanalyse von Schwankungsanteilen des Neutronenflusses (incore und excore) und von nichtnuklearen Signalen wie Körperschall, Druckfluktuation und Beschleunigungen beruhen.
Um eine wirklich sensitive Fehlerfrüherkennung zu erreichen, wird ein theoretisches Schwingungsmodell auf der Basis Finiter Elemente (FE) entwickelt. Dieses Modell gestattet die Interpretation von gemessenen Schwingungssignalen in dem Sinne, daß die gemessenen Resonanzpeaks den Eigenschwingungen des gekoppelten mechanischen Systems zugeordnet werden können.
Darüber hinaus werden Sensitivitätsstudien durchgeführt, die die Veränderungen des Schwingungsverhaltens bei mechanischen Komponentenschäden verdeutlichen.

CONFERENCE CONTRIBUTIONS

Altstadt, E.; G. Grunwald
Analytical and Experimental Investigations for Modelling the Fluid-Structure-Interaction in Annular Gaps
Jahrestagung Kerntechnik 1994; Stuttgart, 17. - 19. Mai 1994
see list of publications

Altstadt, E.; P. Liewers, M. Scheffler, P. Schumann, F.-P. Weiß
Component Vibration of VVER-Reactors - Diagnostics and Modelling
IMORN-25, Raleigh USA, 13. - 15. Juni 1994
se list of publications

Barz, H.-U.; B. Böhmer, J. Konheiser, I. Stephan
Aufgaben und Probleme bei der Bestimmung der Neutronenbelastung für den WWER-1000
5. Deutsch-Russisches WTZ-Seminar der Arbeitsgruppe Komponentensicherheit, Stuttgart, 03. - 05. Oktober 1994

Es werden Erfahrungen der auf diesem Gebiet in Rossendorf tätigen Mitarbeiter bei der Berechnung und Messung von Neutronenfluenzen sowie bei der Anwendung der Spektrumsjustierung dargelegt. An Hand dieser Erfahrungen wird auf noch offene Probleme eingegangen, die insbesondere bei der Neutronendosimetrie des WWER-1000 auftreten. Es werden Möglichkeiten zur Bewältigung dieser Probleme diskutiert und auf eigene Vorstellungen eingegangen. Insbesondere wird betont, daß man mit Hilfe moderner Verfahren der Varianzreduktion die genaue 3-dimensionale Monte-Carlo Methode als Standardverfahren für die Transportrechnungen anwenden kann.

Barz, H.-U.; B. Böhmer, J. Konheiser, I. Stephan
High Precision Neutron Fluence Calculations, Activation Measurements and Spectrum Adjustment for the Rheinsberg Pressure Vessel Steel Irradiation Program
Presentation to the EWGRD, WGRD-VVER Meeting, Rez, Tschechien, April 18 - 22, 1994

The overall approach comprises the pure calculation part, the gamma spectrometric analyses of fluence monitors and the comparison of theoretical and experimental results using the spectrum adjustment procedure. Monte Carlo methods were used to perform the transport calculations. By application of special measures of variance reduction the statistical errors could be reduced so much that accurate 3-dimensional Monte Carlo methods could be generally used with reasonable calculation time. The uncertainties of the results due to the use of different group values of neutron cross sections were assessed by testing different group sets. In that way it could be shown that the kind of group data is of minor influence.

Barz, H.-U; B. Böhmer, J. Kohnheiser
Neutron Fluence Calculations and Spectrum Adjustments for the Rheinsberg Pressure Vessel Steel Irradiation Program
Jahrestagung Kerntechnik, Stuttgart, 17. - 19.Mai 1994
see list of publications

Block, F.R.; R. Dittmer, G. Gerbeth
Electromagnetic Detection of Nonconducting Inclusions in a Liquid Metal Flow
Int. Symposium on Electromagnetic Processing of Materials
Nagoya (Japan), Oct. 1994
see list of publications

Böhmert, J.; H.-W. Viehrig
Irradiation Programme in the Rheinsberg VVER-2 Reactor to Evaluate the Susceptibility of Russian Reactor Pressure Vessel Steels against Neutron Embrittlement
Jahrestagung Kerntechnik, Stuttgart, 17. - 19. Mai 1994
see list of publications

Böhmert, J.; G. Brauer, M. Große, F. Eichhorn
Characterisation of Irradiation-Induced Precipitates in VVER-Type RPV Steel 15Kh2MFA by Anomalous Small Angle Ray Scattering
5th Meeting of the International Group on Radiation Damage Mechanisms, Santa Barbara, May 1994

Irradiation-induced precipitates are the cause for neutron embrittlement of reactor pressure vessel steels. It can be shown that for the VVER-type steel 15Kh2MFA the shift in the ductile-brittle transition temperature depends nearly linearly on the volume fraction of these precipitates.
The nature of the irradiation-induced precipitates has been investigated for the steel 15Kh2MFA. This steel differs from ASTM-type A503 and 533 steels mainly in its content of the carbide forming elements chromium, molybdenum and vanadium.
Small angle neutron scattering (SANS) experiments using the SANS-2 facility at the FRG-1 reactor in Geesthacht (Germany) were employed in the past. SANS gives information about size and volume fraction of the precipitates, but hardly about the chemical composition.
In order to prove and to characterize the nature of the irradiation-induced precipitates anomalous small angle X-ray scattering (ASAXS) has been carried out at the JUSIFA facility of the Hamburg synchrotron laboratory HASYLAB (Germany).
ASAXS experiments with contrast variation at energies near the vanadium-K_α-absorption-edge reveal the content of vanadium within the irradiation-induced precipitates. The scattering density of the precipitates is lower than the scattering density of the iron matrix. The chemical shift of the vanadium K_α-absorption-edge shows that vanadium does not precipitate in an elementary state. Assuming, the precipitates are vanadium carbide, these results can be explained. The results are in accordance with those of SANS experiments and former positron annihilation spectroscopy experiments.

Böhmert, J.; M. Große
Evidence of Irradiation Defection VVER Steels by Small Angle Scattering Experiments - Contribution to the Analysis of Irradiation Effects
5th Specialists Meeting on Scientific and Engineering Cooperation Agreement - Safety of Components, Stuttgart, 04. - 07.10.1994

Up to now there are only few investigations on the microstructural change of VVER-type reactor pressure vessel steels after neutron irradiation. Consequently, the understanding of the mechanism of neutron embrittlement is not physically but only empirically based. Apart from the modern methods of high resolution analytical electron microscopy the small angle scattering with neutrons and X-rays enables experiments that gain information on size, volume fraction and composition of the structure of nanometer-scale precipitates as they are typical for irradiation-induced damages. First experiments with these techniques have shown the irradiation-induced microstructural changes significantly to differ from the changes which were found in ASTM-type steels. To continue such investigations a programme for joint Russian-German research is suggested.

Bojarevics, A.; Yu. Gelfgat, G. Gerbeth
Thermocapillary Convection in a Liquid Metal Under the Influence of the Magnetic Field - Experimental Techniques and Results of the Tests
Energy Transfer in MHD Flows, Conference, Aussois France, Sept. 1994
see list of publications

Brünig, D., Naehring, F., Rindelhardt, U.
Solar Warm Water Heating and Feeding Solar Surplus into the Return Flow of a District Heating System
4. Symposium Thermische Solarenergie, Staffelstein, 9./10. June 1994
see list of publications

Daniels, W.; J. Kuntzsch, U. Rindelhardt
Wind Energy Ressources in Saxony: An Experimental Approach
European Wind Energy Association Conference, Thessaloniki, Greece,
10. - 14. Oktober 1994
see list of publications

Eckert, S.; G. Gerbeth, H. Langenbrunner, W. Witke, O. Lielausis, I. Platnieks
Anisotropic Transport in MHD Turbulence: Experimental Results Using Small Gas Bubbles as Local Tracers
Energy Transfer in MHD Flows, Conference, Aussois Frankreich, Sept. 1994
see list of publications

Eckert, S.; G. Gerbeth, G. Mihalache, J.-P. Thibault
Influence of External Magnetic Fields on Slip Ratio in LMMHD Two-Phase Flow
Energy Transfer in MHD Flows Conference, Aussois Frankreich, Sept. 1994
see list of publications

Futterschneider, H.; H. Morgenstern, U. Rindelhardt
Solar betriebene netzunabhängige Meßstation - Energiebilanzen eines einjährigen Betriebes
9. Internationales Sonnenforum, Stuttgart, 28. 06. - 01.07. 1994
see list of publications

Galindo, V., G. Gerbeth, D. Langbein, M. Treuner
Unsteady Thermocapillary Drop Migration in a Uniform Temperature Gradient
Drop Tower Days'94, Bremen, July 1994
see list of publications

Gerbeth, G.
Contactless Control of Nonlinear Flow Phenomena in the Czochralski Crystal Growth of Silicon by Use of Magnetic Fields
Workshop Potential of Nonlinear Dynamics for Technological Applications, BMFT-VDI, Frankfurt/M., 24.11.1994

Control of melt motions is important for most of the crystal growth technologies in order to improve the crystal quality and the yield. There were several attempts in the past to use steady magnetic fields for damping of instabilities. Much more possibilities for flow control exist if unsteady magnetic fields are used, preferably in combination with steady fields. This new active melt control is attractive for industrial use. Principal mechanisms of this type of flow control are presented in this lecture, particularly adressed to the needs of the Si-Cz-technology. The research project is performed together with the institute of physics Riga and Wacker Chemitronics Ltd. Burghausen.

Gerbeth, G.
LMMHD Activities at Research Center Rossendorf
Kawasaki, Japan: Nippon Steel Corp., 31.10.94
Tokyo, Japan: Tokyo Institute of Technology, 31.10.1994

A review on R&D activities of the FZR group in the field of Liquid Metal MHD is given in this lecture. Particular emphasis is put on the measurements and theoretical results with respect to heat and mass transfer in anisotropic MHD turbelence. Corresponding models, experimental set-ups, and measuring techniques are described. Two-phase flow measurements are presented which were obtained at the FZR sodium facility. The prospects of cylindrical turbulence promoters are discussed.

Gerbeth, G.
MHD Research at Research Center Rossendorf - Relations to LMFBR
O-arai, Japan: O-arai Engineering Center, PNC, 02.11.1994

A review on R&D activities of the FZR group in the field of Liquid Metal MHD is given in this lecture. Special attention is paid to sodium related experiences (facility, experimental programme, measuring techniques) being of interest for the breeder development. In particular, first tests of a contactless gas phase detection system are presented. This system was developed by RWTH Aachen and FZR, and tested for the

first time at FZR. It allows a detection of small, even single gas bubbles independent of their acoustic activity.

Gerbeth, G.
Some Proposals for Marangoni Experiments with a Pre-Prepared Temperature Gradient
Drop Tower Days'94, Bremen, July 1994

Often a serious disadvantage of a lot of microgravity experiments on Marangoni convection is the fact that most of the valuable time under microgravity is lost for preparing the necessary temperature gradient. Therefore, the paper discusses two possibilities of short-term marangoni experiments where the temperature gradient over a plane fluid layer can be prepared in advance, but keeps the fluid motionless. At first, a convective motion will be started simply by switching off gravity which can result in long-wave surface capillary waves. Such a motion due to surface deformations is suppressed under earth conditions.
Second, various types of Marangoni motions will be discussed for liquid metals exposed to an external magnetic field. Instability thresholds are increased by the magnetic field, i.e. the liquid can be kept motionless by means of the magnetic field under a given temperature gradient.
The paper will discuss the feasibility of such investigations in drop tower experiments.

Gerbeth, G.; Galindo, V. u.a.
Thermocapillary Bubble Migration at Higher Marangoni Numbers
- Theory and Experiment
1994 Meeting of the Division of Fluid Dynamics, American Physical Society, Atlanta, 20. - 22. November 1994
see list of publications

Große, M.; G. Brauer, J. Böhmert
Aktuelle Ergebnisse der Untersuchungen zum Mechanismus der Neutronenversprödung in Reaktordruckbehälterstahl
Seminar GKSS, Geesthacht, 1994

Bestrahlungsinduzierte Ausscheidungen gelten als die strukturelle Ursache der Neutronenversprödung von Reaktordruckbehälterstahl (RDB-Stahl). Am Beispiel des WWER-440 RDB-Stahls 15Cr2MFA wird die Korrelation zwischen dem Volumenanteil an bestrahlungsinduzierten Ausscheidungen und der Erhöhung der Sprödbruchübergangstemperatur diskutiert. Es wird eine bimodale Abhängigkeit dieser beiden Größen gefunden. Ursache des bimodalen Verhaltens sind möglicherweise unterschiedliche Arten von bestrahlungsinduzierten Ausscheidungen, die vom Gehalt an Verunreinigungselementen bestimmt sind.
Erste resonante Röntgenkleinwinkelstreuexperimente an Material mit niedrigem Cu-Gehalt zeigen, daß Vanadium ein wesentlicher Bestandteil der bestrahlungsinduzierten Ausscheidungen ist. Die Ergebnisse von Neutronenkleinwinkelstreuung und Positronenannihilationsspektroskopie unterstützen die Hypothese, daß es sich bei den Ausscheidungen im RDB-Stahl 15Cr2MFA um Vanadiumkarbide handelt.

Große, M.; J. Böhmert, F. Eichhorn et. al.
ASAXS and SANS Investigations of the Chemical Composition of Irradiation-Induced Precipitates in Nuclear Pressure Vessel Steels
1st European Confrence on Synchrotron Radiation in Material Science Chester (UK), 02. - 08. Juli 1994
see list of publications

Große, M.; F. Eichhorn, J. Böhmert, G. Brauer
Characterization of Irradiation-Induced Precipitates by Small Angle Scattering Experiments
17th International Symposium on Effects of Radiation on Materials
Sun Valley 1994, 20. - 23. Juli 1994
see list of publications

Große, M.; F. Eichhorn, J. Böhmert u.a.
Characterisation of Nanoscale Precipitates in Reactor Pressure Vessel Steel 15Kh2MFA by Small Angle Scattering Experiments
EUROMAT'94, Balatonszeplak, Hungaria, 30.Mai.bis 01.Juni 1994
see list of publications

Große, M.; J. Böhmert, H.-W. Viehrig
Structural Reasons of the Through-Thickness Variation of Mechanical Properties in Large Forgings of Nuclear Reactor Pressure Vessel Steel
EUROMAT'94, Balatonszeplak, Hungaria, 30.Mai.bis 01.Juni 1994
see list of publications

Grundmann, U.; U. Rohde
Investigations on a Boron Dilution Accident for a VVER-440 Type Reactor by the Help of the Code DYN3D
ANS Topical Meeting on Advances in Reactor Physics:
Reactor Physics Faces the 21st Century,
Knoxville (Tennessee), 11.-15.April 1994, Proceedings Vol.III, S. 464-471
see list of publications

Grundmann, U.; U. Rohde
3-Dimensional Analysis of a Boron Dilution Accident by Using the Code DYN3D/M2
Jahrestagung Kerntechnik 1994
Stuttgart, 17. - 19. Mai 1994
see list of publications

Grundmann, U.
Results of the Second Kinetic AER-Benchmark
4th AER Symposium, Sozopol, Bulgaria, October 10 - 13, 1994
see list of publications

Hirsch, W.; R. Lischke, J. Matthäi, U. Rindelhardt
Untersuchungen zur Windenergienutzung in Sachsen
"TERRATEC"-Fachmesse und Kongreß
Leipzig, 08.- 12. März 1994
see list of publications

Jahn, U.; I. Grochovsky, T. Tegtmeyer, U. Rindelhardt, G. Teichmann
Detailed Monitoring Results and Operating Experiences from 250 Grid Connected Photovoltaic Systems in Germany
12th European Photovoltaic Solar Energy Conference and Exhibition
Amsterdam, 11. - 15. April 1994
see list of publications

Krepper, E.
ATHLET-Rechnungen zum IAEA-Standardproblem SPE-4
3. ATHLET-Anwendertreffen, Garching, Oktober 1994

The experiment pertaining to the IAEA standard problem exercise No. 4 was a 3.2 mm break at the downcomer head. The high pressure injection cooling was assumed to be not available. As an accident management measure, bleed and feed at the secondary side of the steam generator was applied. Research Center Rossendorf contributed to the SPE-4 experiment by supplying needle shaped conductivity probes for the measurement of local void fractions in the primary circuit of the PMK-II test facility. In the course of the standard problem exercise RCR then contributed post-test calculations using the thermalhydraulic code ATHLET.
The calculations showed, that the code was suitable to reproduce the main events of the test. Reasons for some deviations and modelling problems were discussed.

Krepper, E.
Rechnungen zum Naturumlaufexperiment ISP-33 an der Anlage Pactel mit dem Code ATHLET
Jahrestagung Kerntechnik 1994
Stuttgart, 17. - 19. Mai 1994
see list of publications

Krepper, E.; U. Rohde
Natural Circulation Instabilities During a LOCA at VVER-Type Reactors
International Conference New Trends in Nuclear System Thermohydraulics
Pisa, May 30th - June 2nd, 1994
see list of publications

Lucas, D.
Kopplung von ATHLET mit dem 3-dimensionalen Coremodell DYN3D
3. ATHLET-Anwendertreffen, Garching, Oktober 1994

Die Kopplung fortgeschrittener Thermohydraulikprogramme mit dreidimensionalen Neutronenkinetikcodes ordnet sich in das Bestreben ein, konservative Abschätzungen durch "best estimate Rechnungen" zu ersetzen. Der DYN3D-Code wurde im For-

schungszentrum Rossendorf für die Analyse von reaktivitätsinduzierten Störfällen in Reaktoren mit hexagonalen Brennelementen entwickelt und beinhaltet neben der 3D-Neutronenkinetik auch Modelle für die Thermohydraulik im Corebereich und für den Wärmeübergang vom Brennstoff zum Kühlmittel. Daher gibt es zwei grundlegende Möglichkeiten für die Realisierung der Kopplung mit dem Thermohydraulikcode ATHLET der Gesellschaft für Anlagen- und Reaktorsicherheit.
Bei der einen Kopplungsart wird nur der Neutronenkinetikteil von DYN3D an ATHLET angekoppelt (interne Kopplung). Diese Kopplung längs des Cores ist sehr eng und auf Grund der vielen zu übergebenden Parameter mit hohem Programmieraufwand verbunden.
Bei der hier vorgestellten Kopplungsart wird der Corebereich ganz aus dem ATHLET-Anlagenmodell herausgeschnitten und vollständig von DYN3D modelliert (externe Kopplung). Die Schnittstellen sind in diesem Fall der Coreeintritt und -austritt. An diesen Schnittstellen sind nur die Drücke, Massenströme, Enthalpien und Borsäurekonzentrationen zu übergeben. Diese Kopplungsart kann sehr einfach durch Zwischenschaltung einer Interfaceroutine realisiert werden. Sie wird durch das "General Control and Simulation Modul" (GCSM) von ATHLET wirkungsvoll unterstützt. Es sind kaum Veränderungen der einzelnen Programme notwendig. Weiterhin hat sie den Vorteil, daß die aufeinander abgestimmten DYN3D-Modelle auch in dem gekoppelten Programm genutzt werden können.
Die Kopplung wurde explizit realisiert, da eine geschlossene implizite Zeitintegration der thermohydraulischen Gleichungen wie in ATHLET entweder rechenzeitintensive Iterationen zwischen den Programmteilen oder umfangreiche Änderungen der Codes erfordern würde. Die explizite Kopplung beider Programmteile erlaubt nur sehr kleine Zeitschritte. Die numerischen Probleme bei größeren Zeitschritten können aber durch Zwischenschalten eines Tiefpaßfilters erster Ordnung für die von ATHLET an DYN3D als Randbedingung übergebene Druckdifferenz über das Core überwunden werden. Auf die zu berechnenden Transienten hat dieses Tiefpaßfilter praktisch keinen Einfluß. Anhand eines Demonstrationsbeispiels wird gezeigt, daß es auch für sehr schnelle und starke Übergänge zu keinen Verfälschungen kommt. Für einen weiteren Testfall werden erste Vergleichsrechnungen zwischen Punktkinetik, interner und externer Kopplung vorgestellt.

Mittag, S.
Solution of the AER Benchmark Problem on Control Rod Worth of the Paks VVER-440 by the Code DYN3D
4th AER Symposium, Sozopol, Bulgaria, October 10 - 13, 1994
see list of publications

Mutschke, G.; G. Gerbeth
Control of Cylinder Wake Instabilities by an External Magnetic Field
1994 Meeting of the Division of Fluid Dynamics, Americal Physical Society, Atlanta, 20. - 22. November 1994
see list of publications

Mutschke, G.; G. Gerbeth
Magnetohydrodynamic Flow Around a Circular Cylinder
- Numerical Simulation up to Renolds numbers of 1000
DFG-Kolloquium, Bonn, 24.06.94

Noack,K.
PO-3 - the Best Reflector for the IBR-2
International Seminar on Advanced Pulsed Neutron Sources
Dubna, Russia, June 14-16, 1994

The pulsed fast reactor IBR.2, Dubna, is at present the most powerful pulsed neutron source used for condensed matter research. The neutron pulses are generated periodically by reactivity modulation, which is accomplished by a rotating two-reflector system. The neutron physics which has been involved in the development of various reflectors is analysed with respect to the neutron pulse length. Two new reflectors are proposed.

Prasser, H.-M.; W. Zippe, D. Baldauf, L. Szabados, Gy. Ezsöl, G. Baranyai, I. Nagy
Tow-Phase Flow Behaviour During a Medium Size Cold Leg LOCA Test on PMK-II (SPE-4)
Jahrestagung Kerntechnik 1994
Stuttgart, 17. - 19. Mai 1994
see list of publications

Prasser, H.-M.; F. Hensel, P. Schütz
Messung der Volumenströme von Gas und Flüssigkeit in einer Zweikomponentenströmung mit Ultraschall und Mustererkennung
Ultrasonic Two-Phase Flow Measurements Based on Pattern Recognition Techniques
ACHEMA'94; IMEKO, Torino, September 5 - 9, 1994
see list of publications

Priede, J.; A. Thess, G. Gerbeth
Theoretical Aspects of Thermocapillary Convection in Liquid Metals under Magnetic Field Influence
Electromagnetic Processing of Materials, Conference EPM 94
Nagoya (Japan), Oct. 1994
see list of publications

Priede, J.; G. Gerbeth
Hydrothermal Wave Instability of Thermocapillary Driven Convection in a Plane Layer Subjected to a Uniform Magnetic Field
30th COSPAR-Scientific Assembly Conference, Hamburg, July 1994
see list of publications

Priede, J.; A. Thess, G. Gerbeth
Thermocapillary Instabilities in Liquid Metals: Hartmann-Number Versus Prandtl-Number
Energy Transfer in MHD Flows, Conference, Aussois Frankreich, Sept. 1994
see list of publications

Richter, Holger
Bewertung von akustischen Emissionssignalen, aufgenommen mit einer hammerfinnenintegrierten AE-Sonde
Arbeitskreis "Instrumentierter Kerbschlagbiegeversuch" des DVM Berlin,
19. September 1994

Anhand von Beispielen wurden elastische low blow's und deren komplexes akustisches Verhalten an einer ungekerbten hochfesten Stahlprobe unter Ausschluß von plastischer Deformation und Rißbildung diskutiert. Störsignale, die durch verschiedene Prozesse generiert werden, sollen somit besser verstanden und letztlich vom Nutzsignal separiert werden. Die Korrelation der gemessenen Störsignale zu charakteristischen Ereignissen, wie Reibungsquellen und mechanischen Kontakten, gelang noch nicht. Deshalb wird eine zusätzliche AE-Instrumentierung von Probe und Widerlager in Betracht gezogen, die bei der Störquelleninterpretation hilfreich sein wird.

Richter, Holger; H.-W. Viehrig, S. Winkler
Ermittlung dynamischer Rißeinleitungszähigkeiten mit dem instrumentierten Kerbschlagbiegeversuch bei elastisch-plastischem Werkstoffverhalten
26. Vortragsveranstaltung des DVM-AK "Bruchvorgänge"
Magdeburg, 22. - 23. Februar 1994
see list of publications

Rindelhardt, U.; G. Teichmann
Erfahrungen und Ergebnisse des 1000-Dächer-Programms in Sachsen
9. Symposium Photovoltaische Solarenergie
Staffelstein, 16. - 19. März 1994
see list of publications

Rindelhardt, U.
Photovoltaics in the New German Federal States - Results of the 1000-Roofs Programme in Saxony
Deutsch-Russische Konferenz "Die erneuerbaren Energiequellen und ihre energiepolitische Bedeutung in Rußland und Deutschland", Freiburg/Br., 24. - 26. Oktober 1994
see list of publications

Rindelhardt, U.
Photovoltaik - Beispielhafte Anlagen in Sachsen
Konferenz Erneuerbare Energien in Sachsen, Chemnitz, 1. Juni 1994

Aufgrund verschiedener Förderprogramme des Bundes bzw. des Freistaates Sachsen wurden bis Mai 1994 in Sachsen netzgekoppelte Photovoltaikanlagen mit einer Leistung von insgesamt 400 kW_p errichtet. Im Vortrag wird hauptsächlich auf die Ergebnisse der Anlagen eingegangen, die im Rahmen des Bund-Länder-1000-Dächer-Photovoltaik-Programmes errichtet wurden. Weiterhin werden die 40-kW_p-Anlage zur Versorgung der Kirnitzschtalbahn (Sächsische Schweiz) und die mit amorphen Si-Modulen ausgerüstete 7,5-kW_p-Anlage im SOS-Kinderdorf Zwickau vorgestellt.

Shatrov, V.; G. Mutschke, G. Gerbeth
Numerical Simulation of the Two-dimensional MHD Flow Around a Circular Cylinder
Energy Transfer in MHD Flows, Conference, Aussois Frankreich, Sept. 1994
see list of publications

Stephan, I.; D. Gawlik, W. Gatschke, M. Matthes
Bestimmung der Neutronenflüsse in der drehbaren Bestrahlungseinrichtung im BER-II des HMI Berlin
Jahrestagung Kerntechnik 1994
Stuttgart, 17. - 19. Mai 1994
see list of publications

Treuner, M.; D. Langbein, H.-J. Rath, V. Galindo, G. Gerbeth
Thermocapillary Bubble Migration in a Drop Tower experiments
Drop Tower Days'94, Bremen, July 1994
see list of publications

Viehrig, H.-W.; H.U. Barz, U. Bergmann, J. Böhmert, J. Kohnheiser
Characterization of the Initial State of the Reactor Pressure Vessel Steels of the Rheinsberg Irradiation Programme - Survey on Mechanical Testing including Fracture Mechanics and Fluence Investigation in the Research Centre Rossendorf
5th Specialists Meeting of Scientific and Engineering Cooperation Agreement - Safety of Components, Stuttgart, 04. - 07.10.1994

A German/Russian irradiation programme was performed in the high flux irradiation channels of the PWR VVER-2 Rheinsberg from 1984 to 1987. Within the programme Charpy-V-, COD-, 0,5-CT-, X-CT- and 1-CT specimens of reactor pressure vessel (RPV) steels 15Kh2MFA and 15Kh2NMFA(A) and RPV weld metal 10KhMFT, 10Kh2MFA(U) and 10KhNMA(A) were irradiated. These materials are used in the Russian type pressurized water reactors VVER-440 and VVER-1000. Each irradiation cycle lasted one year. In this paper the unirradiated initial state of the material is characterized. It presents mechanical properties and fracture mechanical parameters which were measured in Charpy-V notch impact tests and static 3-point bending tests. Furthermore the neutron fluences of the specimens were calculated in dependence on the position in the high flux irradiation channels.

Viehrig, H.-W.; J. Böhmert, U. Bergmann, H. Richter
Zusammenhang zwischen bruchmechanischen und mechanisch-technologischen Kennwerten für Reaktordruckbehälterstähle
Werkstoffprüfung'94, Bad Nauheim, 01. - 02. Dezember 1994

Im Rahmen der wissenschaftlich-technischen Zusammenarbeit zwischen Deutschland und Rußland und einem koordinierten Forschungsprogramm der IAEA wird das Bestrahlungsverhalten russischer und westlicher Reaktordruckbehälter(RDB)-stähle untersucht. Im unbestrahlten Ausgangszustand weisen die Chargen des Grundwerkstoffes 15Ch2MFA des russischen Druckwassereaktors WWER-440 eine große Streuung in den im Charpy-V Test ermittelten Übergangstemperaturen und Hochlagenenergien auf. Eine geringere Streuung in diesen Kennwerten haben die untersuchten Chargen des Grundwerkstoffes 15Ch2NMFA(A) des russischen Druckwasserreaktors WWER-1000. Die ermittelten Übergangstemperaturen liegen niedriger als bei den ASTM RDB-Stählen A533B Cl. 1 und ASTM A508 Cl. 3. Die J-Integralwerte für technische ($J_{0,2}$)- und physikalische Rißinitiierung der untersuchten RDB-Stähle und der dazugehörigen Schweißgüter wurden mit den Hochlagenenergien aus dem Charpy-V Test und den Streckgrenzen des Zugversuches korreliert.

Weier, T.; G. Mutschke, G. Gerbeth, A. Alemany, A. Pilaud
Stability of MHD Flow Around a Cylinder in an Aligned Magnetic Field
Energy Transfer in MHD Flows, Conference, Aussois Frankreich, Sept. 1994
see list of publications

Weiß, F.-P.; E. Altstadt, P. Liewers, M. Scheffler, P. Schumann
Komponentenschwingungen an WWER-Reaktoren - Diagnose und Modellierung
Jahrestagung Kerntechnik 1994
Stuttgart, 17. - 19. Mai 1994
see list of publications

Weiß, F.-P.
Beiträge des FZ Rossendorf zur Sicherheit von WWER-Reaktoren
WTZ-Statusseminar, Moskau, 08. - 09. Februar 1994

FZR-REPORTS AND OTHER PUBLICATIONS

Barz, H.-U.; J. Konheiser
Fluenzberechnungen für das Bestrahlungsprogramm Rheinsberg von Materialproben im Rheinsberger Reaktor im Zeitraum 1984-1988
Report, FZR-51, August 1994

Im Zeitraum von 1984 - 1988 wurde am Rheinsberger Reaktor ein umfangreiches Bestrahlungsprogramm für Stahlproben aus verschiedenen Druckbehältermaterialien durchgeführt. Zielstellung des Vorhabens ist die Ermittlung der Veränderung der bruchmechanische Eigenschaften durch den Einfluß der Neutronenstrahlung.
Ein Teilaspekt für diese Zielstellung ist die Bestimmung der Parameter für die Neutronenbelastung. In diesem Bericht werden das methodische Vorgehen zur Gewinnung dieser Werte beschrieben, mögliche Fehlerquellen diskutiert sowie ein umfangreicher Überblick über die Ergebnisse gegeben.
Grundlage der transporttheoretischen Berechnungen bei gegebenen Spaltquellen war die Vielgruppen-Monte-Carlo-Methode mit speziellen Verfahren zur Minimierung der statistischen Fehler, so daß Ergebnisse mit kleinem statistischen Fehler für jede Einzelprobe, die im allgemeinen noch in vertikaler bzw. horizontaler Richtung unterteilt wurde, erzielt werden konnten.
Zur Berechnung der Spaltquelle wurde die für ein Zeitraster für jedes Kassettenelement gegebenen Abbranddaten zugrunde gelegt, auf deren Basis für jeder Reaktorbetriebsperiode die integralen Spaltquellverteilungen für verschiedene Spaltisotope berechnet wurden.
Dargestelt werden die für die Neutronenversprödung relevanten Ergebnisse, nämlich die kumulativen Neutronenflüsse im Energiebereich größer 0,5 und 1 MeV sowie eine dpa-Rate. Als allgemeines Resultat kann man die starke Abhängigkeit der Ergebnisse in radialer Richtung vom Reaktormittelpunkt anführen. Dagegen ergaben sich in azimulater und vertikaler Richtung nur relativ schwache Veränderungen.

Bemmann, T.
Auslegung des Wärmeverteilsystems einer zu errichtenden großen solarthermischen Anlage
Diplomarbeit Techische Universität Dresden, Institut für Thermodynamik und Technische Gebäudeausrüstung, April 1994
(Betreuer: Dr. Naehring)

Für ein im Bau befindliches konventionelles Heizsystem auf Erdgasbasis wurden technische Varianten einer einzubindenden Solaranlage untersucht. Dabei stand die optimale Nutzung und Verteilung der von der Solaranlage zu liefernden Wärme im Vordergrund. Als ausschlaggebend erwiesen sich die Berücksichtigung unterschiedlicher Temperaturniveaus der verschiedenen untersuchten Abnehmer (Wohngebiet, Schule). Für 2 Varianten erfolgte eine Systemauslegung und eine Abschätzung der zu erwartenden solaren Gewinne.

Beyer, M.; H. Carl, L.Langer, K. Nowak, P. Schumann, A. Seidel, P. Tolksdorf, J. Zschau
Aufbau eines technischen Systems zur Verbesserung der betrieblichen Überwachung der KKW durch die staatlichen Aufsichtsbehörden
(Saporoshje) - Kurzfassung - Bericht, FZR-44, Juni 1994

Es wird ein techisches System zur Verbesserung der betrieblichen Überwachung eines WWER-1000-Reaktorblockes im KKW Saporoshje vorgestellt, das die Aufsichtsbehörde in die Lage versetzen soll, diesen Block unabhängig vom Betreiber zu beaufsichtigen, seinen Sicherheitszustand zu beurteilen und durch Auflagen zu beeinflussen. Das System gestattet auf Grund moderner Ausrüstung eine frühzeitige Meldung von Störungen aller Art und der damit verbundenen Aktivitätsfreisetzungen. Es stellt eine Grundlage das für die Frühwarnung der Öffentlichkeit in Gefahrensituationen sowie für eine effektive Einleitung von Notfallschutzmaßnahmen. Dazu werden 49 betriebliche Parameter vom Reaktorblock, 18 block- und analgenspezifische radiologische und 6 meteorologische Meßgrößen überwacht. Die geschätzten Kosten für die Realisierung einer Minimalvariante (ohne Baumaßnahmen und Installationsaufwand) belaufen sich auf ca. 1,3 Mio. DM, zuzüglich 650 TDM für notwendige Ertüchtigungen der Meßtechnik. Der Anschluß eines weiteren WWER-1000-Blockes verursacht entsprechende Kosten von etwa 200 TDM.

Beyer, M.; H. Carl, L.Langer, K. Nowak, P. Schumann, A. Seidel, P. Tolksdorf, J. Zschau
Aufbau eines technischen Systems zur Verbesserung der betrieblichen Überwachung der KKW durch die staatlichen Aufsichtsbehörden
(Saporoshje) - Anlage A: Textteil, Bericht, FZR-45, Juni 1994
Kurzfassung siehe vorhergehenden Bericht

Carl, H.; P. Schumann, J. Zschau
Schaffung eines Internationalen Zentrums für Information und Frühwarnung bei nuklearen Ereignissen in mittel- und osteuropäischen Kernkraftwerken
Report, FZR-57, Oktober 1994

Im Rahmen eines vom Sächsischen Staatsministeriums für Wissenschaft und Kunst geförderten Vorhabens wurden 1994 die Untersuchungen zu den Aufgaben, zu den zu erwartenden Kosten und zu den Realisierungschancen für ein internationales Zentrum für Informatino und Frühwarnung bei nuklearen Ereignissen in mittel- und osteuropäischen Kernkraftwerken planmäßig fortgesetzt und das laufende Projekt mit dem Abschlußbericht zum 31.12.1994 abgeschlossen.
Für die anstehenden Aufgaben, nämlich Abschätzung der Emissionen, Prognose der Radioaktivitätsausbreitung, Verfolgung der Lageentwicklung und Mitwirkung bei der Vorbereitung von Notfallschutzmaßnahmen sind im wesentlichen radiologische Meßwerte über die freigesetzten radioaktiven Stoffe und meteorologischen Kennwerte zur Beschreibung der Ausbreitungsbedingungen an das Zentrum zu übertragen. Betriebliche Informationen über den Anlagenzustand sind nur im Sinne von Hintergrundinformationen erforderlich, wozu 8 bis 10 ausgewählte sicherheitsrelevante Betriebsparameter ausreichend sind.

Obwohl der Sinn eines solchen Vorhabens außer Frage steht, sind die Realisierungschancen ohne eine umfassende Förderung durch die EG und andere internationale Organisationen - World Association of Nuclear Operators WANO, International Atomic Energy Agency IAEA - gering.

Grundmann, U., U. Rohde
Verfikation des 3-dimensionalen Kernmodells DYN3D/M2
Report FZR-47, April 1994
Technischer Fachbericht zum Vorhaben:
"Weiterentwicklung und Verifikation eines dreidimensionalen Kernmodells für Reaktoren vom Typ WWER und seine Ankopplung an den Störfallcode ATHLET"
BMFT-Förderkennzeichen 150 0925

Es wird eine Übersicht über die wesentlichsten Ergebnisse bisheriger Arbeiten zur Verifikation des dreidimensionalen Kernmodells DYN3D/M2 für Reaktoren mit hexagonalen Brennelementen gegeben. Verifikationsuntersuchungen für stationäre und instationäre Leistungsdichteberechnung, Thermohydraulik und Brennstabmodell sowie das Gesamtmodell werden beschrieben. Die Verifikation erfolgte durch Nachrechnung von Einzeleffekttests und Experimenten an WWER-spezifischen Versuchsanlagen, Vergleich mit anderen Codes und Benchmarklösungen sowie teilweise durch Vergleich berechneter Parameter mit Betriebsmeßdaten aus KKW mit WWER. Verifikationsbedarf besteht insbesondere noch für das Gesamtmodell und die Anwendung auf den WWER-1000.

Heinze, K.
Konfiguration und Parametrierung eines Meßsystems zur Erfasung der Wärmeflüsse in einer Wohnsiedlung
Diplomarbeit Technische Universität Dresden, Institut für Energiemaschinen und Maschinenlabor, Dezember 1994
(Betreuer: Dr. Naehring)

Für die Wohnsiedlung Rossendorf wurde ein Meßsystem zur Erfassung der Wärmeflüsse für Heizung und Warmwaser entworfen, realisiert und erprobt. Zum Einsatz kam ein industrielles Meßsystem mit Prozeßrechner der Firma Johnson Controls. Durch Testmessungen wurde der Nachweis der Funktionsfähigkeit der Anlage erbracht. Als kritisch erwies sich die genaue Bestimmung der Wärme- bzw. Volumenströme.

Hollstein, F.
Nodales Modell zur Berechnung der Neutronenflußdichteschwankungen infolge stochastischer Schwingungen von Regelelementen mit hexagonalem Querschnitt
Report, FZR-52, August 1994

Auf der Basis eines dreidimensionalen nodalen Geometriemodells für den WWER-440-Reaktor mit Nodes in Hexagonal-z-Geometrie werden die Beziehungen zur iterativen Berechnung der mittleren Neutronenflußdichte in einer Node sowie deren Schwankungen infolge stochastischer Regelelementschwingungen dargestellt.

Für die Rauschquellenmodellierung werden entsprechend der Konstruktion eines Regelelementes als räumliches Doppelpendel mit Absorber- und Brennstoffteil zwei verschiedene geometrische und neutronenphysikalische Ansätze verwendet.
Das durch Schwingungen der Brennstoffteile verursachte Neutronenflußrauschen wird auf Flächenquellen zurückgeführt. Die Flächenquellen werden dabei durch Materialparameterschwankungen infolge der Regelelementverlagerung innerhalb des Führungskanals induziert.
Für den Absorberteil wird das Modell des "thermisch schwarz" absorbierenden Hohlzylinders auf Körper mit hexagonalem Querschnitt übertragen.
Beide Rauschquellen werden als Störungen der über die Nodeoberflächenteile gemittelten partiellen Neutronenstromdichten in der Zweigruppendiffusionsnäherung beschrieben.
Die Übertragung der Rauschsignale wird in der Prompt-Response-Approximation behandelt. Die Kopplung von "Zweigruppen-Quell-Nodes" mit "Eingruppen-Übertragungs-Nodes" wird auf der Basis der modifizierten Eingruppendiffusionsnäherung realisiert.
Die dargestellten Algorithmen sind Grundlage für die Entwicklung eines Rechenpgrogramms zur Untersuchung der ortsabhängigen Übertragungsfunktionen von Neutronenflußdichteschwankungen mit stochastischen Regelelementschwingungen als Rauschquelle.

Kunze, R.
Ultraschallverfahren zur Erfassung von Rißbildung und Rißfortschritt bei quasistatischer Belastung
Diplomarbeit Technische Universität Dresden, Fakultät Maschinenwesen, Juli 1994
(Betreuer: Dr. Böhmert)

Es wurde ein Ultraschallverfahren zur Rißlängenmessung während des Dreipunktbiegeversuchs entwickelt, das auf der Beugung von Ultraschallwellen an der Rißspitze beruht. Die Information über Rißlänge und Rißfortschritt wird aus der Laufzeit der gebeugten Ultraschallwellen gewonnen. Das vorgestellte Verfahren ist das einzige der bisher bekannten Ultraschallverfahren, das an einer so kleinen Probenform erfolgreich angewendet wurde.

Mittag, S.
Recherche zu Gruppendatenbibliotheken für die Anwendung des Programmes DYN3D auf Reaktoren vom Typ WWER
Report FZR-46, Juni 1994
Technischer Fachbericht zum Vorhaben:
"Weiterentwicklung und Verifikation eines dreidimensionalen Kernmodells für Reaktoren vom Typ WWER und seine Ankopplung an den Störfallcode ATHLET"
BMFT-Förderkennzeichen 150 0925

Für die Berechnung des Reaktorverhaltens mit Kernmodellen (wie DYN3D) werden sog. Weniggruppen-Neutronendaten benötigt. Es wird eine Übersicht zu entsprechenden Datenbibliotheken für die Spaltzonen von russischen WWER-Reaktoren aufgestellt. Die Informationen über verwendete Primärdaten und die Genauigkeit der Zellcodes für die Gruppendatengenerierung werden im wesentlichen in Tabellenform

gegeben. Zur Beurteilung der Qualität der Daten werden Vergleiche zwischen gemessenen und berechneten Reaktorparametern zusammengestellt. Die verfügbaren Informationen ergeben keine signifikanten Qualitätsunterschiede zwischen den einzelnen Datenbibliotheken.

Kalinenko, V.
Analysis of Transients for NPP with VVER-440 using the Code SiTAP
Report FZR-54, Juni 1994

The report contains results of the analysis of the transients "Loop connection" and "SG tube rupture" for NPP with VVER-440 type reactors. To obtain detailled informations about NPP's dynamic characteristics, various variants of initial and boundary conditions are considered.
Calculation of these transients was performed with use of the code SiTAP developed at the Nuclear Safety Institute of Russian Research Centre "Kurchatov Institute". SiTAP is a multi-functional computer tool for fast analysis of transient and accidental processes of VVER type reactors for engineers working in the field of NPP dynamics. SiTAP can be used for comparative analysis of several variants of accident scenarios to find out the conditions leading to the most severe consequences from safety point of view. For this cases, additional analyses using best-estimate codes should be carried out.
The results from SiTAP for faulty loop connection leading to a boron dilution accident are intended to be used as boundary conditions for a more detailled analysis by the help of the three-dimensional reactor core model DYN3D, developed in the Research Centre Rossendorf for the simulation of reactivity initiated accidents.

Stephan, I.; D. Gawlik, W. Gatschke, M. Matthes
Bestimmung der Neutronenflüsse in der drehbaren Bestrahlungseinrichtung im BER-II des HMI Berlin
Bericht FZR-33, März 1994

Zur Aktualisierung der Neutronenparameter in der drehbaren Bestrahlungseinrichtung des rekonstruierten BER-II wurde der im Forschungszentrum Rossendorf entwickelte Mehrkomponentenaktivierungsdetektor eingesetzt.
Durch das umfangreiche Datenmaterial sind axiale und radiale Neutronenflußverläufe bestimmt und es gelingt ein eindeutiger Bezug von Meßwert zur Bestrahlungsprobe.

Thess, A.; K. Nitschke
A Note on Benard Marangoni Instability in the Presence of a Magnetic Field
Report, FZR-61, November 1994

We formulate the asymptotic theory of thermocapillary instability in a planar fluid layer heated from below in the presence of a strong magnetic field corresponding to high Hartmann number. Explicit asymptotic expressions are derived for the velocity perturbation, temperature perturbation and electric current density. Their spatial structure is characterized in terms of Hartmann boundary layers - a concept which permits a physical understanding of more complicated situations involving surface deformation, buoyancy and thermoelectric effects. The physical nature of large scale instabilities in the case of a deformable surface is clarified.

Meetings and Workshops

MEETINGS AND WORKSHOPS

1. Rossendorf Workshop
   Entscheidungstheorie und Expertensysteme im Umweltbereich
   Rossendorf, 08.02.94
   ca. 20 German participants

2. IAEO-Workshop
   Use of the Code DYN3D for the Evaluation of Reactivity Accidents in NPP with Hexagonal Core Geometry
   Rossendorf, 14.03. - 18.03.94
   ca. 35 participants from Germany, Eastern Europe and Austria

3. Meeting of Working Group D "Reaktor Safety Analysis"
   of Atomic Energy Research
   Rossendorf, 03.05. - 06.05.94
   ca. 20 participants from Finland, Hungary, Czech Republic, Russia, Germany

4. 1st Specialists Meeting
   "Betriebliche Überwachung des KKW Saporoshje"
   Rossendorf, 01.08. - 05.08.1994
   15 participants from Ukraine and Germany

5. Windenergy-Workshop
   Rossendorf, 07.09.94
   ca. 20 participants from Germany and Czech Republic

6. 2nd Specialists Meeting
   "Betriebliche Überwachung des KKW Saporoshje"
   Rossendorf, 18.11. - 26.11.1994
   12 participants form Ukraine and Germany

7. 5th Workshop
   "Betriebliche Überwachung des KKW-Saporoshje"
   Rossendorf, 05.12. - 09.12.1994
   14 participants from Ukraine and Germany

8. Workshop on Vibration Modelling of VVER Type Reactors
   Rossendorf, 13.12. - 16.12.94
   15 participants from Germany, Russia and Hungary

Seminars

SEMINARS 1994

1. Microstructural Characterization of Neutron Irradiated VVER-type RPV Steels
   Ref.: Dr. J. Kočik, UJV Rez
   T.: 12.01.94

2. Ein Programmsystem für die Berechnung des Plasmas in Spiegelmaschinen mit Monte-Carlo-Methoden - Konzeption und erste Ergebnisse
   1. Darstellung des Themas
   2. Transport Schneller Ionen
   3. Neutralgastransport
   Ref.: Dr. K. Noack, Dipl.-Phys. St. Krahl
   T.: 01.03.94

3. Analytische und experimentelle Untersuchungen zur Modellierung der Fluid-Struktur-Wechselwirkung im Ringspalt
   Ref.: Dr. G. Grunwald, Dr. E. Altstadt
   T.: 10.03.94

4. Integration solarer Warmwasserbereitung in ein Fernwärmesystem auf Erdgasbasis in Freital
   Ref.: Dr. D. Brünig, B. Blandon
   T.: 21.03.94

5. Spezifikation eines technischen Systems zur Fernüberwachung des KKW Saporoshe (Block 5)
   Ref.: Dr. H. Carl, Dr. P. Schumann, Dr. J. Zschau
   T.: 24.03.94

6. Stand und Pläne des Institutes für Sicherheitsforschung (IFS)
   Ref.: Prof. Birkhofer, Dr. Wolfert, Dr. Erlenwein
   T.: 28.03.94

7. Monte-Carlo-Methoden für transporttheoretische Berechnungen von Neutralteilchen - Anwendungen für Neutronenfluenzberechnungen
   - Experiment-Theorie Vergleich mit Hilfe der Spektrumsjustierung
   Ref.: Dr. H.-U. Barz, B. Böhmer
   T.: 14.04.94

8. Untersuchung einer Zweiphasenströmung mit Leitfähigkeitsmeßsonden in der PKL-Anlage
   Ref.: S. Kusch, TU Berlin
   T.: 20.04.94

9. Übersicht über die Arbeiten im Bereich "Physik der Kernreaktoren" des Kurtschatow-Instituts Moskau unter besonderer Berücksichtigung von Transportrechnungen zur Bestimmung der Neutronenbelastung von Reaktordruckbehältern
Ref.: Dr. S.M. Zaritsky, Kurtschatow-Institut Moskau
T.: 27.04.94

10. Überblick über die geplanten Arbeiten am rekonstruierten Impulsreaktor des JINR Dubna und Diagnoseinstallationen zur Betriebsüberwachung des Impulsreaktors
Ref.: Dr. A.V. Vinogradov, Dr. Y.N. Pepelyshev, JINR Dubna
T.: 28.04.94

11. Overview on Research Work for New Generation NPP in the Kurchatov Institute
Ref.: Dr. I.V. Elkin, Kurchatov Institut Moskau
T.: 08.06.94

12. Messung der Zähigkeitskennwerte im Bereich der Hochlage der Kerbschlagarbeit
Ref.: Prof. Dr. K. Reiff, Fachhochschule Osnabrück
T.: 10.06.94

13. Anwendung von Positronenemittern zur Analyse von Zweiphasenströmungen - Stand der Arbeiten
Ref.: F. Hensel
T.: 08.07.94

14. Messung von Rißfortschritt bei quasistatischer Biegebelastung mit Ultraschallverfahren
Ref.: R. Kunze, TU Dresden
T.: 25.07.94

15. Status of a Plasma Neutron Source Project at Novosibirsk
Ref.: Dr. A. Ivanov, Budker Institut Novosibirsk
T.: 18.08.94

16. Beladeoptimierung mit evolutionären Algorithmen auf Parallelrechnern
Ref.: Dr. Axmann, TU Braunschweig
T.: 29.08.94

17. Marangoni Instability under Microgravity Conditions: The Effect of Geometry and Magnetic Field
Ref.: Dr. S.K. Wilson, Strathclyde University, Glasgow
T.: 05.09.94

18. Selbstorganisierte Strukturbildung in Flüssigkeiten und in chemischen Systemen
Ref.: Dr. M. Bestehorn, Univ. Stuttgart,
Inst. für Theoretische Physik und Synergetik
T.: 09.09.94

19. Modellierung mechanischer Schwingungen am WWER-440 mit finiten Elementen
Ref.: Dr. E. Altstadt
T.: 20.09.94

20. The Structural Reasons of the Radiation Embrittlement of VVER-440 Type Pressure Vessel Steels
Ref.: Dr. V. Levit, RRC "Kurchatov" Institute Moscow
T.: 27.09.94

21. 1. Present-day methods on two-phase flow measurements
2. Acoustic methods of two-phase flow diagnostic
Ref.: Prof. V.I. Melnikov, Technical University of Nishny Novgorod, Russia
T.: 14.10.94

22. First Russian Standard Problem Exercise and other Small-Break LOCA tests at the ISB-VVER facility
Ref.: Gaschenko, Maria Petrovna,
Research and Engineering Center Elektrogorsk, Russia
T.: 20.10.94

23. Merkmalsextraktion aus Ultraschallsignalen zur Erkennung von Strömungsmustern in Zweiphasenströmungen
Ref.: Dr. N. Kossok
T.: 27.10.94

24. Parallelisierung des Reaktor-Codes DYN3D - Erste Erfahrungen auf einer Sun Sparc 10/514
Ref.. Dr. S. Mittag
T.: 15.11.94

25. Beiträge der Positronenannihilationsspektroskopie zur Aufklärung der Neutronenversprödung von Reaktordruckbehälterstählen
Ref.: Dr. G. Brauer, TU Dresden, Abt. Physik, WIP-Gr.
T.: 01.12.94

26. Berechnung von Neutronenflußdichteschwankungen infolge stochastischer Schwingungen von Regelstäben mit Hexagonal-Z-Geometrie
Ref.: Dr. F. Hollstein
T.: 14.12.94

Reserach Center Seminars

Sicherheitsforschung zu Risiken großtechnischer Systeme
Prof. Dr.-Ing. E.F. Hicken, KFA Jülich

F/E-Arbeiten des Kernforschungszentrums Karlsruhe zur Sicherheit von Leichtwasserreaktoren
Dr.-Ing. B. Kuczera, KFK Karlsruhe

Seminars held by PhD-Students

Felder und Wellen in Festkörpern und ihre Anwendung zur Rißlängenmessung
Dr. Bergner, TU Dresden

Erfassung und Interpretation von akustischen Signalen im instrumentierten Kerbschlagbiegeversuch
Richter, Holger

Entwicklung eines Ultraschallmeßverfahrens für Rißfortschritt an Dreipunktbiegeproben
Bergmann, Ute

Untersuchungen zum Naturumlaufverhalten der Versuchsanlage PKM-NVH bei reduziertem Kühlmittelinventar (LOCA-Störfälle)
Schäfer, Frank

Entscheidungsanalytische Hilfsmittel für die Altlastensanierung
Kruber, Stefan

Experimentelle Untersuchungen zu MHD-Zweiphasenströmungen
Eckert, Sven

Experimentelle Untersuchungen zur oberflächenspannungsgetriebenen Benard-Konvektion
Nitschke, Kerstin

Fluid-Strukturwechselwirkung in einem Ringspalt: Formulierung der dynamischen Gleichung für eine numerische Lösung
Zoller, Jürgen

Lectures

1. U. Rindelhardt: Renewable Energies
   Lectures at HTWS Zittau/Görlitz

2. U. Rindelhardt: Photovoltaic/Wind Energy
   Lectures at TU Dresden, Fakultät für Maschinenwesen

3. U. Rindelhardt: Renewable Energies
   Lectures at Universität Leipzig,
   Fakultät für Physik und Geowissenschaften

4. F.-P. Weiß: Reliability and Safety of Technical Systems
   Lectures at TU Dresden, Fakultät für Maschinenwesen

5. U. Rindelhardt; G. Teichmann: Photovoltaic
   Practicum held for the TU Dresden, Fakultät für Maschinenwesen

6. Schmitt, W.; Hessel, G.; Weiß, F.-P.:
   Neutron Noise in Zero Power Reactors
   Practicum held for the TU Dresden, Fakultät für Maschinenwesen

7. Schmitt, W.; Hessel, G.; Weiß, F.-P.:
   Power Noise in Pressurized Water Reactors
   Practicum held for the TU Dresden, Fakultät für Maschinenwesen

Departments of the Institute

Research Center Rossendorf, Inc. Organigram

Institute for Safety Research
01314 Dresden, PF 510119

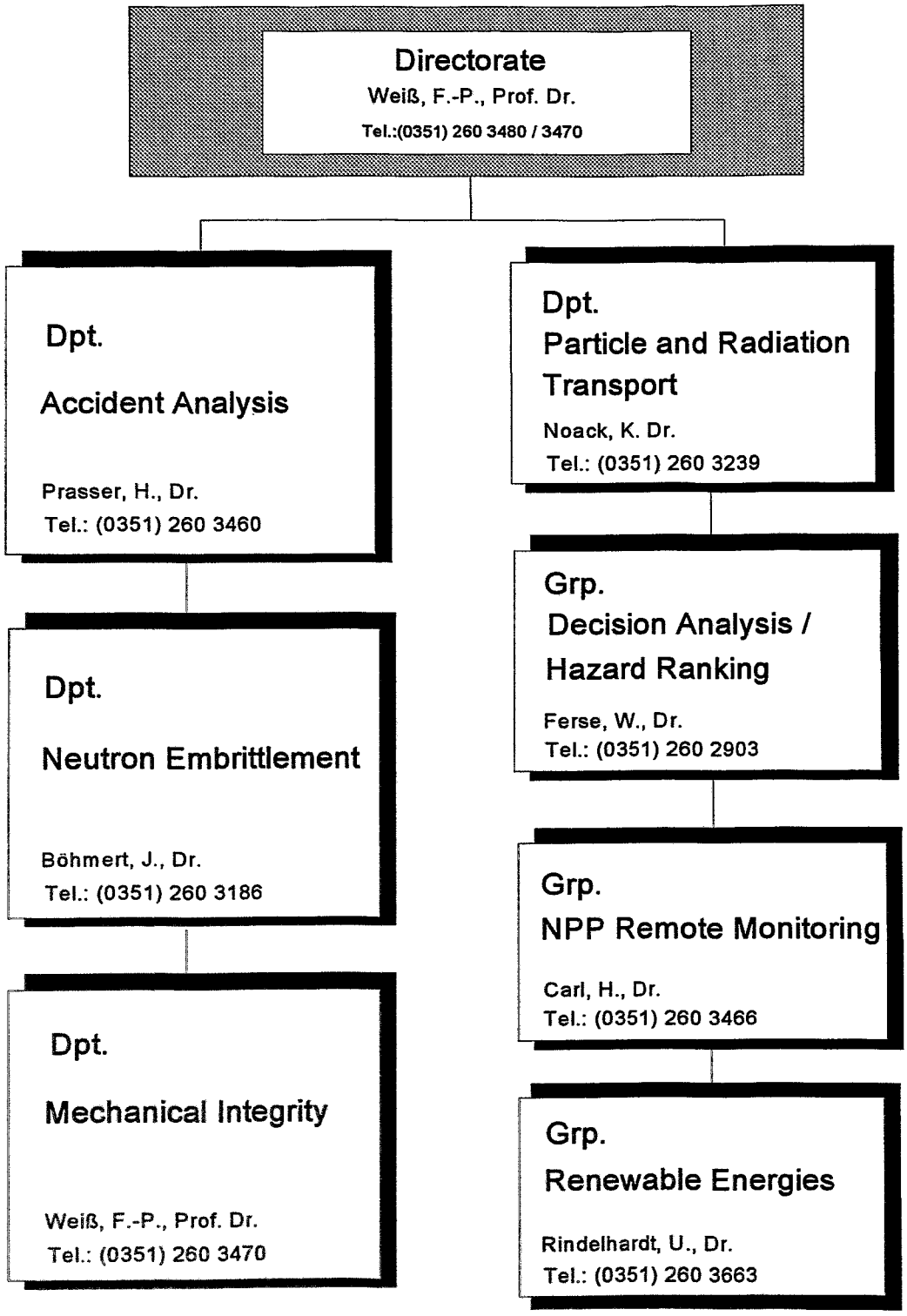

Personnel

Director: Prof. Dr. F.-P. Weiß

Scientific Staff

Altstadt, Eberhard Dr.
Barz, Hansulrich Dr.
Barz, Ralph-Uwe Dr.
Bergmann, Uwe
Beyer, Matthias
Brünig, Dietlinde Dr.
Böhmer, Bertram
Böhmert, Jürgen Dr.
Erlebach, Stephan
Carl, Helmar Dr.
Ferse, Wolfgang Dr.
Galindo, Vladimir Dr.
Gerbeth, Günter Dr.
Große, Mirco
Grundmann, Ulrich Dr.
Grunwald, Gerhard Dr.
Hessel, Günter
Hirsch, Werner Dr.
Hollstein, Frank Dr.
Jüttner, Bernhard
Kliem, Sören
Kolevzon, Vladimir
Konheiser, Jörg
Krahl, Steffen
Krepper, Eckhard Dr.
Kumpf, Hermann Dr.
Langer, Lutz
Lielausis, Olgerts Prof.
Lucas, Dirk Dr.
Maletti, Rainer Dr.
Mittag, Siegfried Dr.
Mutschke, Gerd
Naehring, Friedrich Dr.
Noack, Klaus Dr.
Prasser, Hans-Michael Dr.
Priede, Janis Dr.
Rindelhardt, Udo Dr.
Rohde, Ulrich Dr.
Scheffler, Michael
Schikora, Bernd
Schmitt, Wilfried Dr.
Schröder, Frank
Schubert, Dietmar
Schütz, Peter
Schumann, Peter Dr.
Seidel, Andre
Steinkamp, Helmut Dr.
Stephan, Ingrid Dr.
Teichmann, Günther
van der Vorst, Klaus
Viehrig, Hans-Werner Dr.
Weiß, Frank-Peter Prof. Dr.
Witke, Willy
Zschau, Jochen Dr.
Zippe, Winfried Dr.

Post Doc

Steinkamp, Helmut Dr.

PhD Students:

Bergmann, Ute
Eckert, Sven
Hensel, Frank
Nitschke, Kerstin
Richter, Holger
Schäfer, Frank
Zoller, Jürgen

Technical Staff

Baldauf, Dieter
Behrens, Sieglinde
Blumentritt, Thea
Böttger, Arnd
Borchardt, Steffen
Eichhorn, Christine
Enkelmann, Wolfgang Dr.
Elert, Edith
Fischer, Manfred
Futterschneider, Hein
Gebel, Margitta
Heinze, Gerda
John, Annett
Kaule, Christian
Keulicht, Anke
Kunadt, Heiko
Lang, Dorothea
Leonhardt, Wolf-Dietrich
Leuner, Bernd
Leuschke, Grit
Losinski, Claudia
Lotzmann, Roland
Otto, Gerlind
Pietzsch, Jens
Richter, Annett
Richter, Henry
Richter, Joachim
Richter, Karl-Heinz
Richter, Petra
Rott, Sonja
Russig, Heiko
Schmidt, Johannes
Seidler, Christa
Skorupa, Ulrich
Tamme, Marko
Tamme, Günter
Webersinke, Wolfgang
Weichelt, Steffen
Weiß, Rainer
Werner, Matthias Dr.
Willkomm, Heike
Zimmermann, Wilfried